THE LARGE SCALE STRUCTURE OF THE UNIVERSE IN PANCAKE MODELS OF GALAXY FORMATION

James G. More

Doctor of Philosophy
University of Edinburgh
1988

This thesis is my own composition except where specific reference is made to the work of others.

James G. More

August 1988.

TO MUM AND DAD

for their support and encouragement
in everything I do

Science is not just a collection of laws, a catalogue of unrelated facts. It is a creation of the human mind, with its freely invented ideas and concepts. Physical theories try to form a picture of reality and to establish its connection with the wide world of sense impressions. Thus the only justification of our mental structures is whether and in what way our theories form such a link.

Albert Einstein and Leopold Infeld.

Abstract

This thesis investigates the evolution of characteristic structures in neutrino or adiabatic baryon-dominated models of galaxy formation. We discuss the collapse of protocluster or protosupercluster clouds in terms of the behaviour of non-rotating, homogeneous triaxial ellipsoids, predicting that galaxies should populate filamentary or quasi-spherical structures rather than the generic flat structures (pancakes). Secondly we have designed a numerical code which allows us to do fast cosmological hydrodynamics. We investigate the effect of explosions on the standard pancake picture for galaxy formation. Blast waves created by the early evolution of galaxies can not produce the anti-biasing effect required to reconcile the rapid evolution of clustering in n-body simulations of neutrino models with observations of galaxies at redshifts greater than one.

Acknowledgements

I am indebted to my supervisor Alan Heavens for his ideas and advice throughout the period of study and to John Peacock, Mike Wilson and Arthur Trew who collaborated on some of the work presented in this thesis.

My thanks are also due to many of the students and members of staff at the Observatory both for their friendship and their contribution to my understanding of astrophysics. Special mention must be made of the library staff for their help with photocopying and in obtaining relevant papers, the Observatory secretaries for finishing my education, and in particular the university secretary, Liz Gibson, for her additional willingness to sort out any administrative difficulties I encountered.

On the domestic front I must thank my landlady Mrs M^{c}Robie for keeping my body (and trying to keep my soul) together.

Finally I would like to thank the Science and Engineering Research Council for the award of a studentship, giving me the opportunity to enjoy what has been a rewarding 4 years of research.

Contents

Chapter 1
Introduction

The observed properties of galaxies may be divided generally into two categories: individual properties such as mass or angular momentum and collective features such as their spatial distribution. The work presented in this thesis addresses the latter property in the context of pancake models of galaxy formation. We shall not be concerned with statistical measures, such as the n-point correlation functions, but rather physical processes which will alter the 'standard picture' whereby galaxies exist in thin planar structures.

1.1 Concepts in galaxy formation theory

The standard big bang model (see e.g. Gunn 1978) is accepted as a good zero-order description of the evolution of the universe. In particular nucleosynthesis of light elements in the early stages of evolution compared to observed abundances (recently reviewed by Yang et al. 1984) and the detection of the predicted background radiation by Penzias and Wilson in 1965 give solid support to its validity. In the context of this work it is obviously incomplete: the universe is not homogeneous locally. A great deal of observational work has been done to determine the nature of the galaxy distribution. In particular recent analysis of the CfA redshift survey by various authors e.g. Davis & Peebles 1983, de Lapparent et al. 1986, has revealed considerable clustering of luminous material on a wide range of scales. To explain such clumping of matter in the standard model we must invoke density fluctuations as an *ad hoc* initial condition. Further problems with the basic model, the so-called 'horizon' and 'flatness' inconsistencies, have recently found a possible solution in the theories of particle physics (the inflation concept) which have been developed to explain the early high temperature, high-density stage of the Universe. (Guth & Steinhardt, 1984 give a simple discussion and further more detailed notes in the context of cosmology are contained in a review by Barrow 1983). The most encouraging aspect of these investigations is that a physical theory for the origin of fluctuations may be emerging, providing us with information on how to characterise energy density variations on

different length scales, though as yet the magnitude of such variations are uncertain. Particle theories may provide us with a physical origin for the perturbed standard big bang model which is presently assumed as a starting point for theoretical work on galaxy formation.

The role of large scale structure formation theory could be defined as follows: to investigate the behaviour of density in a representative section of the universe for different cosmological models with given constituents and some assumed initial density distribution. The results are compared to various observations, for example measurements of the microwave background (MWB) isotropy. (This topic has been reviewed recently by Kaiser & Silk (1986)). The standard framework for these calculations is the Friedmann model characterised by density parameter Ω_0 and Hubble constant H_0, often expressed via $h \equiv H_0/100$ $kms^{-1}Mpc^{-1}$. These fundamental parameters are not very well determined (for a critical discussion see Gunn 1978) and consequently previous work has concentrated on ruling out certain formation models with chosen Friedmann constants. The principal difficulty arises in matching theoretical dynamical arguments which predict the spatial distribution of *mass* to observations of the light distribution (galaxies etc.) quantified through correlation function analysis (Peebles 1980). There is good evidence for a large amount of dark matter in galaxies and clusters in an as yet unknown form and the common 'maximum ignorance' assumption that light traces mass (i.e. light density is proportional to mass density) may not be valid. Such segregation of mass and light arises naturally in so-called 'biased' galaxy formation models, the simplest of which is where we assume that the light comes only from the high peaks in the density distribution. This phenomenon also allows us to reconcile low dynamical estimates of the density parameter with $\Omega_0=1$ predicted by inflation. Furthermore the prediction, and subsequent detection of new types of particles which may dominate the mass density has led to a fundamental revision of our ideas on evolution of density fluctuations. These ideas are discussed concisely by Primack (1984).

A few general concepts in fluctuation analysis should be introduced at this stage. The initial density field is assumed to be Gaussian, and the components of its Fourier decomposition $\delta(k)$ are assumed to have random phases. (Work on confirming this standard

assumption is currently being tackled by Gott III et al. 1987). We will not consider non-Gaussian conditions e.g. cosmic strings (see Hogan 1984 and references therein), although we will introduce explosions in Chapter 3. The linear evolution $\delta\rho/\rho \ll 1$ can be summarised in terms of some transfer function T(k,t):

$$\delta(k)_{\text{recombination}} = T(k,t)\ \delta(k)_{\text{initial}} \qquad 1.1)$$

where the initial spectrum is normally assumed to be $|\delta(k)|^2 \propto k^n$. The case n=1, the Harrison-Zel'dovich spectrum, is of particular interest as it has some basis in the theories of particle physics; the size of mass fluctuations on any scale as they come within the horizon is constant. An alternative expression of this is that in a zero-curvature Friedmann model, there is no imprinted scale. A choice of $n \neq 1$ implies a preferred scale where the r.m.s fluctuations on entering the horizon are unity. The amplitude or normalisation of $\delta(k)_{\text{initial}}$ is difficult as it depends on matching theory to observation. Let us consider the processes encompassed by T(k,t) in the linear stage of fluctuation evolution.

Traditionally, for universes composed of baryonic matter and radiation the behaviour of fluctuations can be followed by perturbing, to first order, the standard fluid equations in comoving coordinates about the Hubble expansion. This allows us to derive a second-order equation for fluctuation strength as a function of time which can be solved for a given equation of state relating pressure and density (see for example Weinberg 1972, p571).

Radiation-dominated regime	$P = (1/3)\rho$	$\delta \propto t \propto a(t)^2$	1.2)
Matter-dominated regime	$P = 0$	$\delta \propto t^{2/3} \propto a(t)$	

where a(t) is the universal scale factor. In low-Ω_0 universes growth slows down at $z \approx 1/\Omega_0$. Mészáros (1974) first pointed out that the presence of a uniform relativistic background would slow down the growth of matter perturbations. Strictly the above treatment applies to all scales greater than the horizon. As a given scale enters the horizon, causal processes affect its evolution. Two length scales are of major importance: the Jeans scale, first worked out by James

Jeans in 1902, gives the minimum size of baryon perturbation which can collapse; the Silk damping scale (see Efstathiou & Silk 1983, Fig. 4.1) specifies the photon diffusion length up to which radiation density fluctuations can be erased and hence for adiabatic fluctuations (which we will assume throughout and may arise naturally in the early universe), the scale on which baryon fluctuations are erased until they decouple at recombination.

Universes where various types of dark matter, for example massive neutrinos or photinos, dominate the mass density have more complicated behaviour (see Bond & Szalay 1983 for a detailed discussion). The most important features of the linear evolution are: the erasure of fluctuations on scales less than the free-streaming scale for the particle in question; the retardation of growth on scales less than the Jeans mass at recombination, as a result of dark matter perturbations coming within the horizon before they dominate the energy density, and hence finding themselves in a uniform background field (an extension of the Meszaros effect). The principal difficulty in baryon-dominated universes, the MWB problem (see later), is eased as baryon fluctuation growth is accelerated post-recombination to match the already growing dark matter perturbations, which do not show up as MWB fluctuations as they decouple from the radiation field at an earlier epoch. The linear evolution is now well understood, the main uncertainty being the normalisation of the amplitude of the density fluctuation field. This requires a match of theory to observation, which requires an understanding of non-linear evolution which we now discuss.

1.2 Approaches to non-linear behaviour

Linear evolution theory predicts the shape of the recombination epoch fluctuation spectrum, $\delta(k)_{\text{recombination}}$. We are naturally led to the top-down formation picture in adiabatic neutrino- or adiabatic baryon-dominated models where large scales have most power and collapse first. Galaxies must arise from fragmentation of these protocluster- and protosupercluster-scale objects. The cold dark matter picture leads to collapse of globular-cluster-size objects first and larger objects form by hierarchical clustering. The uncertain regimes in such evolution are where scales collapse beyond the linear

phase $\delta>1$. Order of magnitude estimates yield $\delta=2$ for the Local Supercluster and $\delta=10^4$ for rich clusters i.e. most observations probe this uncertain region. There are two possible approaches to calculating this non-linear phase of evolution of structure: (i) use n-body simulations (e.g. Efstathiou et al. 1985) which model a large region of the universe but have limited spatial resolution and as yet treat purely gravitational forces; (ii) calculate the behaviour of individual structures in a given model. Obviously interaction effects between neighbouring structures are neglected in this approach so the two types of investigation must be regarded as individually incomplete but complementary. To date the n-body approach has provided most of the important conclusions on the successes and problems of various models. However the treatment of bias is rather *ad-hoc* in these calculations and a study of the physical processes giving rise to the segregation of mass and light in a given model is very important.

1.3 Pancake models

We will concentrate on theories where large-scale damping of density fluctuations is important. Our models will look at evolution of initially homogeneous structures on scalelengths corresponding to: i) Silk damping, $\lambda=2.1(\Omega_o h^2)^{-5/6}$Mpc (Efstathiou & Silk 1983); ii) Neutrino free-streaming, $M_\nu=4\times10^{15}(m_\nu/30ev)^{-2}M_\odot$ (Bond et al. 1980) i.e. $\lambda=13.8(\Omega_o h^2)^{-1}$ Mpc where $\Omega_o h^2=0.31(m_\nu/30eV)(T_o/2.7K)^3$ describes the mass m_ν of neutrinos required to close the universe for a given Hubble constant h. This so-called 'pancake' theory developed by the Zel'dovich school (Sunyaev & Zel'dovich 1972) involves formation of high-density flattened regions which can fragment to galaxies. Recently, Shapiro and Struck-Marcell (1985) have discussed the behaviour of the coupled baryon and dark matter distributions as they collapse to a pancake. The baryon component, held up by radiation pressure until the recombination epoch, is rapidly pulled into the already growing dark matter potential wells. It has much of its kinetic energy transformed into heat in a plane shock set up in the baryon fluid and consequently settles into a dense, rapidly cooling central layer where conditions are suitable for fragmentation. The dense central layer then acts to enhance the flattening of the

dark matter distribution over a purely collisionless collapse.

Adiabatic baryon-dominated and hot dark matter models at present seem most compatible with observations, particularly taking into account streaming motion work (Aaronson et al. 1982, Collins et al. 1986, Peacock et al. 1987, Lynden-Bell et al. 1988), the discovery of giant voids (~50Mpc) in the galaxy distribution (e.g. Kirshner et al. 1987) and recent work by Einasto et al. (1986) which suggests a galaxy correlation length r_0 greater than the canonical $5h^{-1}$Mpc. The Einasto work has been confirmed by as CfA survey analysis (Geller, 1988). If these results are substantiated it appears that currently fashionable cold dark matter (CDM) models may be ruled out as they have little power on large scales. The observed structure and coherent motions on such scales are difficult to explain if the calculations are normalised to reproduce the small scale structure (White et al. 1987). The theoretical calculations of streaming motion are dependent on two key features; i) the normalisation of the amplitude of the density contrast; ii) the window function which is used to simulate observational procedure through its convolution with the peculiar velocity field to predict streaming motions. For detailed arguments on the theoretical work see Hoffman (1987), Kaiser (1987), Peacock et al (1987). At the moment it is unclear how the contrasting effects discussed by these authors can be reconciled into an agreed theoretical prediction. Also there are still great arguments over systematic effects in the observational determinations of streaming motions.

In contrast to CDM, there is some experimental evidence for the existence of massive neutrinos from tritium β decay studies, $17 \leqslant m_\nu \leqslant 40$eV (Lyubimov et al. 1980, 1986), though the implications from observations of SN 1987A (Bahcall & Glashow 1987) place a conflicting upper limit on the mass of the electron neutrino of $m_\nu \leqslant 11$eV. Conclusive evidence should come from the planned Los Alamos group experiment on atomic tritium where the experimental problems will be better understood. Molecular tritium measurements (Robertson et al. 1986) have yielded an upper limit of 29.3eV on the electron neutrino mass.

However several problems with pancake models have not been satisfactorily answered. Two general criticisms are that the fragmentation of protocluster-scale objects into galaxies is a largely

unknown process, so the small scale clustering of galaxies and the origin of Lyα clouds is not clear, and that evidence for processed material in voids in the galaxy distribution (Brosch & Gondhalekar, 1984) is hard to explain. Standard pancake models have no processed material between the dense pancakes, these regions being evacuated by infall.

Baryon pancake models are principally constrained by nucleosynthesis arguments $\Omega_b h^2 < 3.5\times10^{-2}\ (T/2.7K)^3$ (Yang et al. 1984) and by microwave background measurements. Even for a flat baryon model, where maximum possible fluctuation growth occurs but we must postulate a low value of h (see Shanks 1985), recent MWB fluctuation measurements by Davies et al. (1987) on large angular scales are in conflict with calculations (Wilson & Silk 1981) unless we choose apparently unphysical initial fluctuation spectra with $n > 1$. In their recent paper (see above) Peacock et al. conclude that flat baryon models are tenable provided galaxy formation is very recent ($z \lesssim 1$).

White et al. (1983) outlined the major argument against neutrino models; if the present galaxy correlation length is 5 h^{-1} Mpc (Davis & Peebles 1983) they concluded that for reasonable values of Ω_o and H_o the first structures must have collapsed too recently ($z \lesssim 1$) to explain observations of quasars at high redshift. There are many problems with this approach but the analysis ultimately rests on identifying the present epoch in their n-body simulations by matching the mass autocorrelation function to the present galaxy correlation function. If the galaxy correlation length is actually $10h^{-1}$ Mpc as Einasto et al. suggest, we can relax the formation epoch to be as high as 3 depending on H_o. Also the assumption that light traces mass may be too simplistic. Gas dynamic effects from the first objects to form could stimulate/suppress collapse of nearby objects, making the galaxy correlation function significantly different from the mass autocorrelation function. Reduction of the correlation on small scales (anti-biasing) would relax further the formation epoch constraint (Braun et al. 1988). This argument is also important in alleviating the formation epoch problem in baryon models discussed by Peacock et al. .

White et al. (1984) have further argued that 'neutrino clusters' in simulations have masses and binding energies too large to be

identified with observed Abell clusters. They point out that even if galaxy formation could be suppressed in these high density regions, to fix up the clustering problem outlined above, a simple estimate of x-ray emission from hot gas in the cores is excessively large. However, Bond et al (1984b), (see also Shapiro & Struck-Marcell 1985) have shown that only 10-20% of the gas shock heated as it collapses to a high density pancake can cool sufficiently to condense into such neutrino potential wells, perhaps reducing the predicted x-ray emission to reasonable levels. As Bond et al. discuss, a hot intergalactic gas providing a large fraction of the baryon density may fit the observed discrepancy between the nucleosynthesis constraint and estimates of the luminous matter density in galaxies, so the neutrino theory may survive.

The dark to luminous mass ratio as a function of scale and the nature of dark matter on a given length scale provide stringent constraints on the type of particle dominating the mass density and hence the galaxy formation scenarios considered. The observed constancy of (Mass/Luminous Mass) with scale (Rees, 1984) has no obvious physical origin in top-down pictures. Observational evidence that galaxies have non-baryonic haloes would rule out massive neutrinos as the dominant dark matter *on such scales* according to the phase space argument of Tremaine & Gunn (1979):

$$m_\nu^4 > \text{const} / \sigma_v\, r^2 \qquad 1.3)$$

where σ_v is the velocity dispersion and r the core radius of the neutrino distribution defined by the virial condition:

$$r^2 = 9\sigma_\nu^2 / 4\pi G\rho_0 \qquad 1.4)$$

ρ_0 is the central density. The result depends critically on the assumed final state of the neutrino distribution associated with the galaxy; an isothermal sphere of given radius r and isotropic velocity distribution. Madsen and Epstein (1984, 1985) point out that computing the most compact neutrino mass distribution and allowing for an anisotropic velocity distribution relaxes these limits somewhat. However unequivocal evidence for dark haloes in *dwarf* galaxies would require neutrinos of mass $m_\nu \gtrsim$ 50eV in conflict with experimental limits. Kormendy (1987) notes that observationally the core radius of dwarf galaxies is hard to determine (the visible matter may be clustered on a smaller scale than the dark material), and that ρ_0 and σ_ν should be used as diagnostics. He points out that rotation

curve analysis may as yet underestimate σ_v and hence overestimate the lower limit on the neutrino mass. Finally the analysis of stellar velocity dispersions in Local Group dwarfs by Aaronson & Olszewski (1987) which suggests $m_\nu \gtrsim 400eV$ is dependent on assuming that light traces mass. In conclusion more work is required to prove the existence of dark haloes and further to show they are non-baryonic, if we are to rule out neutrinos as the dominant mass in these galaxies. This argument of course would not rule them out as being cosmologically important as the dark matter on galactic scales could be baryonic, (but see the work of Hegyi & Olive 1986). Cowsik and Ghosh (1987) present a model where the dark matter does not take part in the clustering below cluster scales. Luminous material is embedded in a smooth neutrino distribution. The relevant scale r for the neutrino mass constraint is thus the cluster scale, and the phase space constraint then does not conflict with observations.

We conclude that, although one or two problems exist, the pancake theory has many promising features for the large scale galaxy distribution. The small scale behaviour, where non-linear effects are important, has not yet been accurately modelled. Hydrodynamics must play an important part. When this has been included in the calculations we will have a better idea of how successfully pancake models fit the observed universe. Determination of the neutrino mass by experiment and observational work on the dynamics of galaxies will be important constraints on neutrino models.

1.4 Aims of the thesis

The philosophy behind our work is essentially this: The CDM model is currently the most fashionable and has had notable successes, such as predicting flat rotation curves for galaxies. Although a great deal of effort has been made by many workers to circumvent the problems faced by that model in explaining large scale structure (see earlier), the situation is as yet unresolved. Until (if ever) CDM gives us all the answers, and the postulated dark matter is detected, it seems sensible to investigate other possible models in similar detail.

We concentrate on two problems in top-down theories which have direct consequences for the large scale galaxy distribution. Our

approach will be to model the evolution of individual structures in these theories where density fluctuations have damped out to large scales.

In chapter 2 the gravitational collapse of non-rotating, homogeneous, triaxial ellipsoids is followed through and beyond the formation of a two-dimensional caustic surface ('pancake'). This should be a realistic model of the gravitational collapse of a protocluster or protosupercluster as fluctuations on smaller scales will have been largely eradicated by the processes mentioned at the end of section 1.1. We investigate the effect of varying the assumptions regarding the behaviour of background material on the nature of the collapse of such objects, comparing critically with the analysis of White and Silk (1979). In previous work on this problem, 'filaments' (one-dimensional structures) correspond only to the degenerate case of collapsing prolate spheroids; all other shapes, except spheres, collapse to pancakes. In this work, we find that, assuming dissipation or relaxation processes keep the surface relatively thin after formation, pancakes undergo further collapse in their planes, forming either filamentary structures or more isotropic configurations which we call clusters. Filaments thus do not correspond to a degenerate case, but arise naturally from this secondary collapse phase. Some pancakes may nevertheless persist indefinitely, never undergoing the secondary collapse to a filament. However, if we compare the initial shapes required for this behaviour with the initial shape distribution expected for maxima in three-dimensional Gaussian noise, we find that long-lived pancakes should be rare, particularly for high Ω_0 values. We can generally state that galaxies should populate filamentary or spherical structures rather than flat sheets as customarily assumed for these models. In addition we find a very simple yet powerful result on the collapse epoch of objects of a given overdensity with different initial shapes, generalising work on the collapse of spherical structures (e.g. Zel'dovich & Novikov 1983, Peebles 1980).

In chapter 3 we investigate the consequences of the dense pancakes releasing large quantities of energy, in the spirit of explosive models of galaxy formation. The reason for performing this study can be viewed in two ways: in the conventional neutrino model, the galaxies inhabit only the shocked layer of the pancake, and are

consequently strongly clustered. If the explosion mechanism can lead to galaxy formation outside the planes, the clustering problem may be relieved. From an alternative perspective, explosion models have some difficulty producing large scale structure (Ostriker, 1986); a possible resolution would be to imprint the large scale structure by using pancakes as 'seeds' for the explosion process. Our discussion will largely be in terms of the former description although both are in some ways different sides of the same coin. We have modified an Eulerian difference scheme, which solves the equations of inviscid flow to produce a powerful numerical code on which we can do fast cosmological hydrodynamics. The input of energy sends a blast wave through the baryonic material which is still falling in towards the pancake plane. We are interested in the possible cooling of this shocked gas as its subsequent fragmentation would lead to the required population of galaxies outside the pancake plane. The scale height of cooled material is discussed and we check that the shocked gas does not violate X-ray background and Sunyaev-Zeldovich constraints. We compare our results directly with other discussions on these topics and give a simple but very useful result on the comoving thickness of the baryon pancake which extends previous analytical work (Szalay et al. 1984). Our basic finding is that explosions can not produce the anti-biasing mechanism required to alleviate the timing problem faced by standard pancake models without violating observational limits sensitive to the amount of hot gas produced by the explosive process. Alternatively, pancakes may not be used as effective seeds, as the strong gravitational field confines galaxies to be very near the pancakes.

Chapter 2.

The gravitational collapse of triaxial protoclusters

2.1 Introduction

Since the pioneering work of Lin, Mestel & Shu (1965), it has been well known that the anisotropic gravitational field of a uniform density ellipsoid leads to the accentuation of asphericity with time. As the collapse proceeds, a two-dimensional elliptical caustic surface is produced, with infinite density. Only in the degenerate case of an ellipsoid with two equal axes will collapse lead to a one-dimensional filament. Spherically symmetric collapse to a point occurs only if all three axes are equal.

Doroshkevich (1970) discussed the nature of constant overdensity surfaces for random density perturbations in the context of the Zel'dovich formalism; high density regions may be approximated by homogeneous ellipsoids and the shapes of the constant overdensity surfaces thus give the initial axes of the ellipsoids. He showed that these surfaces are generally aspherical, and the probability that two principal axes (of the deformation tensor) are equal is particularly low, so it might seem that filament and point structures should be very rare. However, let us consider the evolution of an homogeneous ellipsoid beyond its collapse to a two-dimensional pancake. If the formation of such a caustic surface results in dissipation of the motion perpendicular to the surface, then the anisotropic gravitational and velocity fields will lead to further growth of anisotropy, in the sense that the eccentricity of the elliptical pancake increases with time.

In the adiabatic theory of galaxy formation (see section 1.3), fluctuations in density are damped below a mass scale $M_D \simeq 1.3\times10^{12}(\Omega_o h^2)^{-3/2}\ M_\odot$, or $4\times10^{15}(m_\nu/30eV)^{-2}\ M_\odot$ ($h=H_o/100 kms^{-1}\ Mpc^{-1}$) if the mass of the Universe is dominated by one light neutrino of mass m_ν. In these cases, the identification of ellipsoids with supercluster scale regions of higher than average density is not too unrealistic. In this picture, as collapse proceeds any new layers of gas which accrete onto the pancake have most of their kinetic

energy transformed into heat by a pair of shocks set up in the baryon fluid either side of the caustic surface (Sunyaev & Zel'dovich 1972). This heat can then be dissipated in the dense central region by radiative cooling which is more rapid than the dynamical time-scales characterising the flow and so a thin dense layer persists. If the Universe is dominated by light collisionless particles, then we expect dissipative pancakes to form by baryons falling into the potential wells of the large-scale dissipationless material. This has been confirmed by Shapiro & Struck-Marcell (1985). Their detailed hydrodynamical calculations of the coupled growth of such baryon/collisionless particle pancakes show that not only do baryons cool and compress into a dense central layer on short time scales but the distribution of collisionless particles also remains highly flattened for some time after the caustic forms. Indeed, the presence of the baryon component serves to decrease the scale height of the collisionless particle distribution further. This confirms the argument of Dekel (1983), who considered an adiabatic invariant treatment of non-dissipative pancakes in their planes and demonstrated that, although the pancake thickness grows as it expands, it becomes relatively flatter in time. It seems justifiable then to neglect motions perpendicular to the plane and assume a planar velocity field within the pancake since this approximation is valid as long as the thickness of the pancake remains smaller than the two principal axes.

The procedure for this calculation splits into two parts: first (Section 2.2) we follow the collapse of ellipsoids to the formation of a caustic surface, in the spirit of White & Silk (1979), hereafter WS (see also Barrow & Silk 1981). We take this opportunity to vary some of the simplifying assumptions of WS, to test the sensitivity of their results to different simplifications. Secondly, we follow the subsequent collapse of pancakes in their planes (Section 2.3). This is an extension of unpublished work by Dr.A.F.Heavens & Dr.J.A.Peacock. At the instant of formation of the pancake, the short axis is expanding less quickly than the long axis, as our calculations demonstrate. The short axis, or indeed both axes, may be contracting, depending on the initial axial ratios of the ellipsoid when the overdensity of the ellipsoid $\delta\rho/\rho$ is much less than unity.

2.2 Pre-pancaking evolution

2.2.1 THE MODEL

The evolution of regions of overdensity in an expanding universe is, in general, extremely complicated. It is possible, however, to gain some insight into the behaviour using a simplified approach following the methods developed by Lin et al (1965) and WS on the collapse of homogeneous ellipsoids. This is the most general three dimensional problem which can be handled exactly by current analytic means. One of the main difficulties with this method is how to treat the gravitational effect of the material outside the ellipsoid. WS assumed it remained uniform at the average universal density. This requires matter to fall continuously into the surroundings of the ellipsoid. Alternatively, we may instead allow the external density to differ from the average density of the universe as a whole. The justification for this is as follows; if space is populated by these ellipsoids, then neighbouring objects will on average prevent the infall of matter to keep the surrounding density high. We make what is in essence an opposite assumption: we assume that there is no infall from outside a sphere of comoving radius r equal to the initial semi-major axis of the ellipsoid, a. Mass inside r is conserved, with average density equal to the average density of the universe (so the ellipsoid is surrounded by an underdense region with density determined by the ellipsoid shape). We could, of course, generalise this approach by assuming there is no infall from outside some general radius $r \geqslant a$. WS's approximation amounts to $r \to \infty$, hence the two approximations can be thought of as the opposite extremes of this method. A further minor alteration to WS's method is that we follow a pure growing mode, so include a velocity perturbation in the initial conditions. This will be appropriate if perturbations have been able to grow before recombination, when we start our calculation; this is the case for perturbations in a high-density universe dominated by 'hot' collisionless particles. Including the growing mode is almost equivalent to reducing the initial overdensity by a factor 5/3 in the problem solved by WS, whose initial condition on velocity was pure Hubble flow. Now Peebles' (1980) calculation of the growing and decaying modes is valid for the matter dominated regime. Our

calculation, which assumes only the growing mode at recombination, therefore accurately represents the behaviour of a fluctuation in high-density universes where matter domination occurs before recombination and the decaying mode has time to die out. For lower-density universes where recombination and matter domination occur more or less simultaneously, there will be in addition a decaying mode. We ignore all other tidal forces and magnetic fields.

Given a quadratic form for the potential, the basic requirement for evolution through a series of homogeneous ellipsoids is that the initial velocity perturbations should be in proportion to the axial ratios (Lin et al. 1965). This can be demonstrated for the growing mode perturbation as follows:

The large scale peculiar velocity field associated with large scale irregularity in density is given in proper coordinates (Peebles 1980, p.65) by

$$\underline{v} = \frac{Hf}{4\pi} \nabla \int \frac{d^3r^1 \rho(r^1)}{|\ \underline{r} - \underline{r}^1|} \qquad (2.1)$$

where $f=(a/\delta)(d\delta/da)$ with overdensity $\delta(\underline{r}^1)=\{\rho(\underline{r}^1)-\rho_b\}/\rho_b$ and scale factor a(t). ρ_b is the mean density of the universe, and H is the Hubble parameter (not to be confused with the present day Hubble constant H_o). Whilst linear perturbation theory applies and we are at a late enough epoch so that only the growing mode solution is present and the relativistic background can be ignored, then f is independent of r and is a function of the density parameter only. We will adopt Peebles' approximation $f(\Omega)=\Omega^{0.6}$; this is only used to set up the initial conditions and will be sufficiently accurate at a starting redshift at recombination of 1500 where Ω is very close to one.

Denoting initial quantities by the subscript (i) where necessary, if we specify the initial overdensity of the ellipsoid, $\delta_{(i)} = (\rho_e-\rho_b)/\rho_b$, we can calculate the density ρ_s outside the ellipsoid, given the assumption that the average density inside a sphere of radius $a_{1(i)}$ is ρ_b. It is given by

$$\rho_s = \rho_b \left[\ 1 - a_{2(i)}a_{3(i)}\{\ 1+\delta_{(i)}\}\ \right]/\{\ 1 - a_{2(i)}a_{3(i)}\} \qquad (2.2)$$

where the $a_{j(i)}$ are the principal axes of the ellipsoid

$\{a_{1(i)} \geqslant a_{2(i)} \geqslant a_{3(i)}\}$ and we choose our length unit such that $a_{1(i)}=1$. The overdensity of the matter immediately outside the ellipsoid is

$$\delta_s = - \left[\frac{a_2 a_3}{1-a_2 a_3} \right]_{(i)} \delta_{(i)}. \qquad (2.3)$$

Clearly the assumption will not be so good for near spherical objects, as formally $\delta_s \to -\infty$, whereas we expect underdensities of the same order as the overdensities in all but the most unusual density fields. However, only when $a_{3(i)} \geqslant 0.9$ does the underdensity outside the ellipsoid greatly exceed the overdensity inside, so the inapplicability to near-spherical objects is not serious in practice.

Splitting the integral into two parts over a homogeneous sphere, overdensity δ_s and a homogeneous ellipsoid, overdensity $\delta_{(i)}-\delta_s$ which can be solved exactly and performing the divergence operation we find that the initial growing mode velocity perturbation is given by components [dropping subscript (i) for equations (2.4) and (2.5) only]

$$v_j = - \frac{\Omega^{0.6} H \delta r_j}{2(1-a_2 a_3)} (\alpha_j - a_2 a_3) \qquad (2.4)$$

with the α_j coefficients defined by

$$\alpha_j = a_1 a_2 a_3 \int_1^\infty (a_j^2 + \lambda)^{-1} \prod_{k=1}^{3} (a_k^2 + \lambda)^{-1/2} \, d\lambda \qquad (2.5)$$

The chosen initial axial ratios $a_{j(i)}$ with $\alpha_{j(i)}$ values from (2.5) and proper velocities from (2.4) adding in a Hubble term constitute the initial conditions.

The potential for a homogeneous ellipsoid, of density ρ_e is

$$\Phi = \pi G \sum_{j=1}^{3} \{(\rho_e - \rho_s)\alpha_j + \frac{2}{3}\rho_s\} r_j^2 \qquad (2.6)$$

[cf. WS equation (5)] where, if we ignore all other tidal effects, Birkhoff's theorem means that we can ignore forces from the surrounding average density universe.

This enables us to determine the equations of motion for the principal axes of the ellipsoid a_j. If we change the independent variable to z using

$$dz/dt = -H_0 (1+z)^2 (\Omega_0 z + 1)^{1/2} \qquad (2.7)$$

(e.g. Longair 1984), express all densities in terms of Ω_0 (the present value of Ω), we can eliminate H_0 to yield

$$\frac{d^2a_j}{dz^2} = - f_1(\Omega_0,z)\frac{da_j}{dz} - \frac{f_2(\Omega_0,z)}{\rho_b} a_j\{ \alpha_j\rho_e + (\frac{2}{3} - \alpha_j) \rho_s\} \quad (2.8)$$

where

$$f_1= \frac{5\Omega_0 z + \Omega_0 + 4}{2(1+z)(\Omega_0 z+1)} \; ; \quad f_2= \frac{3\Omega_0}{4(1+z)(\Omega_0 z+1)}$$

If we convert equation (2.8) into two first-order equations and use the auxiliary formulae (7) of WS we can set up a system of differential equations in $a_j,\dot{a}_j,\alpha_j$ which are solved numerically subject to the conservation equations

$$\rho_e a_1 a_2 a_3 = \text{constant} \; ; \quad \rho_s(s^3 - a_1 a_2 a_3) = \text{constant} \qquad (2.9)$$

where s is the comoving radius of the sphere containing our perturbation. For the particular case of oblate or prolate spheroids the α_j values can be written in closed form [adapted from equations (21)-(24) of Lin et al. with a misprint corrected].

We began each calculation at a redshift 1500, in the recombination era. For our purposes the initial epoch is not too important as the shape is more or less preserved while $\delta\rho/\rho \ll 1$. The behaviour of the principal axes of some representative ellipsoids is shown in Fig.(2.1).

2.2.2 RESULTS

We can now compare the results of the two models and offer some physical explanation of the differences. The general behaviour of the perturbation is rather similar to that of the WS model and their basic conclusions on the effect of varying input parameters are confirmed:

(i) At a given initial overdensity highly eccentric objects collapse fastest.

(ii) Deviation from self-similar evolution is larger in low density

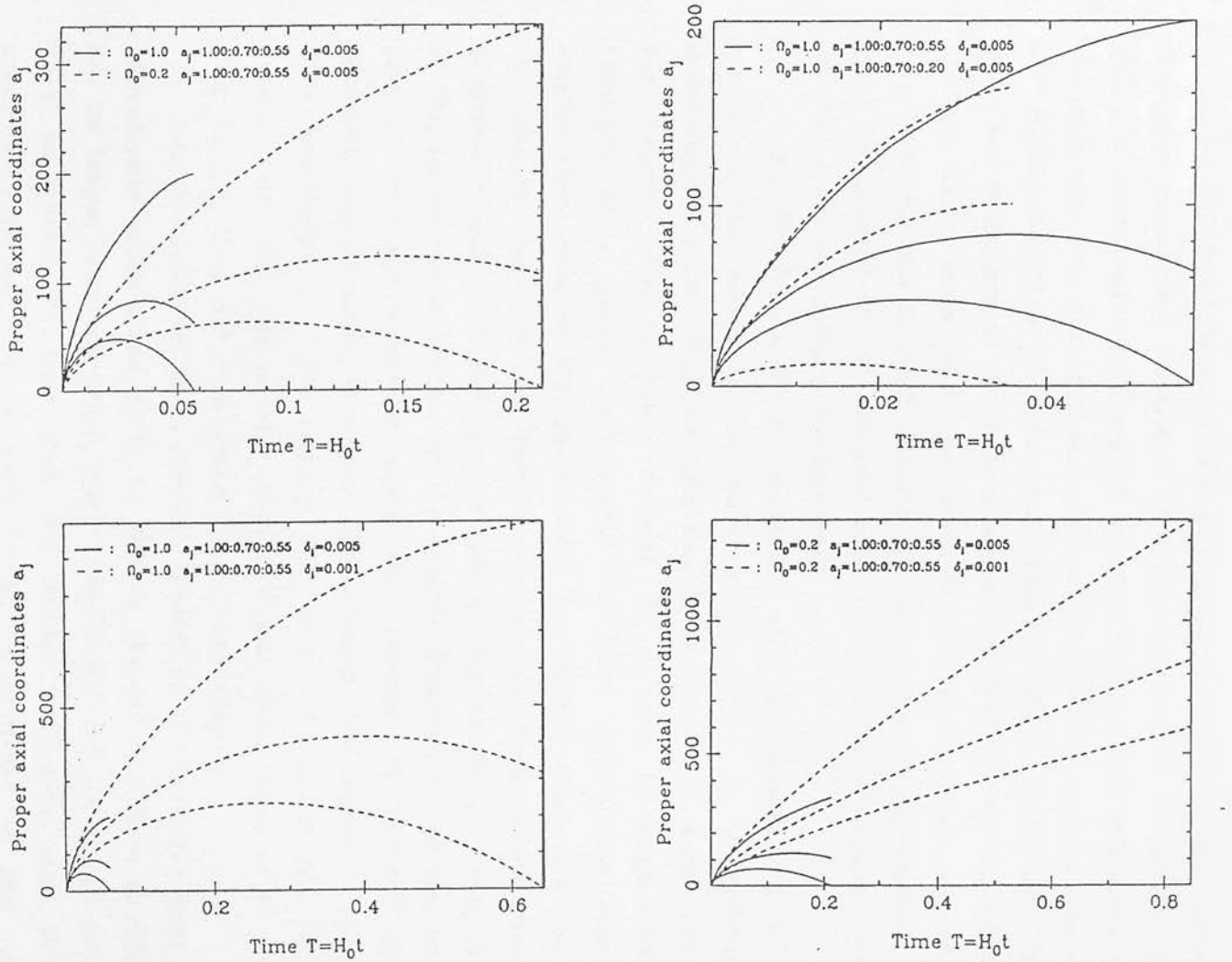

Figure 2.1 The pre¬pancaking behaviour of the principle axes of a few representative ellipsoids is shown to illustrate the effect of a change in background density, ellipsoid density, and initial configuration. The axes, normalised to the initial major axis, are plotted against dimensionless time $T=H_0t$

universes where significant overdensity is achieved earlier, due to the more rapid background expansion.
(iii) Kinematic properties of a pancaked ellipsoid depend both on the initial shape of the perturbation and on the background density.

We will have more to say with regard to (ii) in the context of the post pancaking behaviour (Section 2.3) but it is informative to apply a quantitative analysis of the last point which will allow us to compare the two approximations directly. The two calculations agree for highly eccentric objects given similar initial conditions. This is what we would expect since at a given overdensity the flat ellipsoids contain little mass and the surrounding underdense region has approximately background density. As sphericity is approached, more mass is enclosed in the ellipsoid and the underdense region deviates further from the uniform background.

As WS found, when compared with the collapse of isolated ellipsoids, the effect of the surrounding region is to reduce the deceleration of the shortest axis and to increase the deceleration of the longest axis. In other words, the growth of asphericity is reduced. At a given overdensity our tidal forces are generally smaller than those of WS, particularly for objects which are not very flat. The net result is that fairly round objects form caustic surfaces at earlier epochs with our approximation. This result, and indeed that of WS, is not quite trivial, as the smaller deceleration of the longest axis in our approximation slows the increase of density of the ellipsoid, counteracting somewhat the reduced tidal support. However, with knowledge of WS's results and those of Lin et al., we can predict that our objects will collapse faster than those of WS, since they believe they are in a lower-density universe.

As a result of the different treatment of the tidal field, the approximate expressions given by WS for the velocity field at collapse are no longer very accurate, par ticularly for objects which are not very eccentric. We find that the middle and long axes behave somewhat differently from each other, in contrast to the rather remarkable result of WS. Accurate expressions can be obtained for our approximation at the cost of some complication. The expressions below are, however, accurate for a very wide range of shapes

$$1-H_1/H_{(p)} = 0.66\,\Omega_{(p)}^{0.55}\{s_1(a_1/a_3-1)\}^{-1.13} \quad s_1=1+10a_3^{3.5}(a_1-a_3)$$

$$1-H_2/H_{(p)} = 1.11\,\Omega_{(p)}^{0.55}\{s_2(a_2/a_3-1)\}^{-1.24} \quad s_2=1+10a_3^{3.5}(a_2-a_3) \quad (2.10)$$

where $H_j \equiv (1/a_j)da_j/dt$ and $H_{(p)}$ and $\Omega_{(p)}$ are the Hubble parameter and density parameter at the formation of the caustic surface. These are accurate to $0.2H_{(p)}$ for all ellipsoids with $a_{3(i)} < 0.9$ provided the axes are not collapsing too fast $\{|H_j| < H_{(p)}\}$. As we might expect, the approximations break down for the most spherical objects.

The essential results are that the ellipsoids collapse earlier and the pancakes expand faster than those of WS. As expected, for highly eccentric objects ($s \to 1$) our velocity expressions agree reasonably with WS's approximate results.

2.3 Post-pancaking evolution

2.3.1 THE EQUATIONS OF MOTION

We now continue the evolution of the collapsed ellipsoids further. Assuming the caustic surface to remain thin (see Section 2.1), we may investigate further behaviour in a similar way to the method of Section 2.2. The elliptical pancake formed, with principal axes $a_{1(p)}$ and $a_{2(p)}$, is the limiting case of a highly flattened ellipsoid and, given the dissipation of motions perpendicular to the plane, has surface density

$$\sigma_{(p)}(x,y)=\tilde{\sigma}_{(p)}\{1-x^2/a_{1(p)}^2-y^2/a_{2(p)}^2\}^{1/2} \quad (2.11)$$

where conservation of mass implies that

$$\tilde{\sigma}_{(i)}=2a_{2(i)}a_{3(i)}\{1+\delta_{(i)}\}\rho_{b(i)}/\{a_{1(p)}a_{2(p)}\} \quad (2.12)$$

The pancake axial ratio and velocities along with (2.11) constitute the initial conditions for the post-pancaking evolution. The equation of motion is determined by the gravitational field of the elliptical pancake and the background matter. The gravitational potential of an elliptical surface with surface density of the form (2.11) is given in

the plane by

$$\Phi(x,y)= \frac{\pi^2 G\tilde{\sigma}}{4a_1} \{ A(e)x^2+ B(e)y^2\} \qquad (2.13)$$

with

$$A(e)= \frac{2(1-e^2)^{1/2}}{e^2}\{ F(1/2,1/2;1;e^2) - F(-1/2,1/2;1;e^2) \}$$

$$B(e)= \frac{2}{(1-e^2)^{1/2}e^2}\{ F(-1/2,1/2;1;e^2) - F(1/2,1/2;1;e^2)(1-e^2)\}$$

$$e^2=1-a_2^2/a_1^2 \qquad (2.14)$$

and F(a,b;c;z) the hypergeometric function (Abramowitz & Stegun 1968). To this we add the potential of the uniform background matter, as in Section 2.2, to obtain

$$\Phi(x,y)= \frac{\pi^2 G\tilde{\sigma}}{4a_1} \{A(e)x^2+ B(e)y^2\} + 2/3\pi G\rho_s(x^2+y^2) \qquad (2.15)$$

Since the potential is quadratic in x and y, the surface density of the ellipse maintains its form:

$$\sigma(x,y,t)=\tilde{\sigma}(t)(1-x^2/a_1^2 - y^2/a_2^2)^{1/2} \qquad (2.16)$$

where $a_1(t)=a_{1(p)}X(t)$, $a_2(t)=a_{2(p)}Y(t)$ and $\tilde{\sigma}=\tilde{\sigma}_{(p)}/XY$ with X and Y evolving according to

$$\frac{d^2X}{dt^2} = \frac{-\pi^2 G\tilde{\sigma}_{(p)}A(e)}{2a_{1(p)}XY} - \frac{4\pi}{3} G\rho_s(t)X$$

$$\frac{d^2Y}{dt^2} = \frac{-\pi^2 G\tilde{\sigma}_{(p)}B(e)}{2a_{1(p)}X^2} - \frac{4\pi}{3} G\rho_s(t)Y \qquad (2.17)$$

given the initial conditions X=Y=1, $dX/dt=H_{1(p)}$, $H_{2(p)}=dY/dt$. If we let $T=H_0t$ and define the elongation parameter

$$\Delta \equiv 1-a_2/a_1= 1-(Y/X)a_{2(p)}/a_{1(p)} \qquad (2.18)$$

then we have

$$\frac{d^2X}{dT^2} = - \frac{\Omega_0}{2}\left[FX(1+z)^3+ \frac{S\ A(e)}{X^2(1-\Delta)}\{1+z_{(p)}\}^3 \right]$$

$$\frac{d^2\Delta}{dT^2} = \frac{\Omega_0}{2}\left[\frac{S\{1+z_{(p)}\}^3}{X^3}\{B(e) - A(e)\}\right] - \frac{2}{X}\frac{dX}{dT}\frac{d\Delta}{dT} \qquad (2.19)$$

where

$$F \equiv 1-a_{2(i)}a_{3(i)}\{1+\delta_{(i)}\}$$

and

$$S \equiv \frac{3\pi a_{2(i)}a_{3(i)}}{4a_{1(p)}^3}\left[\frac{1+z_{(i)}}{1+z_{(p)}}\right]^3\{1+\delta_{(i)}\} \qquad (2.20)$$

measures the relative importance of the disc gravitational field to that of the background matter at pancaking. Converting to independent variable z as before (equation 2.7) we can integrate this pair of equations using series expansions for A and B. In the later stages of collapse,

$$\epsilon = 1-e^2 \ll 1,$$

we can use the asymptotic expansions

$$A(e)\rightarrow\frac{2}{\pi e^2}\epsilon^{1/2}\left[\ln 16 - 2 - \frac{(1+e^2)}{e}\ln\epsilon\right] \; ; \; B(e)\rightarrow\frac{2}{\pi\epsilon e^2}\left[1+e^2 - \frac{\epsilon\ln\epsilon}{2} - \frac{\epsilon\ln 16}{2}\right] \qquad (2.21)$$

(Abramowitz & Stegun 1968). As will be apparent from (2.19), the ellipse increases its eccentricity with time. The minor axis may then reach zero in a finite time, and a filament will be formed. Whether this happens or not depends on the shape of the pancake, its density and expansion velocities at formation. In low-density universes ($\Omega_0<1$), it is possible for the ellipse to expand asymptotically at constant velocities in both of its principal directions.

2.3.2 RESULTS

For a given value of Ω_0 and pancake collapse redshift, the evolution is described entirely by the axial ratios $(a_2/a_1)_{(i)}$ and $(a_3/a_1)_{(i)}$. The evolution of the three axes is shown in some

representative cases in Fig.(2.2). Essentially three types of behaviour are possible:

(i) The middle axis collapses before the present epoch, while the long axis is still contracting.

(ii) The middle axis collapses before the present epoch, while the long axis is still expanding.

(iii) The pancake has not collapsed to a filament by the present epoch.

In the third case, corresponding to highly flattened ellipsoids, the pancake may exist for a long time. Indeed, in a low density universe, the pancake may undergo asymptotic undecelerated expansion, never forming a filament. In other cases, the eccentricity increases with time until the middle axis collapses, and a filament is formed. In the absence of further dissipation (i.e. if all matter fragments into collisionless galaxies at pancaking), the filament will not remain thin, but possibly relax into a cigar shape. We make a crude distinction between those filaments which are still expanding along the long axis when the middle axis collapses, and those which are contracting. We assume that the latter relax into more isotropic configurations, which we shall describe as 'clusters' for the purposes of discussion. The former we assume will remain as filaments, although some will be bound and some unbound.

It is convenient to display the results for different initial axial ratios on a triangular diagram, as shown in Figs (2.3,2.4,2.5). A point on this diagram represents one particular shape of ellipsoid characterised by the two coordinates $(a_2/a_1)_{(i)}$ and $(a_3/a_1)_{(i)}$. The apex represents spheres, the right hand side oblate spheroids, and the diagonal prolate spheroids. The figures show the divisions between clusters, filaments and pancakes (characterising the three cases above) for different initial shapes and background densities. This begs the question 'What is a typical initial shape ?' This has been tackled by Peacock & Heavens (1985), hereafter PH, who analysed Gaussian random density perturbations to obtain shapes of primordial maxima. If we compare Figs. 2.3 and 2.5 with their Fig. 3, we see that, for a given overdensity, more structures survive as pancakes in a low-density universe than in a high-density universe.

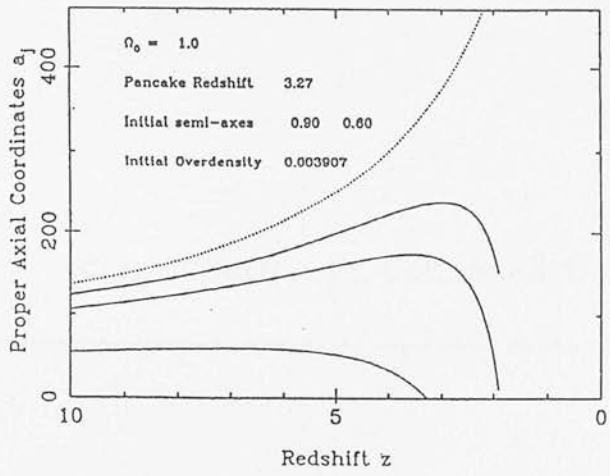

(i)

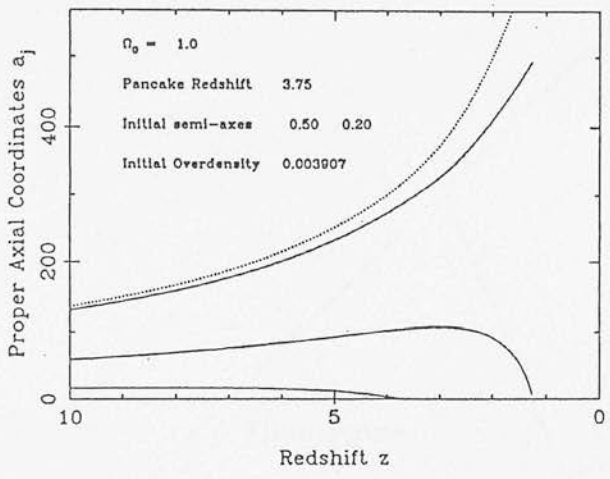

(ii)

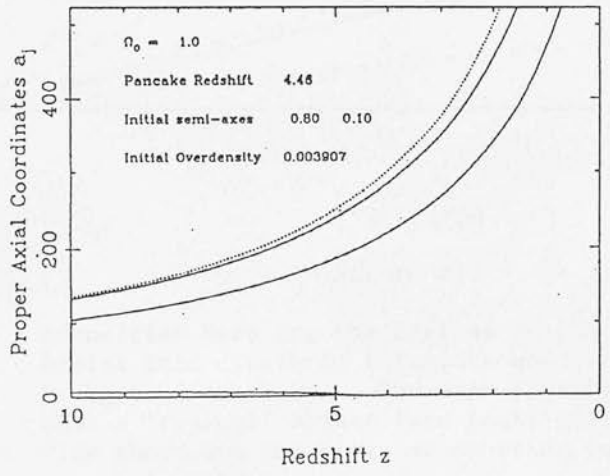

(iii)

Figure 2.2 We illustrate the behaviour of the ellipsoid axes through pancaking identifying three cases: (i) Clusters - the long axis is contracting when the middle axis collapses (ii) Filaments - the long axis is expanding when the middle axis collapses. (iii) Pancakes - the major axes have not collapsed by the present.

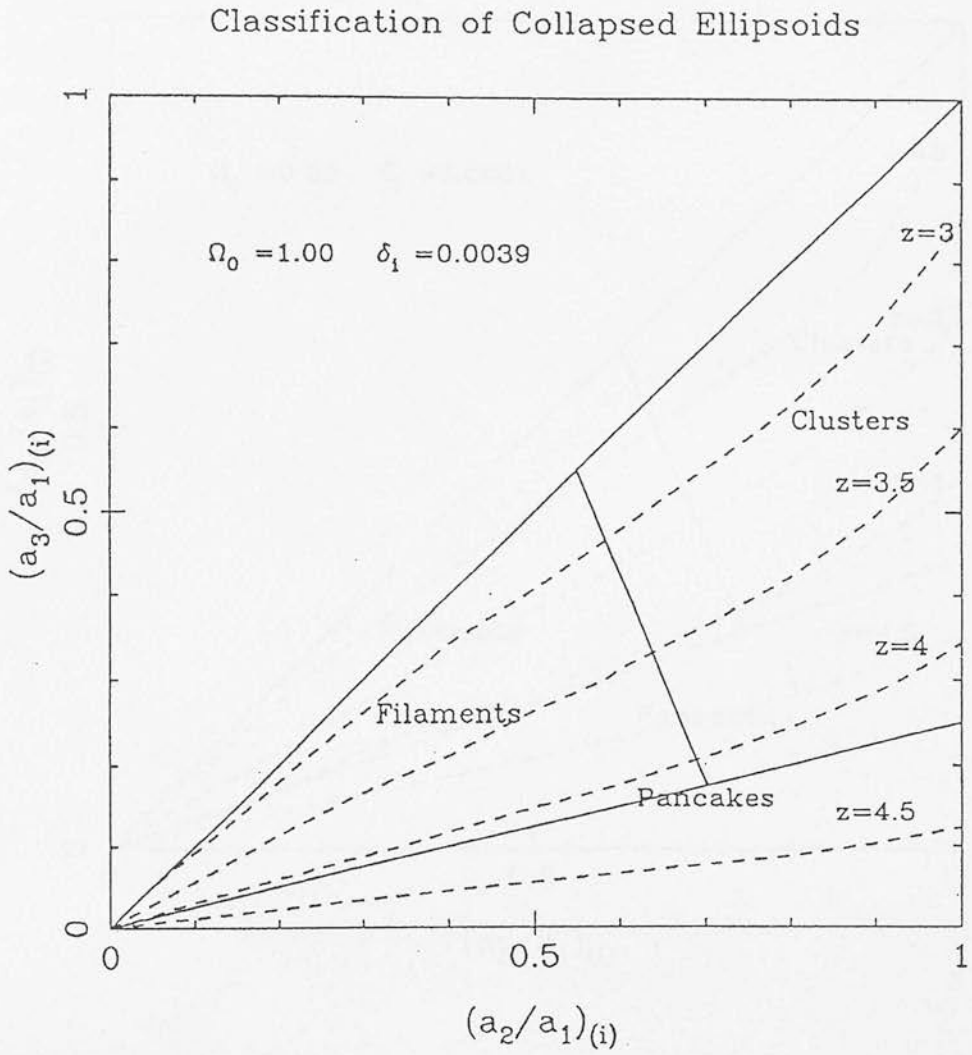

Figure 2.3

Figures 2.3-2.5 Identified here are the regions in the initial shape plane which evolve into clusters, filaments and pancakes for different background densities. The over density $\delta\rho/\rho$ is chosen so that a 'typical' object (see text) collapses at redshift 3. Also shown are the lines of constant collapse redshift.

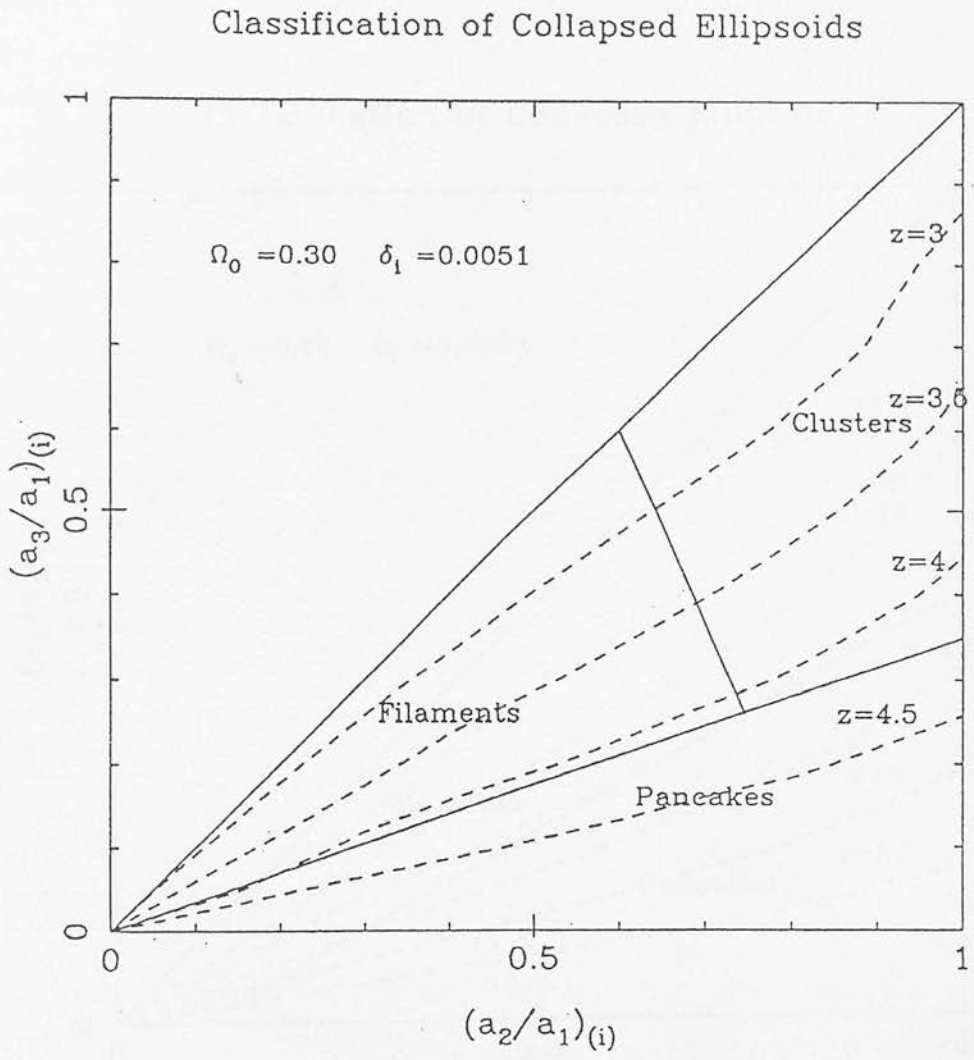
Classification of Collapsed Ellipsoids
Ω_0 =0.30 δ_1 =0.0051
z=3
z=3.5
Clusters
z=4
z=4.5
Filaments
Pancakes
$(a_3/a_1)_{(i)}$
$(a_2/a_1)_{(i)}$
0
0.5
1

Figure 2.4

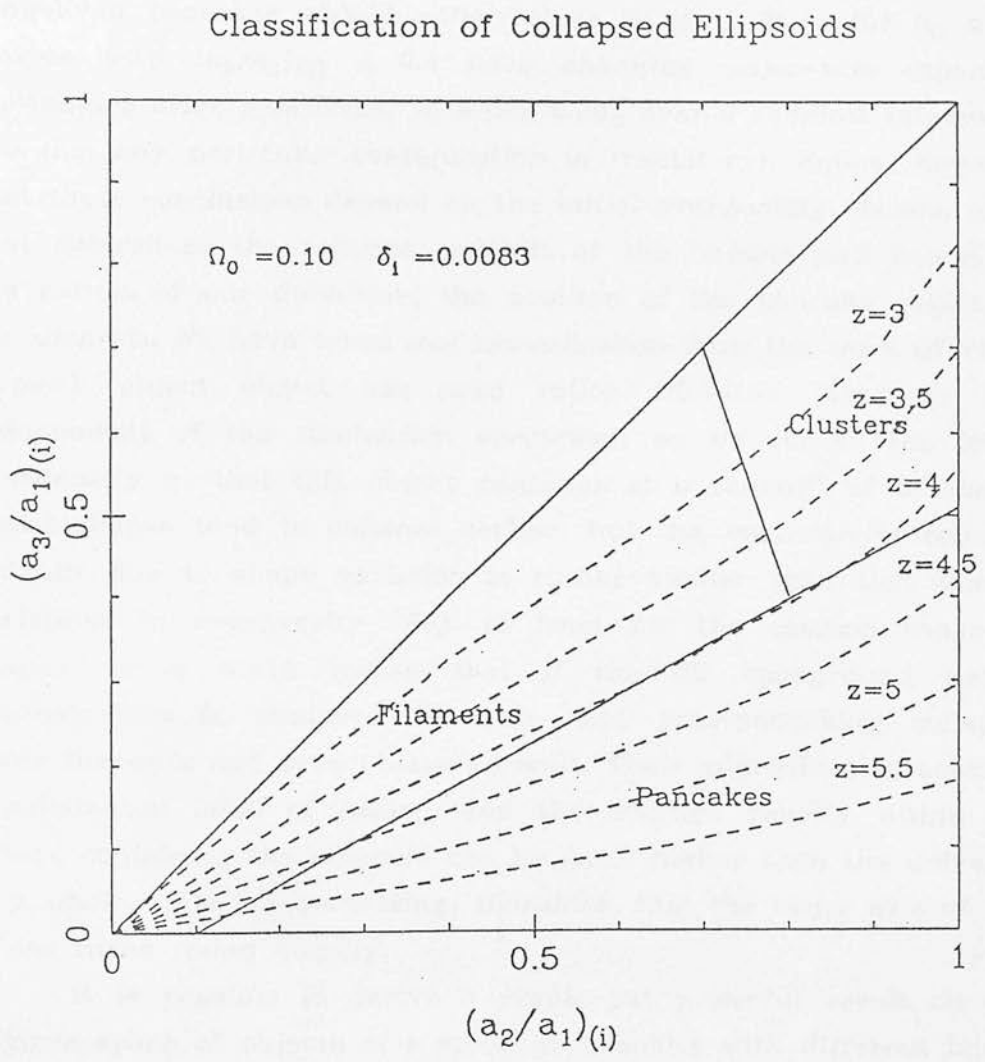
Classification of Collapsed Ellipsoids
Ω_0 =0.10 δ_1 =0.0083
z=3
z=3,5
Clusters
z=4
z=4.5
z=5
z=5.5
Filaments
Pancakes
$(a_3/a_1)_{(i)}$
$(a_2/a_1)_{(i)}$
0
0.5
1

Figure 2.5

This fits in with result (ii) of the pre-pancaking evolution since earlier deviation from self similar evolution is more likely to lead to collapse of the minor axis, leaving two expanding axes. The most interesting result of such a comparison is the extreme rarity of objects which are expected to persist indefinitely as pancakes. There are very few local density maxima with $(a_3/a_2)_{(i)} \leqslant 0.4$ in the work of PH (a result which is insensitive to the precise details of the perturbation spectrum). We see from Figs.(2.3,2.4,2.5) that virtually no long-lived pancakes should exist unless $\Omega_0 \leqslant 1$. Even for $\Omega_0 = 0.1$ maxima with $(a_3/a_2)_{(i)} \leqslant 0.4$ have changing major-axis expansion parameters after pancaking, of order $0.2H_0$ over a redshift interval of $2 \rightarrow 0$ (i.e. any particular configuration is transitory). Notice, however, that these conclusions depend on the initial overdensity chosen, since that determines the collapse redshift of the objects and hence, by the nature of our definition, the position of the pancake region on the diagram. We have taken our normalisation from the work of PH. A 'typical' object object has axial ratios 1:0.7:0.55 (more or less independent of the fluctuation spectrum), so we choose the initial overdensity so that this object pancakes at a redshift of 3. Flatter initial shapes tend to collapse earlier, but the variation in collapse redshift due to shape variation is rather smaller than that due to variations in overdensity (PH), at least for the common range of shapes. It is worth noting that if the WS background matter approximation is employed for pre- and post-pancaking collapse, fewer filaments and more clusters result. Their approximation assumes a substantial infall of matter, and the average density within the sphere containing the ellipsoid can be much higher than the universe as a whole. It is not surprising, therefore, that the major axis of the ellipse turns round quickly.

It is possible to derive a simple yet powerful result on the collapse epoch of objects of a given overdensity with different initial shapes. In the spherical model for collapse in a flat universe (see e.g. Zel'dovich & Novikov 1983) pancaking occurs when the linear theory predicts that the overdensity $\delta_{lin} = 1.69$ where

$$\delta_{lin} = \delta_{(i)} \frac{\{1+z_{(i)}\}}{\{1+z_{(p)}\}} \qquad (2.22)$$

If we put $\delta_{(i)} = 0.0039$ (see Fig.2.3) and $z_{(i)}=1500$ this gives the

* INSERT:

For an oblate spheroid with infinitessimally small minor axis a_3 the equation of motion is (see 2.6):

$$\frac{d^2a_3}{dt^2} = -2\pi G\rho_o(t)[2(1+\delta(t))-4/3]\, a_3$$

The density outside a highly flattened spheroid follows the background $\rho_o(t) = \rho_i\ (t/t_i)^{-2}$ and the major axis follows the Hubble expansion, $a_1(t) = a_i\ (t/t_i)^{2/3}$. The conservation of mass then implies that

$$1 + \delta(t) = (1 + \delta_i)\ \frac{a_{3i}}{a_3(t)}\ (t/t_i)^{2/3}$$

For $\Omega_o = 1$, $6\pi G\rho_i t_i^2 = 1$, and we can rewrite the equation of motion as

$$\frac{d^2a_3}{dt^2} - \frac{4a_3}{9t^2} = -\frac{2(1+\delta_i)}{3t^2}\ a_{3i}\ (t/t_i)^{2/3}$$

which gives

$$a_3(t) = a_{3i}\ (1 + \delta_i)\ (t/t_i)^{2/3} - \delta_i\ a_{3i}\ (t/t_i)^{4/3}$$

so a_3 reaches zero at t_c given by

$$(t_c/t_i)^{2/3} = \frac{1 + \delta_i}{\delta_i} \simeq \frac{1}{\delta_i}$$

i.e. at $1 + z_c = \delta_i\ (1 + z_i)$. Inspection of equation 2.22 indicates that linear theory predicts $\delta = 1$ at this epoch. This is in agreement with the collapse epochs of highly flattened objects shown in Figs. 2.3, 2.4 and 2.5.

collapse redshift of a spherical object to be 2.47 which gives a consistent limit on our numerical calculations. The fact that the constant collapse redshift lines, or equivalently constant δ_{lin} lines are approximately straight allows us to find an approximate relation between δ_{lin} and $(a_2/a_3)_{(i)}$. It is a good approximation to say that collapse occurs when linear theory predicts that

$$\delta_{lin} = 1 + 0.6(a_3/a_2)_{(i)} \qquad (2.23)$$

i.e. at

$$1 + z = \delta_{(i)}\{ 1+z_{(i)}\}/\{ 1+0.6a_{3(i)}/a_{3(i)}\} \qquad (2.24)$$

This result is valid for a wide range of initial shapes and overdensities. The lower limit $a_{3(i)}\rightarrow 0$, giving $\delta_{lin} = 1$, which implies that instantaneous pancaking does not occur, is entirely consistent with an analytic solution of the acceleration equation (2.8) for an oblate spheroid with infinitesimally small minor axis, and represents the fact that as we flatten the object at a given overdensity less matter is driving the collapse.

2.4 Discussion

2.4.1 COLLAPSE TO FILAMENTS

In this chapter, we have extended the work of Lin et al. (1965) and White & Silk (1979) on the gravitational collapse of homogeneous triaxial ellipsoids. Including the effect of background matter in an idealised manner, we find that (assuming the caustic surface, formed during the collapse, remains thin), the anisotropic collapse continues after pancake formation, increasing the eccentricity of the pancake with time. This is partly effected by the anisotropic gravitational field in the plane of the non-circular pancake, but is principally due to the fact that the anisotropic collapse prior to the formation of a pancake imparts an anisotropic velocity field to the pancake. The short axis expands less quickly (if indeed it expands at all) than the long, and collapses prior to the long axis.

In many cases, then, the anisotropic collapse of the pancake in its plane leads to the formation of a filament, which may be expanding or contracting along its axis. For highly flattened ellipsoids, however, the resulting pancake may persist for a long time. In a low-density universe the pancake may asymptotically expand undecelerated and never undergo secondary collapse in its plane to a filament. On fragmentation we might expect a sheet-like distribution of galaxies with approximately Hubble velocity expansion in the plane.

The secondary collapse of a pancake to a filament may result in further fragmentation of some of the gas which did not fragment before. Galaxies formed at pancaking may be regarded as collisionless, and will not be confined to a thin line. The galaxy distribution around a filament may therefore be expected to be closer to a cigar shape than to a one-dimensional structure.

In summary, the types of objects expected given the possibility of secondary collapse are filaments, pancakes and more isotropic 'clusters', depending on the initial ellipsoid axial ratios. Filaments do not correspond to a degenerate case, as in existing pancake theories, but arise naturally after pancake formation.

2.4.2 THE LOCAL SUPERCLUSTER

The general features of the pre-pancaking collapse (i.e. production of highly flattened structures with velocities in the plane retarded with respect to the Hubble flow), provide an interesting comparison with the observations of superclusters in general (see Oort 1983) and in particular those of the Local Supercluster (LS; see e.g. Tully 1982). There are two possible explanations for the LS observations as mentioned by WS: first, that we are simply observing the LS near pancaking in a small scale damping picture with galaxies forming prior to superclusters, or secondly, that it represents an object which collapsed whilst still gaseous at some earlier epoch. In principle, observation of the velocities normal to the plane can distinguish these two cases as the dissipative formation will result in low values. We can now discuss these descriptions in more detail. The observed flattening and velocity behaviour reported by Tully can be reproduced in two ways :

(1) The initial structure was highly eccentric:

$$(a_3/a_1)_{(i)} \cong 1/8 \qquad \Omega_0 = 1.0$$
$$(a_3/a_1)_{(i)} \cong 1/4 \qquad \Omega_0 = 0.2 \qquad (2.25)$$

which collapse quite early ($z>4$ for our normalisation). As discussed earlier these are unusual objects, particularly on the $\Omega_0 = 1$ case. If any of these objects exist, our post pancaking calculations show that their major-axis velocity variation will be slow and so Tully's observed 27% deviation from pure Hubble flow in the LS plane does not put tight constraints on the LS collapse epoch.

(2) If we restrict ourselves to shapes of objects which are common in the work of PH we find that, given our normalisation, even in a low-density universe ($\Omega_0 = 0.1$) very few objects will not have undergone secondary collapse by the present. These statements are, however, valid for one normalisation (i.e. one initial overdensity). Varying the overdensity will affect which shapes remain as pancakes at the present and their major-axis velocities. We can set a limit on the collapse redshift for the LS in different background universes by considering the present major axis velocity for ellipsoids with a_2:a_3 of order 1:0.4, representing the limit of common objects (PH Fig.3). Objects flatter than this occur with a probability of 0.07 (PH Fig.4). Requiring the expansion in the plane to be 0.73 H_0 at $z=0$ gives the following limits:

$$\Omega_0 = 0.1 \qquad z_{(p)}<3.31$$
$$\Omega_0 = 0.3 \qquad z_{(p)}<0.61 \qquad (2.26)$$

Earlier collapse will result in velocities in the pancake plane smaller than those observed in the LS. For shapes of order 1:0.5 which may occur reasonably often (12 per cent) we obtain

$$\Omega_0 = 0.1 \qquad z_{(p)}<1.46$$
$$\Omega_0 = 0.3 \qquad z_{(p)}<0.10 \qquad (2.27)$$

We use inequalities here since, for later collapse epochs there will be some (common) initial shapes with $a_3 \gtrsim 0.5$ which have $H_1=0.73H_0$. For $\Omega_0=1.0$ we cannot model the LS field with the above structures, requiring a more eccentric and hence unusual initial perturbation. If we choose the overdensity so that our model of the LS collapses at $z=0$, which corresponds to the least eccentric possible initial structure, we require minor to major axis ratio of 0.36 which has about 5% chance of occuring. This agrees with the WS result that for $\Omega_0=1$ a viable model requires $(a_3/a_1)<1/3$ and demonstrates that the effect of using different background assumptions is not drastic for flat structures.

We see then that, for the higher density universes, LS collapse must have occurred recently and so a hierarchical clustering picture is favoured, whereas in low-density universes it is possible to reconcile the LS velocity behaviour with a pancake picture in which galaxies form later. There are of course ways to avoid this and allow $\Omega_0=1$. The most obvious solutions are to appeal to non-Gaussian initial conditions or to a non-zero cosmological constant. If this seems distastefully *ad hoc*, there remains the possibility of a more complex tidal field than the one we have considered. Allowance for the effects of discrete nearby clusters may relax the above limits somewhat. In the context of this work, however, the LS must have grown from an exceptionally flat perturbation, if $\Omega_0=1$ and the initial perturbations were Gaussian.

Chapter 3

Explosions in pancake models of galaxy formation

3.1 Introduction

Let us briefly recap points made in Chapter 1 which are of direct relevance here. In galaxy formation models involving large scale damping (e.g. adiabatic fluctuations in massive neutrino-dominated universes) large clouds are the first to collapse. Material falling in forms a pair of stand-off shocks, enclosing a dense central layer. Because of the high density, the layer can cool and fragment into galaxies or sub-galactic systems (Sunyaev & Zel'dovich 1972). Such models provide a good explanation for the large scale (~ tens of Mpc) clustering of galaxy clusters and recent observations of streaming motions (Collins et al. 1985, Lynden-Bell et al. 1988).

There are however several problems with the standard picture: if galaxies inhabit only the pancake planes, the high clustering strength seen in N-body simulations implies a very recent formation epoch z~1 (White et al 1983), which is inconsistent with observations of galaxies with old stellar populations at high redshift; there is some evidence for processed material in the voids (Brosch & Gondhalekar 1984) which has no obvious origin; analysis of observations of the Local Supercluster (Tully 1986) indicate clouds of galaxies away from the principal plane defined by the Virgo cluster.

Doroshkevich (1984) mentions the possibility that clump formation in the cooling gas in the dense central layer and the subsequent formation of stars would release energy which would not only affect the pancake internal structure but induce flows and irregularities in the baryonic material falling in towards the pancake. This is an important hydrodynamical process which has not yet been incorporated into N-body simulation work.

In this work, we investigate the consequences of Doroshkevich's conjecture. For sufficiently large energy release, a blast wave travels out of the central layer, influencing the state of the baryonic material as it falls in. In particular we investigate whether any of the shocked gas can cool before the present epoch, leading to formation of galaxies *outside* the pancake plane, in regions normally

expected to be voids. This would help alleviate the clustering problem and provide explanations for the processed gas in voids and Tully's clouds.

The calculation is performed using a fluid-in-cell numerical scheme running on an axisymmetric grid with initial conditions set up on the basis of the Zel'dovich approximation (see section 3.2). We instantaneously release energy ϵ (in units 10^{54} J) at the redshift z_c when the dense central layer is formed. The energy is assumed to be released in the manner proposed by Ostriker & Cowie (1981) and Ikeuchi (1981) i.e. by the cumulative effect of supernovae. It thus suffers from the same weaknesses as the explosion model, except that here we have a well-defined population of seeds.

If cooling of the baryonic material shocked by the blast wave is possible before it falls into the central layer we check that the fragments produced do not immediately collapse into the dense pancake. There are two principal observational constraints, arising from the presence of shocked, high temperature, gas in the voids. The process must not produce too much X-ray emission, nor must it produce excessive fluctuations in the microwave background intensity via the Sunyaev-Zel'dovich effect. We use these observations to constrain the magnitude of the explosions and the epoch at which they are introduced. (Section 3.4)

3.2 The Model

We will follow the evolution of a density fluctuation on a given comoving scale in the fluid approximation The basic equations of inviscid flow are solved on an axisymmetric space grid using a robust, cpu- and storage-economical Eulerian difference scheme called FLIC which uses a time-splitting solution technique and includes artificial viscosity (for details see Gentry et al (1966)).

We are grateful to Dr. M. J. Wilson at Leeds University for providing us with the basic code which we have modified in two ways; we solve the fluid equations in comoving coordinates using transformations given by Shandarin (1980); secondly we use a logarithmic spacing away from the pancake plane to give us high resolution where the most rapid evolution is occurring. For speed

considerations we have adapted the code to run on a 64x64 distributed array processor, initially at the University of Edinburgh and latterly at Queen Mary College. This adaptation resulted in a factor of about 60 improvement in speed over the VAX 11/780, giving us a relatively fast method of modelling cosmological hydrodynamics.

We are concerned with modelling the collapse of massive clouds resulting from the damping of neutrino fluctuations by free streaming. The Zel'dovich (1970) approximation for the growth of such perturbations, which is exact for one-dimensional fluctuations, has been shown to be a good first order description of 3-d behaviour by Shapiro et al. (1983). To set up the initial conditions for collapse we adopt this Zel'dovich description imposing a plane wave perturbation of scale 13.8 $(\Omega_0 h^2)^{-1}$ (see chapter 1) to the matter. The fluid occupying the grid represents the baryon component only. In our simulation, the effect of the massive neutrinos is purely to provide the gravitational acceleration. We ignore the changes to the gravitational field resulting from the disturbed baryon component. As we typically have Ω_b=0.14, Ω_0=1 this omission is not serious. The massive neutrinos are assumed to follow the Zel'dovich approximation. This will be accurate if we are outwith the region near the pancake plane where orbit crossing has taken place. Shapiro and Struck-Marcell have shown that this is confined to the region defined by the stand-off shocks in the baryon component.

3.2.1 EQUATIONS OF FLUID FLOW IN COMOVING COORDINATES

The basic equations of fluid flow (e.g. Landau & Lifshitz 1959), including a gravitational field (see later for calculation), are written in comoving form $\underline{\tilde{x}} = \underline{r} \,/\, a(t)$.

$$\frac{\partial \rho_b}{\partial t} + \frac{3\dot{a}\rho_b}{a} + \frac{1}{a}\nabla.\rho_b\underline{v} = 0$$

$$\ddot{a}\underline{\tilde{x}} + \frac{\partial \underline{v}}{\partial t} + \frac{1}{a}(\underline{v}.\nabla)\underline{v} + \frac{\dot{a}\underline{v}}{a} = -\frac{\nabla P}{a\rho_b} + \underline{f} \qquad (3.1)$$

$$\frac{\partial E}{\partial t} + \frac{1}{a}\nabla.(\underline{v}(E+P)) + \frac{3\dot{a}(E+P)}{a} = \rho_b\underline{v}.(\underline{f}-\ddot{a}\underline{\tilde{x}}) - \frac{\dot{a}\rho_b\underline{v}}{a}$$

where a(t) is the universal scale factor, $\underline{v}$ is the peculiar velocity

and E is the comoving energy density. $\nabla \equiv \partial/\partial\underline{x}$ and subscript b denotes baryon density. Notice that $\underline{f}$ includes the unperturbed gravitational field. Assuming a Friedmann model with negligible pressure

$$\frac{\ddot{a}}{a} = -\frac{4\pi G\rho}{3} \qquad (3.2)$$

we can simplify the equations to include only the peculiar acceleration

$$\underline{F} = \underline{f} + \nabla\Phi \qquad (3.3)$$

The Shandarin (1980) transformation of variables

$$\tilde{\rho} = \rho a^3 \; ; \; \tilde{e} = Ea^5; \; \tilde{P} = Pa^5; \; \underline{\tilde{v}} = a\underline{v} \; ; \; \underline{\tilde{F}} = a^3\underline{F} \; ; \; d\tilde{t} = dt/a^2 \qquad (3.4)$$

with an equation of state $P \propto \rho_b^{\gamma}$ allows us to put the equations into a conservation-law form suitable for use in a finite difference scheme. Remarkably, the resulting equations are identical to the standard equations of fluid dynamics:

$$\frac{\partial}{\partial\tilde{t}} \begin{bmatrix} \tilde{\rho}_b \\ \underline{\tilde{v}} \\ \tilde{e} \end{bmatrix} + \nabla. \begin{bmatrix} \tilde{\rho}_b\underline{\tilde{v}} \\ \underline{\tilde{v}}\;\underline{\tilde{v}} \\ \underline{\tilde{v}}(\tilde{e}+\tilde{P}) \end{bmatrix} = \begin{bmatrix} 0 \\ -\nabla\tilde{P}/\tilde{\rho}_b + \underline{\tilde{F}} \\ \tilde{\rho}_b\underline{\tilde{v}}.\underline{\tilde{F}} \end{bmatrix} \qquad (3.5)$$

We must now consider how the initial conditions are set up.

3.2.2 ZEL'DOVICH APPROXIMATION

If we displace particles initially at comoving position $\underline{q}$ to $\underline{q}-\underline{p}(\underline{q})$ where p is some displacement function then

$$\underline{r} = a(t)\underline{q} - b(t)\underline{p}(\underline{q}) \qquad (3.6)$$

is an approximate solution to the equations of motion if pressure can be neglected. For a one-dimensional perturbation the solution 3.6) is exact if b satisfies

$$\ddot{b}/b = -2\ddot{a}/a \qquad (3.7)$$

where a(t) is the scale factor with redshift dependence $a(z)=(1+z)^{-1}$ and b(z) is given by Zel'dovich(1970)

$$b(z) = (1+\Omega_o z)^{1/2} \int_z^\infty \frac{dz'}{(1+z')^2(1+\Omega_o z')^{3/2}} \qquad (3.8)$$

Ω_o describes the present total mass density. We can calculate the peculiar infall velocity $\underline{v} = \dot{\underline{r}} - (\dot{a}/a)\underline{r}$ and acceleration $\underline{F} = \ddot{\underline{r}} - (\ddot{a}/a)\underline{r}$ directly, and obtain the baryonic density evolution from the mass conservation condition

$$\rho_b d^3\underline{r} = \rho_{bo} d^3\underline{q} \qquad (3.9)$$

Assuming a 1-d sinusoidal perturbation of comoving wavelength $\lambda = 2\pi/k$ along the infall axis

$$p_z(q_z) = B \sin(kq_z) \qquad (3.10)$$

(for neutrino free streaming $\lambda = 13.8\ (\Omega_o h^2)^{-1}$ Mpc e.g. Efstathiou & Silk 1983) and scaling $\mu = q_z/\lambda$ $\mu = [0,1/2]$ then

$$r = a(t)q_z - b(t)B\sin 2\pi\mu \qquad \text{i)}$$

$$v_z = ((\dot{a}/a)b - \dot{b})B\sin 2\pi\mu \qquad \text{ii)}$$

$$F = -1.5\ \ddot{b}\ B \sin 2\pi\mu \qquad \text{iii)} \qquad (3.11)$$

$$\rho_b = \rho_{bo} a^{-3}(1-(b/a)kB\cos 2\pi\mu)^{-1} \qquad \text{iv)}$$

and the radial velocity v_r' is identically zero. B is defined by the epoch of caustic formation, when $\rho \to \infty$ at $\mu = 0$ in a pressure free collapse.

$$B = \lambda a_c/2\pi b_c = \lambda(1+z_c)^{-1}/2\pi b_c \qquad (3.12)$$

It is convenient to transform to dimensionless versions of the Shandarin variables

$$\rho_b' = \tilde{\rho}_b/\rho_o;\ t' = H_o\tilde{t};\ \underline{x}' = \tilde{\underline{x}}/\lambda;\ v_z' = \tilde{v}_z/\lambda H_o;\ F' = \tilde{F}/\lambda H_o^2;\ B' = B/\lambda \qquad 3.13)$$

where H_0 is the Hubble constant to yield

$$
\begin{aligned}
x' &= \mu - \frac{b}{a} B'\sin(2\pi\mu) && \text{i)} \\
v'_z &= \left\{ \frac{\dot{a}b}{a} - \dot{b} \right\} aB'\sin(2\pi\mu)/H_0 && \text{ii)} \\
F' &= -1.5\, B'b\sin(2\pi\mu)\Omega_0 && \text{iii)} \\
\rho'_b &= \frac{\rho_{b0}}{\rho_0}\left(1 - \frac{b}{a} 2\pi B'\cos(2\pi\mu) \right)^{-1} && \text{iv)}
\end{aligned}
\qquad (3.14)
$$

We assume the initial gas temperature was actually set by adiabatic cooling since the last scattering surface at z = 1050 (Jones & Wyse 1985). i.e. it is essentially negligible. More rigorously residual ionisation effects keep the temperature close to the radiation temperature until z=100. This is of no practical importance for our calculation, as the thermal energy is negligible and is soon exceeded by the small thermal energies generated by the finite difference approximation. Defining

$$P' = \rho'_b T' \qquad (3.15)$$

with

$$T' = Ta^2/(\lambda H_0)^2\ (k/\mu m_H) \qquad (3.16)$$

we can complete the setting up of the initial conditions

$$
\begin{aligned}
T' &= 36.0/(\lambda H_0)^2 && \text{i)} \\
P' &= 36.0/(\lambda H_0)^2(1 - (2\pi b/a)B'\cos 2\pi\mu)^{-1} && \text{ii)}
\end{aligned}
\qquad (3.17)
$$

For an ideal gas with adiabatic index γ = 5/3, the internal energy density is 3/2 P and total energy density

$$e' = 1/2\ \rho'_b v'^2_z + 3/2\ P' \qquad (3.18)$$

With this definition and dimensionless time

$$t' = H_0\tilde{t} = (2/\Omega_0)(1 - (1+\Omega_0 z)^{1/2}) \qquad (3.19)$$

the fluid equations retain their conservation law form:

$$\frac{\partial}{\partial t'}\begin{bmatrix} \rho_b' \\ \underline{v}' \\ e' \end{bmatrix} + \nabla.\begin{bmatrix} \rho_b'\underline{v}' \\ \underline{v}'\underline{v}' \\ \underline{v}'(e'+P') \end{bmatrix} = \begin{bmatrix} 0 \\ -\nabla P'/\rho_b' + \underline{F}' \\ \rho_b'\underline{v}'.\underline{F}' \end{bmatrix} \qquad (3.20)$$

where ∇ now represents $\partial/\partial x'$. As mentioned earlier we solve these equations using a modified form of FLIC with a logarithmic spacing along the infall axis which allows us to monitor the rapid fluctuation of density, velocity etc. near the dense central plane. Salient points are outlined in Appendix 1. For a symmetric collapse, the correct lower boundary condition is a rigid wall at $x'=0$. With a logarthmic grid this is of course impossible. We apply a rigid wall at the lower boundary of the grid, typically $x'=10^{-4}$, and measure real vertical distances (for example the pancake thickness) from this point. In general calculation of the initial conditions requires numerical integration for $b(z)$, $\dot{b}(z)$ but for $\Omega_o = 1$ exact solutions can be found:

$$b(z) = \frac{2}{5}(1+z)^{-2} \quad ; \qquad \dot{b}(z) = \frac{4}{5} H_o (1+z)^{-1/2} \qquad (3.21)$$

and equations 3.14) become :

$$x' = \mu - \frac{1}{2\pi}\frac{(1+z_c)}{(1+z)}\sin 2\pi\mu \qquad \text{(i)}$$

$$v_z' = -\frac{1}{2\pi}\frac{(1+z_c)}{(1+z)^{3/2}}\sin 2\pi\mu \qquad \text{(ii)}$$

$$F' = -\frac{3}{4\pi}\frac{(1+z_c)}{(1+z)^2}\sin 2\pi\mu \qquad \text{(iii)} \qquad (3.22)$$

$$\rho_b' = \left[1 - \frac{(1+z_c)}{(1+z)}\cos 2\pi\mu\right]^{-1} \qquad \text{(iv)}$$

As discussed earlier the peculiar acceleration produced by the dynamically dominant neutrinos is obtained from the Zel'dovich solution 3.14iii) or 3.22iii) which accurately specifies their effect outside the central plane.

3.2.3 POST COLLAPSE CONSIDERATIONS

At the collapse redshift z_c pressure effects cause a hot, dense shocked central layer to form, bounded by a pair of stand-off shocks which move slowly away from the central plane (Sunyaev & Zel'dovich 1972). The high density of the shocked material allows rapid enough cooling for fragmentation to occur (Shapiro & Struck-Marcell 1985). Here we consider the consequences of one of the fragments releasing some energy into the surrounding gas, in the manner proposed by Ikeuchi (1981) and Ostriker & Cowie (1981). One mechanism they propose is an initial burst of star formation, leading to a burst of supernova activity.

The energy input ϵ (in units of 10^{54}J), is implemented as an instantaneous increase in thermal energy only for the central grid cells. This is reasonable: Spinrad et al. (1972) have observed colour gradients on galactic core scalelengths for which the free-fall time, indicating the star formation timescale for an ellipsoidal component, is 10^6yr, considerably smaller than the pancake free-fall time; Bookbinder et al. (1980) estimate from theoretical calculations of supernova metal production and observation of galaxy metal content that 10^{54} J of energy may have been emitted in a short-lived early phase of galaxy evolution. We employ a Gaussian weighting function to the energy variable $\hat{e}$ (for a definition see Appendix 1) to avoid the problems an energy spike would cause in the numerical scheme. This results in a shock wave, which, provided it can leave the dense central layer, propagates down the density gradient away from the plane. We discuss the validity of this assumption in section 3.4 on the basis of our results for pancake thickness.

Our prime aim is to investigate whether any of the gas shocked by the blast wave *outside* the central layer may cool before it falls into the central plane. If this does occur, we may expect to form objects outside the (very thin) pancakes formed by neutrino collapse. Obviously the blast wave will also affect material in the pancake plane; we shall address this later.

For this process to be important, the cooled gas must not fall back into the pancake on a timescale less than the cooling timescale, and the high-temperature shocked gas must not emit too much x-ray radiation to exceed the background constraints. We must also ensure

that any hot gas produced does not cause excessive fluctuations in the microwave background radiation via the Sunyaev-Zel'dovich effect.

As noted earlier we can still employ the Zel'dovich force calculation after the introduction of the explosion even though redistribution of the baryonic material occurs, as it has little effect dynamically in neutrino-dominated models.

3.3 Hydrodynamic results

We can illustrate the general behaviour in models by a series of contour plots showing the density, pressure and temperature evolution. These plots are displayed in Appendix 2. In all models we have chosen $\Omega_0=1$, $h=0.5$ and $\Omega_b=0.14$ to fit the nucleosynthesis constraint, so $\lambda=55.2$ Mpc (see section 1.3). For large explosion energies $\epsilon=10^2$ (for example Figure A2.1) the explosion shock propagates to large scale heights above the central plane, producing a high temperature evacuated bubble at approximately constant pressure. With the high resolution our logarithmic spacing along the infall axis provides, we can also distinguish the stand-off shock, which is planar. When the input energy is lower, $\epsilon=10^{-1.5}$, there is very little radial propagation of energy i.e. the behaviour is essentially one-dimensional (Figure A2.2). It is evident that in this model the volume affected is considerably smaller, the post-shock temperature is lower and the shock falls back into the central plane fairly quickly. The one-dimensional nature of the evolution is displayed more clearly if we plot the contours against grid positions rather than the eulerian coordinates (Figure A2.3). This has important consequences in interpreting the results; we shall return to this later. For reference, in all cases the explosion was input over a 10 cell square region with a gaussian width of 3 cells. We shall refer to this as the 'standard explosion'. The behaviour of the stand-off shock is also well illustrated in Figure A2.3.

We have checked the typical temperatures and pressures generated in the plane shock against the approximate analytical solutions of other authors (for example Bond et al. 1984a),b), Shapiro & Struck-Marcell 1985). This confirms the validity of our calculations

for the post-shock material. We have also found that an excellent fit for the comoving thickness as a function of time is

$$R = 7 \left(\frac{\lambda}{55.2}\right) \left(\frac{\tau-1}{\tau}\right)^{1.5} \text{Mpc} \quad ; \quad \tau = \frac{1+z_c}{1+z} \qquad (3.23)$$

where λ is the comoving wavelength of the collapsing region in Mpc. In the limit as z approaches z_c ($\tau \to 1$) this expression agrees well with the approximate solution used by Szalay et al.(1984)

$$R = 1.3 \left(\frac{\lambda}{10}\right) \left(\tau-1\right)^{1.5} \text{Mpc} \qquad (3.24)$$

which is valid for $\tau < 1.5$. Our fit is accurate at least for τ up to 5.5, the limit to which we have information. At late times the Szalay et al. approximation is not good. We will comment later on the importance of this difference when we look at the predicted microwave fluctuations.

3.4 Constraints on model parameters

3.4.1 ESCAPE FROM THE CENTRAL PLANE

We are in a position now to discuss the validity of our assumption (see 3.2.3) that the shock wave can leave the dense central plane. We must ask how this depends on our model parameters ϵ and z_c. In our simulations we introduce the explosion at the epoch of caustic formation. In reality there will be some delay, as cooling takes place and the putative massive stars go through their life cycles. If this delay is too long, there is a chance that the explosion may not, in fact, leave the high pressure central layer at all. In round terms a blast wave of energy E will reach its maximum propagation radius r_{max} when its internal energy density E/r_{max}^3 drops to the ambient pressure. For escape we require that r_{max} must be larger than the pancake thickness at that time. To study this we use the approximation for the central pressure given by Bond et al. (1984b), which for our pancake size is

$$P = 1.49 \times 10^{52} (1+z)^4 \text{ J Mpc}^{-3} \qquad (3.25)$$

and our fit (equation 3.23) for the pancake thickness. If an object

releases energy at redshift z then the energy required to allow escape from the plane is:

$$E = 5.11 \times 10^{54} \left(\frac{\lambda}{55.2}\right)^3 (1+z)^4 \left(1 - \frac{1+z}{1+z_c}\right)^{4.5} J \quad (3.26)$$

Table 3.1 shows the energy requirement for different collapse redshifts assuming a comoving scalelength 55.2Mpc. Provided the time delay is short, a "typical" galaxy in its early evolution can provide the energy required, though this result is marginal for collapse redshift 7 if the time delay is roughly 10^8 years.

Table 3.1

Time delay = 0.001 x t_H				Time delay = 0.01 x t_H			
z_c	z	τ	E (J)	z_c	z	τ	E (J)
1	0.996	1.002	5.8×10^{43}	1	0.963	1.019	1.3×10^{48}
4	3.963	1.007	6.0×10^{47}	4	3.659	1.073	1.3×10^{52}
7	6.882	1.015	1.1×10^{50}	7	5.983	1.146	1.1×10^{54}

Some work is done in evacuating the central plane so our energy parameter ϵ will thus be αE where α is some efficiency factor for the escape from the pancake plane. We have simply considered a point explosion escaping from the central plane, ignoring the possibility of a more planar shock resulting from the merging of a succession of explosions throughout the pancake. We will have more to say on this topic later.

Having confirmed the validity of our earlier assumption let us now look in detail at the observational constraints on the model parameters (z_c, ϵ).

3.4.2 THE X-RAY BACKGROUND

X-ray measurements in the 3-50 kev band (summarised by Schwartz 1979) and analysis of the HEAO-1 data by Marshall et al (1980) consistently give an observed flux limit 1.8×10^{-9} $Jm^{-2}s^{-1}$. We can calculate the x-ray emission, due to optically-thin bremsstrahlung (Rybicki & Lightman 1979), of a model as a function of redshift and observed frequency. Assuming the structures are distributed on the

surface of spheres at even spacing in comoving distance we calculate the total flux at any frequency using the flux-luminosity relation for the Friedmann model (e.g. Longair 1984, eq^{n} 15.26). This spectrum can be integrated up to give the estimated flux in any waveband and compared to the observational limit given above.

3.4.3 THE SUNYAEV-ZEL'DOVICH EFFECT

The Sunyaev-Zeldovich effect, scattering of the microwave background radiation off high-temperature electrons, can also be used to constrain the model. The best large-angle observational data are from the beam switching experiment of Davies et al. (1987), giving a preliminary measurement of:

$$\Delta T/T = 3.7\times10^{-5}$$
$$\text{on angular scale } 8' \text{ at } \nu=10.7\text{GHz} \qquad (3.27)$$

The small-angle experiments of Uson & Wilkinson (1984) have a 4.5 arcmin beam throw. This is smaller than the angular size of the neutrino pancakes (see below), so we would not expect significant variations on such scales. We can calculate the temperature fluctuation for a given direction through the computational grid as a function of epoch z by using the non-relativistic result of Zel'dovich & Sunyaev (1969). Assuming small energy transfer, valid for $T_e \gg T_{rad}$, and that we are in the Rayleigh-Jeans (RJ) regime $h\nu \ll kT_{rad}$ then

$$\Delta T/T = -2y \qquad (3.28)$$

where the Comptonisation parameter is

$$y = 1.12\times10^{-38} \int n_e \, T_e \, dl \qquad (3.29)$$

along some line of sight dl. We calculate the r.m.s. fluctuation in $\Delta T/T$ for an infinitesimal beam width and widely separated beams. In principle, this can be compared with the Davies et al. result if the finite beam width and beam throw are accounted for. The fluctuation is due to variations in the number of pancakes along different lines of sight and variations in the contribution y_j from a given pancake

as a result of different orientations with respect to the line of sight. By choosing to confront observational constraints on angular scales larger than the scale subtending the comoving pancake length at the collapse redshift, we hope that the lines of sight will be virtually independent. For our model ($h=0.5, \lambda=55.2$Mpc) the angular scale of a pancake at $z \gg 1$ is about 16 arcmin for an Einstein-de-Sitter Universe. To subtend an angle of 8° the objects would have to be placed at redshift 0.07! Assuming objects are placed randomly along the line of sight, so that the total number N is distributed as Poisson with standard deviation $\sqrt{N}$, and calculating the variance in the y_j values assuming random orientations, we can make a crude estimate of the variance in $\Delta T/T$ (see Appendix 3 for details). As we have ignored cooling in the numerical scheme (as we must: Falle et al 1984) and the objects are likely to be spaced more regularly than the random assumption our prediction should be an upper limit on $\Delta T/T$ for our model. A more detailed calculation of the anisotropies to be expected in such an experiment should really be attempted before strong conclusions can be drawn, but for these angular scales, the beams should be sampling the full r.m.s. temperature fluctuation. An important effect in this experiment is the dilution because the beam includes many independent lines of sight. This 'beam smearing' effect is complicated as the number of independent objects contributing to a single beam is a function of redshift. We have not calculated this effect in detail, because, as we shall see, the dT/T limits are sufficiently weak that even a small number of pancakes in the beam renders the dT/T constraint obsolete. The x-ray background provides a much stronger constraint.

3.4.4 COOLING TIMES

Let us turn from a discussion of theoretical and observational constraints on the model parameters to address the key issue of the cooling times for material shocked by the blast wave. We calculate a cooling time on the basis of the Fall & Rees (1985) cooling function for a H,He plasma ($10^4 < T < 10^7$ K) and the Ikeuchi et al (1983) approximation to the Bremsstrahlung cooling rate for $10^7 < T < 10^9$ K. We also employ the Ikeuchi et al. approximation to the Compton cooling rate, important at redshifts ≥ 3. We follow the kinematic

* INSERT:

We find shocked material by locating density peaks on the grid. In order to calculate a cooling time for this gas, we need the temperature, which is derived from the pressure. This has to be done with some care, as the artificial viscosity spreads the shock over a number of cells, so there is a spurious precursor of material with pressure intermediate between the pre- and post-shock values. For the purposes of calculating the cooling times, the pressure throughout the numerical shock transition region is assumed to have the immediate post-shock value.

behaviour of material which cools rapidly as it moves in the force field of the dense central layer. This is a particularly simplified calculation, assuming instantaneous cooling of material at the moment it is shocked, redshift z_s, and the formation of collisionless objects by fragmentation. Obviously we should consider hydrodynamic effects for some period after shocking of the material, which will act to hold up the collapse toward the central plane. In this approximate calculation if the idealised fragment collapses into the central layer before the epoch by which the material it represents has cooled then such material does not provide a suitable source for the creation of a bound object off the pancake plane.

3.5 Constraints results

3.5.1 X-RAY BACKGROUND

We display the results for the predicted x-ray flux and microwave fluctuations in figures 3.1 and 3.3. For the x-ray flux, full line contours represent models (z_c,ϵ) which satisfy the observational constraints. The range of energies ϵ we investigate is consistent with our earlier statement concerning the energy expended by the blast wave in escaping from the plane and the magnitude of the likely release of energy in the early phases of galaxy evolution.

Let us consider the x-ray diagram, figure 3.1, first. The basic result is that as the explosion energy input increases the contributed x-ray flux increases. Referring back to our hydrodynamic results (section 3.3), as ϵ increases a larger volume of material is shocked to temperatures high enough to produce x-ray emission by the bremsstrahlung process. Notice that material contributing x-ray photons may have been shocked both by the blast wave and the plane shock which hits it later on. The turnover above redshift 6 has a fairly simple explanation. For large z_c values the post plane-shock temperature, which is mainly a function of the baryon infall velocity at a given redshift, can reach the limiting temperature $3.5\times10^7(1+z)$K at which 3keV xray luminosity is contributed. The material has fallen in from a greater distance above the central plane and has been accelerated to higher velocities in these early collapse models. So the

Figure 3.1

We plot the observed xray flux for a population of pancakes, distributed evenly in comoving distance out to the collapse epoch, all of which form at redshift z_c and are affected by a given explosion characterised by ϵ (see text for further details).

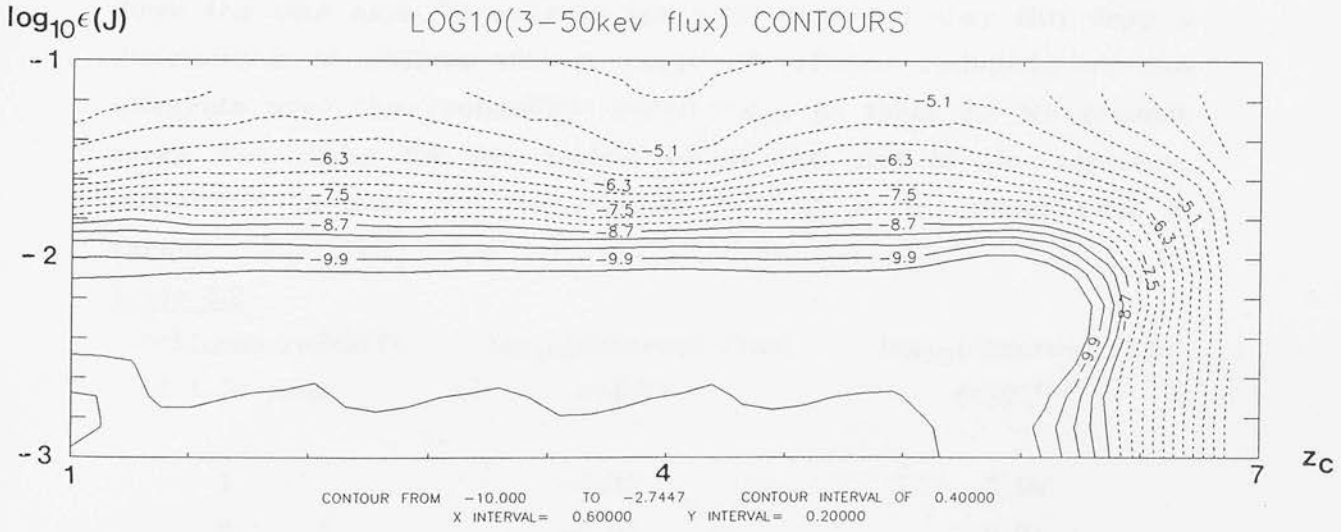

central layer starts dominating the contribution a given pancake makes to the flux, overwhelming the blast wave effect and hence the dependence on ϵ. We can put the following approximate limits on ϵ and z_c.

$$\epsilon < 10^{-1.8} \quad ; z_c < 6.3$$

These could be relaxed somewhat if cooling was considered. Of course our results assume that all objects form at one particular redshift z_c. The x-ray flux contribution from less distant objects is that of pancakes which have evolved considerably since the explosion energy input at z_c. A great deal of work has been done recently on studying the collapse epochs of peaks of varying density contrast in normally distributed density perturbations (Peacock & Heavens 1985, Bardeen et al. 1986). The result for a spectrum similar to the post-recombination spectrum of neutrino perturbations (a Zel'dovich spectrum modified by neutrino free-streaming) is shown in Figure 3.2. The calculation is normalised so that a 1.7σ peak (the mode of the probability distribution) collapses at redshift 2 and it is obvious from the plot that many objects collapse much earlier. As we vary the collapse redshift of a 1.7σ peak the curve translates up and down the time axis. To estimate the total observed x-ray flux from a distribution of objects with a range of collapse redshifts we can integrate over the probability distribution. In table 3.2 we present x-ray flux limits for two models where the size of the explosion introduced is fixed but the collapse redshift of the modal peak is varied.

Table 3.2

Collapse redshift of 1.7σ peak	$\log_{10}$(Observed flux) $\epsilon=10^{-1}$	$\log_{10}$(Observed flux) $\epsilon=10^{-1.5}$
1	-4.43	-5.98
2	-4.54	-6.01
3	-4.48	-5.85
4	-4.25	-5.46

A crucial factor (see Figure 3.1) is obviously how many of the z_c=6.5 and above peaks influence the result. Provided the 1.7σ peak collapses later than redshift 2 or so there are very few objects forming earlier than redshift 7 to contribute to the total flux

Figure 3.2

This shows the probability distribution for the number of peaks forming at any particular epoch. A peak with density contrast 1.7 times the r.m.s density fluctuation collapses at redshift 2.

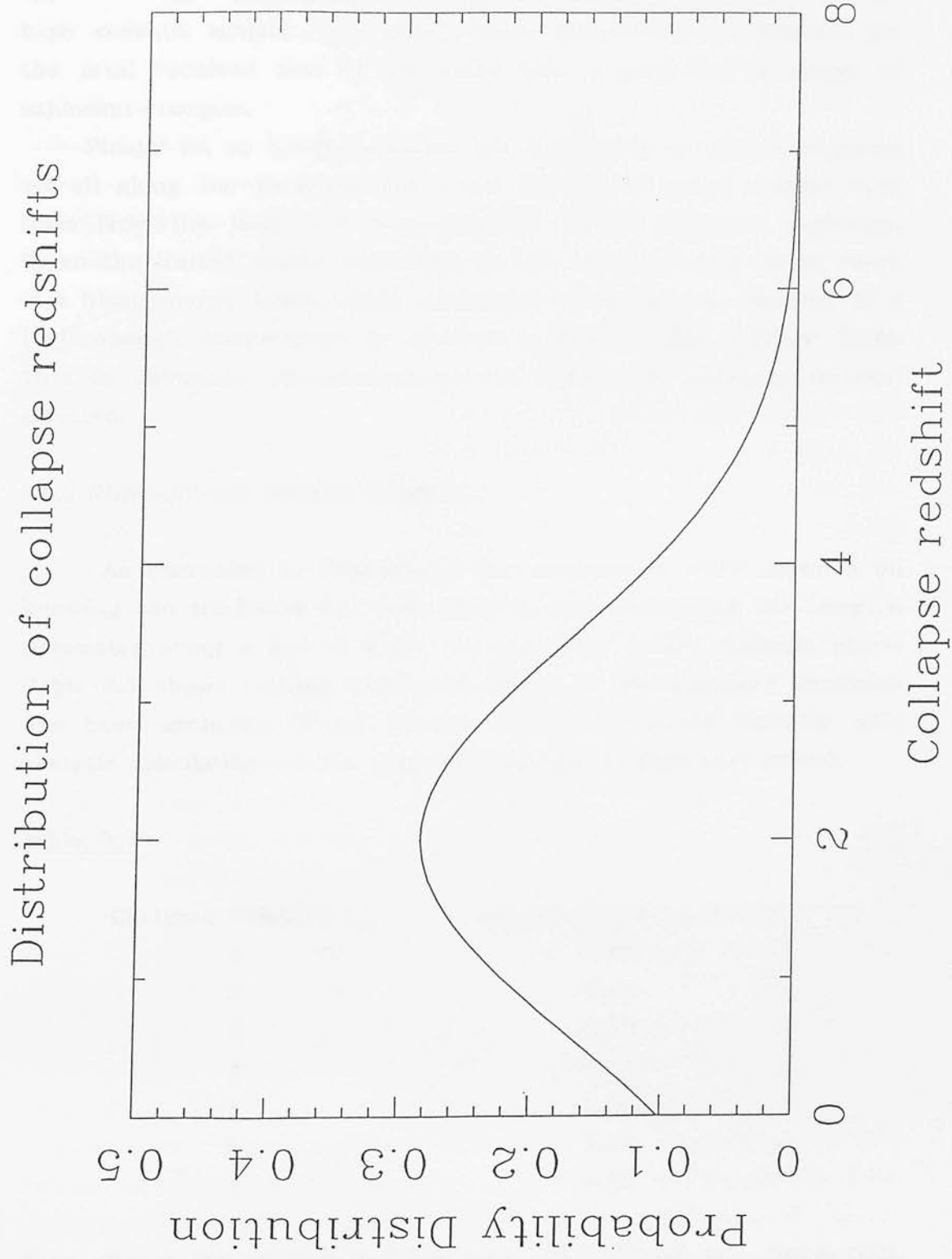

received (see Figure 3.2). It is evident that a very small explosion ($\epsilon \ll 10^{-2}$) would be required to reconcile our models with observation. However the results of section 3.4 (Table 3.1) suggest that, for a given time delay between caustic formation and energy release, the typical energy escaping from the central layer will be smaller for the high redshift models. This effect would reduce our predictions for the total received flux if we could also account for a range of explosion energies.

Finally let us briefly consider the possibility of explosions going off all along the pancake. The x-ray constraint would change very little from the limits set from analysis of the standard explosion. Given the limited spatial resolution in our numerical calculation there is a blast energy below which essentially no material is shocked to a high enough temperature to produce x-rays in the 3-50kev band. This is obviously independent of the volume of baryonic material affected.

3.5.2 SUNYAEV-ZEL'DOVICH EFFECT

As discussed in Appendix 3 the variance in dT/T depends on knowing the thickness for each pancake and calculating the Compton paramater along a line of sight perpendicular to the pancake plane. Table 3.3 shows results where the effect of the standard explosion has been excluded. These results can be compared directly with analytic calculations of the standard pancake picture (see below).

Table 3.3

Collapse redshift z_c	Log_{10}(Variance in dT/T)
1	-5.68
2	-5.16
3	-4.83
4	-4.57
5	-4.35
6	-4.17
7	-4.00

Generally as the collapse redshift goes up the microwave fluctuation

is increasing. We suggest that material hitting the plane shock is being heated to higher temperatures and the line of sight contributing is longer. It is interesting to note that the predictions of Szalay et al. (1984) are roughly 4-5 times as large as our values. We have already mentioned their equation for shock thickness which is a gross over-estimate at late times (large τ), and the baryon density $\rho_b \propto \Omega_b h^2$ is a factor 3 larger for their models. Both of these factors increase the size of the fluctuation predicted. This is balanced somewhat by their larger value of h so that there are fewer pancakes along the line of sight. However this only accounts for an increase by a factor of approximately 2 in dT/T so that the discrepancy noted above is understandable.

We now wish to look at the effect of introducing explosions on the variance in dT/T. We saw that for small explosions, the behaviour of the blast wave is almost one-dimensional (section 3.3) with the blast wave travelling very little in the radial direction. The implication of this is that for these explosions it is the increase in surface energy density which is fundamentally important. In the standard explosion we have introduced 10^{54} ϵ J over a circle of radius ~ 0.69 Mpc, giving an average surface density of 6.7×10^{53} ϵ J Mpc^{-2}. Let us now calculate the variance in dT/T using the appropriate pancake thickness and compton parameter for a line of sight through the blast wave perpendicular to the pancake plane. This effectively assumes that the surface energy density above is released at all points along the pancake. Figure 3.3 shows the results for given standard explosion energies which are best interpreted as the surface energy density input described above. One can see that in fact even for $\epsilon = 10^{-1}$ at $z_c = 4$ the variance in dT/T is only up by a factor of 1.6. So even for this extreme limit assuming explosions all along the pancake rather than the standard case, the additional contribution is fairly small.

An important point to consider is the beam-smearing effect referred to in section 3.4.3. Even if the entire variation in the temperature is due to the S-Z effect, the effect of finite beam size renders this constraint weaker than the x-ray constraint. With the minimal assumption of 4 independent objects in the 8 beam, the r.m.s dT/T would go down by a factor 2 (a logarithmic decrease of 0.3). A glance at Figure 3.3 then confirms that the only models excluded by

Figure 3.3

The predicted r.m.s. variation in microwave distortion dT/T resulting from the effect of material hit by the blast and plane shocks (see text). Again, as for figure 3.1, the population of objects contributing to the compton parameter are characterised by a single z_c and ϵ.

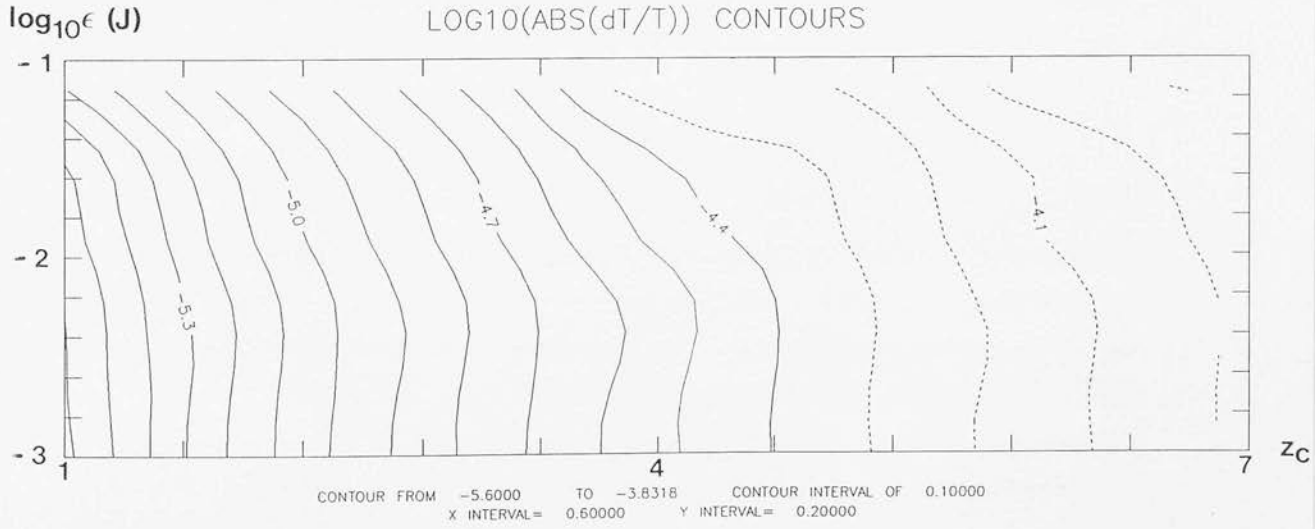

* INSERT:

Our criterion for cooling is as follows. Fluid shocked at z_s after the collapse epoch z_c will eventually fall back into the plane of the pancake. If cooling can take place before this, then it is possible for bound objects to form outside the pancake plane. We can estimate when infall occurs by assuming that gas which can cool efficiently fragments into bound objects whose subsequent behaviour is determined only by the initial velocity and gravity. We calculate a cooling time on the basis of the temperature and density of the shocked gas, and flag any cells which cool (at z_{cool}) before the epoch z_{infall} at which infall into the central layer occurs. The following table shows the cells with the shortest cooling times for a given explosion energy and collapse redshift. These cells lie at the densest part of the blast wave, where it meets the central layer. The best chance for cooling occurs soon after the explosion, when the proper mass density of the fluid is highest. For these small explosions, there is little sideways expansion of the blast, which would cause the internal pressure to drop. The results are summarised in Figure 3.4.

ϵ	z_c	z_s	Cooling time (s)	z_{cool}	z_{infall}
10^{-3}	2	1.98	3.4×10^{16}	1.34	1.6
10^{-2}	2	1.98	4.8×10^{16}	1.17	1.4
10^{-1}	2	1.98	8.7×10^{16}	0.83	1.2
10^{-3}	3	2.99	3.2×10^{16}	1.90	2.7
10^{-2}	3	2.99	6.8×10^{16}	1.28	2.4
10^{-1}	3	2.99	7.3×10^{16}	1.22	2.0
10^{-3}	4	3.98	5.9×10^{15}	3.51	3.5
10^{-2}	4	3.98	7.1×10^{15}	3.43	3.1
10^{-1}	4	3.98	1.7×10^{16}	2.87	2.5
10^{-3}	5	4.98	4.6×10^{15}	4.40	4.2
10^{-2}	5	4.98	1.1×10^{16}	3.83	4.1
10^{-1}	5	4.98	1.5×10^{16}	3.50	3.5
10^{-3}	6	5.97	3.1×10^{15}	5.39	5.3
10^{-2}	6	5.97	5.9×10^{15}	4.95	4.9
10^{-1}	6	5.97	9.1×10^{15}	4.55	4.3

the microwave constraint are at $z \gtrsim 6.5$, already ruled out by the x-ray constraint.

3.5.3 COOLING TIMES

We can now turn to a discussion of the cooling properties. We find material shocked early on by the blast wave can only cool rapidly if the collapse redshift is 4 or greater. At these epochs Compton cooling becomes important. The scale height of such material is very small (<0.01 Mpc) and the cooling material collapses into the central plane rapidly. We are faced with the following problem: for the scale height of cooling material to be interesting the shock must propagate well away from the central plane. Such material must also get a large velocity boost to prevent it falling back into the neutrino potential well too rapidly. But a large energy explosion produces high temperature material which cools slowly and the highest shocked densities, facilitating cooling, are in the part of the blast wave closest to the central plane. We must conclude that there is no possibility of bound objects forming at cosmologically significant distances from the pancake plane.

3.6 Discussion

We have shown that the scale height of cooling material in neutrino models which do not violate observational constraints is very small. The explosive process we have investigated can not significantly affect the large scale distribution of baryonic material and so no answer to the timing problem (see intro) is apparent. We rule out the possibility of promoting galaxy formation away from the dynamically dominant neutrino distribution along the infall axis. A second method of reducing the high level of clustering is to prevent galaxies forming close to each other within the pancake plane. Braun et al. (1988) discuss such "anti-biasing" of galaxy formation; suppressing the clustering of galaxies relative to the neutrinos. If the influence of the first objects to form is to prevent the formation of other objects locally (i.e. Mpc scales) the timing problem can be eliminated. We can say something about the "most extravagant in

energy" suppression mechanism, the blast wave, discussed by the authors. The explosive process we have investigated must affect the internal structure of the pancake, producing a "suppression radius" in the manner discussed by Braun et al. Local evacuation of material in the pancake plane up to a scale $r \cong (\epsilon/P)^{1/3}$ is a possibility. Using the expression for pressure in the pancake plane quoted earlier (eq^{n} 3.25) the proper distance influenced is

$$r \cong 4\ \epsilon^{\gamma/3}(1+z)^{-4/3}\ \text{Mpc} \qquad (3.30)$$

Braun et al. demonstrate that suppressing galaxy formation within a fixed proper radius $5h^{-1}/(1+z_f)$ Mpc after the onset of galaxy formation at redshift z_f reduces clustering in high density regions. This is reasonable: the observed galaxy clustering length is $5h^{-1}$ Mpc, so we clearly have to affect galaxy formation on these scales if we are to modify significantly the clustering length. Identification of the present epoch in biased simulations, where objects collapsing within the suppression radius of an earlier forming galaxy do not become luminous, admits a formation epoch of 3.6, alleviating the timing problem which the standard picture faces. With h=0.5 and z_f=3.6, r=2.17Mpc and we require $\epsilon \cong 4$, a model which would easily violate the xray and dT/T constraints. So this blast wave suppression mechanism would seem to be problematical.

The enrichment of voids and the markedly non-planar distribution of galaxy clouds in the LS remain unexplained by the explosive process. It is also apparent that neutrino pancakes can not be put forward as the seeds for the explosive picture of formation as the energy released can not affect relevant (Mpc) scale regions of space without violating observational constraints.

It is also interesting to look at the fraction of baryonic material which can cool by z=1 in a variety of models. This fraction increases from roughly 12% for z_c=2 to 38% for z_c=6. It is obvious then that the redshift 2 result is only marginally consistent with the observed baryon density from luminous material (Ω_{lum} =0.01 from observations of galaxies). Our results are very different from those of Shapiro and Struck-Marcell who quote the much smaller baryon fraction 10% for their z_c=6 model. The smaller h value in our calculation (0.5 as opposed to 0.75), and hence the larger time availible for cooling between epochs 6 and 1, is counteracted by the smaller baryon density $\rho_b \propto \Omega_b h^2$ in our models (0.035 to 0.056) which should result

in longer cooling times. The difference in the two sets of results may arise because Shapiro and Struck-Marcell include cooling in their numerical scheme. The cooling rate for material must be a function of time whereas our rate is assumed constant at its immediate post-shock value.

Of course, we could appeal to a higher pancake formation redshift so that Compton cooling would be effective in reducing the x-ray emission and microwave distortion. At least 3 problems are immediately apparent: Firstly this cooling would be highly efficient so that most of the baryons would be in neutral states; secondly Bond & Efstathiou (1984) show that small (arcmin) fluctuations in the MWB rule out $z_{formation} \geq 3.5$. Recent revision of the Uson and Wilkinson limit upwards by a factor of two allows us to push back this limit to roughly ten; thirdly, as we have shown in Chapter 2, the transitory nature of pancakes would mean that by the present all structures would have evolved into "clusters".

In passing, it is clear that it is impossible to ionise the voids with explosions which do not violate the x-ray constraint. The Gunn-Peterson test, limiting the neutral hydrogen fraction to $n_{HI} < 10^{-5}\rho/\rho_c$, is violated. The problems of fully ionising the IGM, discussed by Shapiro (1986) among others, remain unsolved.

The conclusion of this work is that explosions can not alleviate the problems of the adiabatic neutrino model of galaxy formation. Figure 3.4 summarises our work. We can define a region in the ϵ, z_c plane populated by models which fit x-ray and microwave constraints and produce off-plane material which can cool. The allowed region is rather small and we have shown that the scale height of cooling material is inconsequential.

Figure 3.4

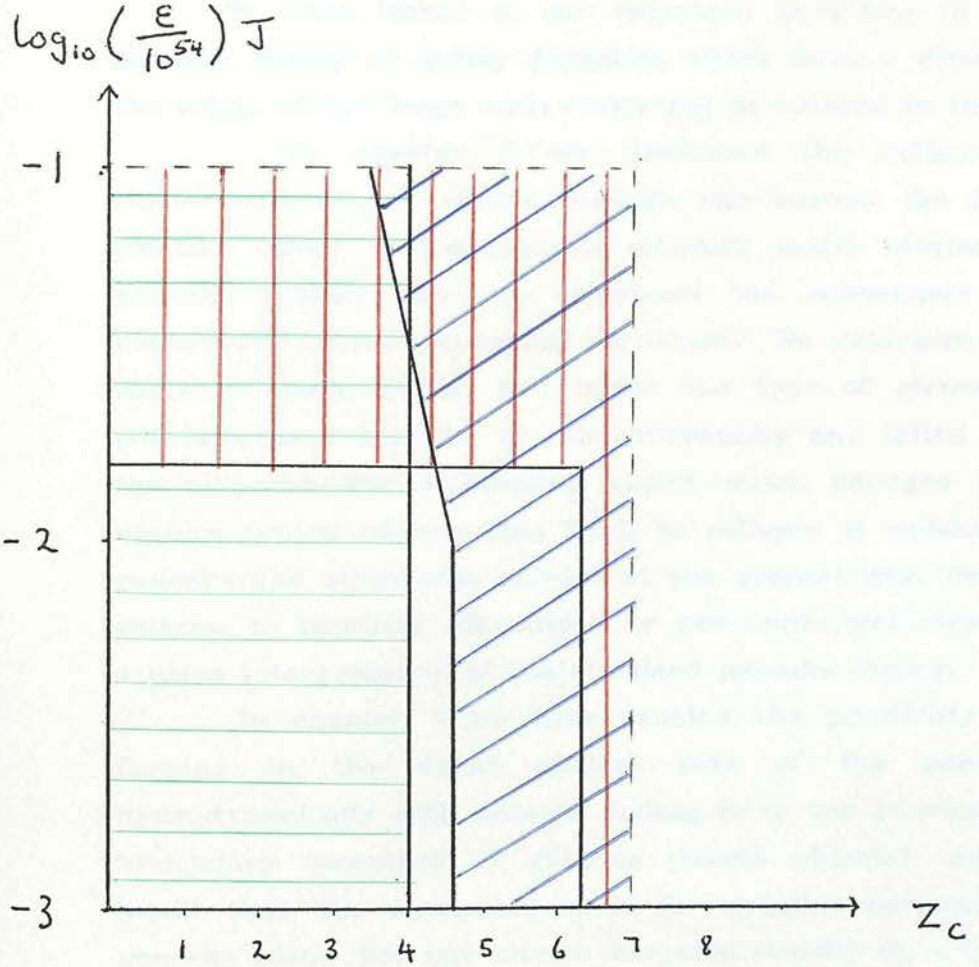

Region excluded by microwave constraint for an infinitesimal beam width.

Region excluded by xray flux constraint

Region where no cooling can take place in off-plane material (see text)

Chapter 4

Summary

4.1 Problems addressed in the thesis

We have looked at two important questions in the so-called pancake theory of galaxy formation which have a direct bearing on the origin of the large scale clustering of material in the universe.

In chapter 2 we discussed the collapse of proto-cluster/supercluster clouds through and beyond the formation of a pancake using a homogeneous ellipsoid model. Assuming that the pancake remains thin we calculated the subsequent evolution to filamentary or more spherical structures. We determined the present shape of such clouds, and hence the type of structures galaxies populate, as a function of the overdensity and initial axial ratio of the ellipsoid. The interesting result which emerges is that if we require typical objects (see 2.3.2) to collapse at redshift 3 very few pancake-like structures survive at the present day. We would expect galaxies to populate filamentary or more spherical structures, unlike a naive interpretation of the standard pancake theory.

In chapter 3 we have tackled the possibility that objects forming in the dense central part of the pancake interact hydrodynamically with material falling in to the pancake producing a 'secondary formation' of galaxies (bound objects). Such a process would alter the clustering scale for galaxies perpendicular to the pancake plane. For our chosen baryonic density $\Omega_b = 0.14$, cooling of material shocked by a blast wave escaping from the pancake plane is only possible at redshifts greater than 4. For models which fit the x-rayflux and microwave constraints such cooling material has a very small scale height above the plane (<0.1Mpc). We conclude that explosions can not provide the biasing mechanism required to alleviate the timing problems (see chapter 1) facing standard pancake models.

4.2 Pancake models: the future.

We have been unable to find a hydrodynamic solution to the clustering problem faced by 'standard' pancake models. Some means

of 'anti-biasing' the formation of galaxies away from the deepest potential wells in the neutrino distribution must be found or such a scenario is untenable. This anti-biasing process will undoubtedly depend on the details of galaxy formation and evolution, as yet poorly understood in pancake models. Of course as theoreticians, we would pride ourselves in being able to concoct some hybrid pancake model involving cold and hot dark matter, or abandon the physically appealing assumptions of $\Omega_0 = 1$ and gaussian fluctuations, to make our model fit crucial observations, but this is far from satisfactory. There must be a simpler answer. Ultimately we must rely on observation to guide our inventive minds. Concrete evidence for a neutrino rest mass, or for non-luminous matter in dwarf galaxies would be important. Better determination of the large scale clustering of galaxies and galaxy clusters, and more accurate velocity measurements to monitor the mass distribution, are a must if theories are to be constrained let alone given a sound basis.

Credit must be given to observation rather than theories, and to theories only in so far as they are confirmed by the observed facts.

Aristotle.

References

Aaronson, M., Huchra, J., Mould, J., Schechter, P.L. & Tully, R.B., 1982. Astrophys. J., 258,64.

Aaronson, M. & Olszewski, E., 1987. I.A.U. Symp., 117. Dark Matter in the Universe, ed Kormendy & Knapp (Dordrecht:Riedel)

Abramowitz, M. & Stegun, I.A. 1968. Handbook of Mathematical Functions Dover, New York.

Bahcall, J.N. & Glashow, S.L., 1987. Nature, 326,476.

Bardeen, J.R., Bond, J.R., Kaiser, N. & Szalay, A.S., 1986. Astrophys. J., 304,15.

Barrow, J.D. & Silk, J.I., 1981. Astrophys.J., 250,432.

Barrow, J.D., 1983. Fundam.Cosmic.Phys., 8,83.

Bond, J.R., Efstathiou, G. & Silk, J., 1980. Phys.Rev.Lett., 45,1980.

Bond, J.R. & Szalay, A.S., 1983. Astrophys.J., 274,443.

Bond, J.R. & Efstathiou, G., 1984. Astrophys. J., 285,L45.

Bond, J.R., Centrella, J., Szalay, A.S. & Wilson, J.R., 1984a. Mon.Not.R.astr.Soc., 210,515.

Bond, J.R., Centrella, J., Szalay, A.S. & Wilson, J.R., 1984b. in "Formation and Evolution of Galaxies" ed. Audouze & Tranh Thanh Van.

Bookbinder, J., Cowie, L.L., Krolik, J.H., Ostriker, J.P. & Rees, M., 1980. Astrophys.J., 237,647.

Braun, E., Dekel, A. & Shapiro, P.R., 1988. Preprint, Weizmann Inst. of Science.

Brosch, N. & Gondhalekar, P.M., 1984. Astr.Astrophys., 140,L43.

Collins, C.A., Joseph, R.D. & Robertson, N.A., 1986. Nature, 320,506.

Cowsik, R. & Ghosh, P., 1987. Astrophys. J., 317,26.

Davies, R.D. et al., 1987. Nature, 326,462.

Davis, M. & Peebles, P.J.E., 1983. Astrophys.J., 267,465.

Dekel, A., 1983. Astrophys.J., 264,373.

Doroshkevich, A.G., 1970. Astrophysics, 6,320.

Doroshkevich, A.G., 1984. Sov.Astr.Lett., 28,378.

Efstathiou, G. & Silk, J.I., 1983. Fundam. Cosmic Phys., 9,1.

Efstathiou, G., Davis, M., Frenk, C.S. & White, S.D.M., 1985. Astrophys.J.Suppl.Ser., 57,241.

Einasto, J., Klypin, A.A. & Saar, E., 1986. Mon.Not.R.astr.Soc, 219,457.

Fall, S.M. & Rees, M.J., 1985. Astrophysics.J., 298,18.

Falle, S.A.E.G., Garlick, A.R. & Pudsley, P.H., 1984. Mon.Not.R.astr.Soc., 208,925.

Geller, M., 1988. in SAAS-FEE "Large Scale Structure of the Universe" in print.

Gentry, R.A., Martin, E.R. & Daly, B.J., 1966. J.Comp.Phys, 1,87.

Gott III, J.R., Weinberg, D.H. & Melott, A.L., 1987. Astrophys.J., 319,1,1987.

Gunn, J.E., 1978. in SAAS-FEE, "Observational Cosmology", ed. Maeder, Martinet & Tamman.

Guth, A.H. & Steinhardt, P.J., 1984. Scientific American, 250,90.

Hegyi, D.J. & Olive, K.A., 1986. Astrophys. J., 303,56.

Hoffman, Y., 1987. Astrophys.J., 318,L7.

Hogan, C., 1984. Nature, 310,365.

Ikeuchi, S., 1981. Publ.astr.Soc.Japan, 211,33.

Ikeuchi, S., Tomisaka, K. & Ostriker, J.P., 1983. Astrophys.J., 265,583.

Jeans, J., 1902. Phil.Trans.Roy.Soc., 199A,49.

Jones, B.J.T. & Wyse, R.F.G., 1985. Astr.Astrophys., 149,144.

Kaiser, N., 1987. Mon.Not.R.astr.Soc., 231,149.

Kaiser, N. & Silk, J., 1986. Nature, 324,529.

Kirshner, R.P., Oemler Jr., A., Schechter, P.L. & Shectman, S.A., 1987. Preprint Yale University.

Kormendy, J., 1987. I.A.U. Symp., 117. Dark Matter in the Universe, ed Kormendy & Knapp (Dordrecht:Riedel).

de Lapparent, V., Geller, M.J. & Huchra, J.P., 1986. Astrophys.J., 302,L1.

Landau, L.D. & Lifshitz, E.M., 1959. Course of Theoretical Physics, Vol.6: Fluid Mechanics, Pergamon Press.

Lin, C.C., Mestel, L. & Shu, F.H., 1965. Astrophys.J., 142,1431.

Longair, M.S. 1984. Concepts of Theoretical Physics, Cambridge University Press.

Lynden-Bell, D., Faber, S.M., Burstein, D., Davies, R.L., Dressler, A., Terlevich, R. & Wagner, G., 1988. Astrophys. J., in press.

Lyubimov, V.A., Novikov, E.G., Nozik, V.Z., Tretyakov, E.F. & Kosik, V.S., 1980. Phys.Lett., 94B,266.

Lyubimov, V.A., 1986. Neutrino 86, Proc. 12th International Conference on Neutrino Physics & Astrophysics, ed. Kitagaki & Yuta, World Scientific.

Madsen, J. & Epstein, R.I., 1984. Astrophys.J., 282,11.
1985. Phys.Rev.Lett., 54,2720.

Marshall, F.E., et al., 1980. Astrophys.J., 235,4.

Mészáros, P., 1974. Astron.Astrophys., 37,225.

Oort, J.H., 1983. A.Rev.Astr.Astrophys., 21,373.

Ostriker, J.P. & Cowie, L.L., 1981. Astrophys.J. 243,L127.

Ostriker, J.P., 1986. in Galaxy Distances and Deviations from the Universal Expansion, ed. Madore & Tully, Dordrecht:Riedel.

Peacock, J.A. & Heavens, A.F., 1985. Mon.Not.R.astr.Soc., 217,805.

Peacock, J.A., Lumsden, S.L. & Heavens, A.F., 1987.
Mon.Not.R.astr.Soc., in press.

Peebles, P.J.E. 1980. The Large Scale Structure of the Universe, Princeton University Press.

Penzias, A.A & Wilson, R.W., 1965. Astrophys.J., 142,419.

Primack, J.R., 1984. Lectures presented at the International School of Physics "Enrico Fermi".

Rees, M.J., 1984. J.Astrophys.Astr., 5,331.

Robertson, R.G.H., et al 1986. Neutrino 86, Proc 12th International Conference on Physics & Astrophysics, ed. Kitagaki & Yuta, World Scientific.

Rybicki, G.B. & Lightman, A.P., 1979. Radiative Processes in Astrophysics. Wiley & Sons Ltd.

Schwartz, D.A., 1979. in X-ray astronomy, ed. Baity & Peterson.

Shandarin, S.F., 1980. Astrophys., 16,438.

Shanks, T., 1985. Vistas in Astronomy, 28,595.

Shapiro, P.R., Struck-Marcell, C. & Melott, A.L., 1983.
Astrophys.J., 275,413.

Shapiro, P.R. & Struck-Marcell, C., 1985.
Astrophys.J.Suppl.Ser, 57,205.

Shapiro, P.R., 1986. P.A.S.P., 98,104.

Spinrad, H., Smith, H.E. & Taylor, D.J., 1972. Astrophys.J., 175,649.

Sunyaev, R.A. & Zeldovich, Ya.B., 1972. Astr.Astrophys., 20,189.

Szalay, A.S., Bond, J.R. & Silk, J.I., 1984.
in "Formation and Evolution of Galaxies" ed. Audouze & Tran Thanh Van.

Tremaine, S. & Gunn, J.E., 1979. Phys.Rev.Lett., 42,407.

Tully, R.B., 1982. Astrophys.J., 257,389.

Tully, R.B., 1986. Astrophys.J., 303,25.

Uson, J.M. & Wilkinson, D.T., 1984. Astrophys.J., 277,L1.

Vittorio, N., Juszkiewicz, R. & Davis, M., 1986. Nature, 323,132.

Weinberg, S., 1972. Gravitation and Cosmology : Principles and Applications of the General Theory of Relativity. Wiley & Sons, New York.

White, S.D.M. & Silk, J., 1979. Astrophys.J., 231,1.

White, S.D.M., Frenk, C.S. & Davis, M., 1983. Astrophys.J., 274,L1.

White, S.D.M., Davis, M. & Frenk, C.S., 1984. Mon.Not.R.astr.Soc., 209,27P.

White, S.D.M., Frenk, C.S., Davis, M. & Efstathiou, G., 1987. Astrophys.J., 313,505.

Wilson, M.L. & Silk, J., 1981. Astrophys.J., 243,14.

Yang, J., Turner, M.S., Steigman, G., Schramm, D.N. & Olive, K.A., 1984. Astrophys.J., 281,493.

Zel'dovich, Ya.B. & Sunyaev, R.A., 1969. Astrophys.Sp.Sci., 4,301.

Zeldovich, Ya.B., 1970. Astr.Astrophys., 5,84.

Zeldovich, Ya.B. & Novikov, I.D., 1983. Relativistic Astrophysics, Vol.2: The Structure and Evolution of the Universe, Chicago University Press.

Appendix 1

Aspects of the FLIC difference scheme

We describe here the modifications which had to be made to the general difference scheme 'FLIC' of Gentry et al. (hereafter GMD) for our specific purposes, how the new scheme was tested and note the relevant programming considerations.

Flic deals with total quantities for cells. We will focus on the basic fluid equation for z momentum (3.1 without the force term) to explain the major points in the numerical scheme before going on to describe the adaptations made.

$$\frac{\partial \rho v_z}{\partial t} + \frac{\partial}{\partial z}(\rho v_z^2 + P) + \frac{1}{r}\frac{\partial}{\partial r}(\rho v_r v_z r) = 0 \quad \text{(A1.1)}$$

is integrated over the cell volume :

$$\frac{\partial}{\partial t}\int \rho v_z dV = \frac{\Delta ZMOM}{\Delta t} = -\int \frac{\partial}{\partial z}(\rho v_z^2 + P)dV - \int \frac{1}{r}\frac{\partial}{\partial r}(\rho v_r v_z r)dV \quad \text{(A1.2)}$$

$$= \overset{1)}{-\int} P dS_z \overset{2)}{-\int} \rho v_z v_z dS_z \overset{3)}{-\int} \rho v_z v_r dS_r \quad \text{(A1.3)}$$

making use of the divergence theorem, where dS_r,dS_z are the incremental surface areas in the z and radial direction. Such terms are dealt with in two stages; an acceleration stage (GMD eqn. 3) where the pressure integral, term 1, is approximated

$$\int P dS_z = \left((p + q)_{i+1/2,j} - (p + q)_{i-1/2,j} \right) \times Sz_{i,j} \quad \text{(A1.4)}$$

(S_z is the top surface area of the appropriate cell, q is an artificial viscosity term which enhances the stability of the scheme and subscript 1/2 indicates values at a cell boundary)

followed by a transport phase (GMD eqns. 8-12) where the z-momentum is convected between cells at the velocity calculated in the acceleration phase:

$$\int (\rho v_z)\, v_z dS_z = \left((\rho v_z)_{k-1}\, (v_z)_{k-1/2} - (\rho v_z)_k\, (v_z)_{k+1/2} \right) \times Sz_k \quad \text{(A1.5)}$$

This two-stage process is done for both radial and z components, so term 2) in eqn. A1.3 is dealt with in the transport phase of the z calculation and term 3) in the corresponding stage of the r calculation.

We want to deal with a logarithmic coordinate along the z-axis as the interesting physics occurs close to the central plane where the variables are fluctuating rapidly. Defining logarithmic coordinate $z=\ln(z')$, and retaining the conservation law form in cylindrical polars equations 3.20) become dropping primes

$$\frac{\partial}{\partial t}\begin{bmatrix}\rho\\ \rho v_z\\ \rho v_r\\ e\end{bmatrix}+\frac{\partial}{\partial z}e^{-z}\begin{bmatrix}\rho v_z\\ (\rho v_z^2+P)\\ \rho v_r v_z\\ v_z(e+P)\end{bmatrix}+\frac{1}{r}\frac{\partial}{\partial r}\begin{bmatrix}\rho v_r r\\ r\rho v_r v_z\\ r(\rho v_r^2+P)\\ r v_r(e+P)\end{bmatrix}=\begin{bmatrix}-e^{-z}\rho v_z\\ \rho F-e^{-z}(\rho v_z^2+P)\\ p/r-e^{-z}\rho v_z v_r\\ \rho v_z F-e^{-z}v_z(e+P)\end{bmatrix} \tag{A1.6}$$

It is difficult to incorporate the large number of 'source terms' (rhs of the above eqn. A1.6) into the Flic scheme. Now we saw that Flic operated on integral quantities; provided we set up the density, energy density and pressure to be the re-defined quantities $\hat{\rho}_B=\rho'_B e^z$, $\hat{e}=e'e^z$, $\hat{P}=P'e^z$ with cell volumes in our new coordinate system $V_{log}=V_{real}e^{-z}$ then Flic will update real cell mass $(\hat{\rho}_B V_{log})$, momentum and energy as before. With this variable definition the equations have a much simpler form:

$$\frac{\partial}{\partial t'}\begin{bmatrix}\hat{\rho}_B\\ \hat{\rho}_B v'_z\\ \hat{\rho}_B v'_r\\ \hat{e}\end{bmatrix}+\frac{\partial}{\partial z}\begin{bmatrix}\hat{\rho}_B v'_z\, e^{-z}\\ (\hat{\rho}_B v_z'^2+\hat{P})e^{-z}\\ \hat{\rho}_B v'_r v'_z e^{-z}\\ v'_z(\hat{e}+\hat{P})e^{-z}\end{bmatrix}+\frac{1}{r'}\frac{\partial}{\partial r'}\begin{bmatrix}\hat{\rho}_B v'_r\, r'\\ r'\hat{\rho}_B v'_r\, v'_z\\ r'(\hat{\rho}_B v_r'^2+\hat{P})\\ r' v'_r(\hat{e}+\hat{P})\end{bmatrix}=\begin{bmatrix}0\\ \hat{\rho}_B F'\\ \hat{p}/r'\\ \hat{\rho}_B v'_z F'\end{bmatrix} \tag{A1.7}$$

It is very much clearer how the first-order equations should be adapted:

1) The acceleration of cell material in r or z directions is calculated as before (eqns. 3)-6) GMD) from real pressure gradients (now $\hat{P}e^{-z}$) adding in the gravitational force term to the z component.

2) In the radial and z direction transport phases we simply convect real cell mass (now $\hat{\rho}_B e^{-z}$), momentum and energy as before at the intermediate velocity calculated in step 1.

If we take the new zmomentum equation

$$\frac{\partial \hat{\rho}_B v'_z}{\partial t'} + \frac{\partial}{\partial z'}(\hat{\rho}_B v'^2_z + \hat{P})\, e^{-z} + \frac{1}{r'}\frac{\partial}{\partial r'}(\hat{\rho}_B v'_r v'_z r') = 0 \qquad (A1.8)$$

we can again identify total quantities for a given grid cell:

$$\frac{\Delta ZMOM}{\Delta t} = -\overset{1)}{\int} \hat{\rho}_B F' dV \; -\overset{2)}{\int} \hat{P} e^{-z} dS_z \; -\overset{3)}{\int} \hat{\rho}_B v_z e^{-z} v_z dS_z \; -\overset{4)}{\int} \hat{\rho}_B v_z e^{-z} v_r dS_r \qquad (A1.9)$$

In the acceleration phase we approximate

$$\int \hat{P} e^{-z} dS_z = \left(((\hat{p}+\hat{q})e^{-z})_{i+1/2,j} - ((\hat{p}+\hat{q})e^{-z})_{i-1/2,j} \right) \times Sz_{i,j} \qquad (A1.10)$$

adding in the force term approximation

$$\int \hat{\rho}_B F' dV = MASS_k \times (F_{k+1/2} - F_{k-1/2}) \qquad (A1.11)$$

The Flic z transport phase approximation to term 3) becomes:

$$\int (\hat{\rho}_B v_z e^{-z}) v_z dS_z = ((\hat{\rho}_B e^{-z} v_z)_{k-1} (v_z)_{k-1/2} - (\rho_B e^{-z} v_z)_k (v_z)_{k+1/2}) \times Sz_k \qquad (A1.12)$$

Operation of the scheme, particularly boundary conditions, was checked carefully by the standard method of testing shock propagation. The behaviour of a plane shock on an otherwise uniform density grid is shown in Figure A1.1) and point, line and plane explosion behaviour in the absence of gravity are given in Figures A1.2)-A1.4). Qualitatively the evolution is reasonable. Notice that the smearing out of the discontinuity is a numerical artefact. Schemes are designed to make a numerical shock as narrow as possible without producing large downstream oscillations. Also obvious in Figure A1.2) is the effect of the finite region over which a 'point' explosion is introduced. The shock becomes spherical fairly close to the origin. This is important if we are to derive meaningful results with regard to the density behaviour in our models. The evolution of the shock

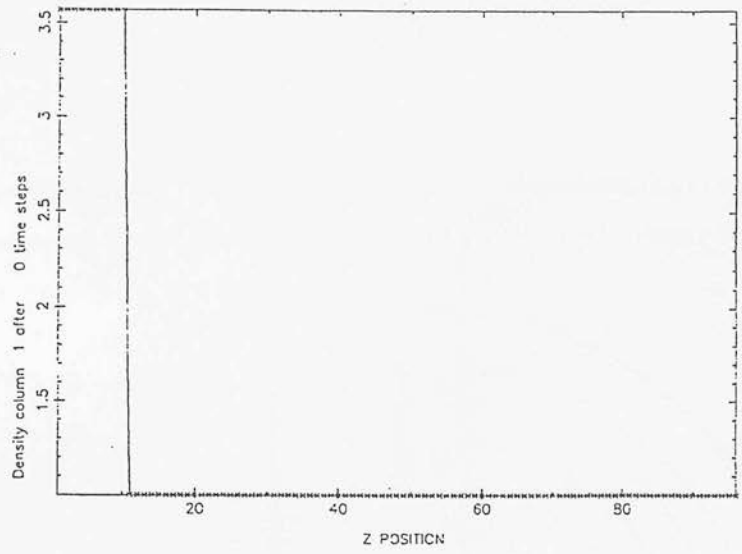

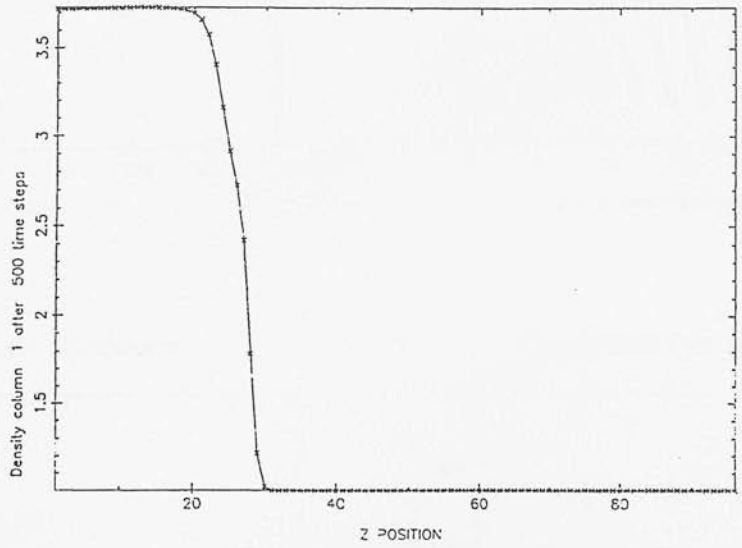

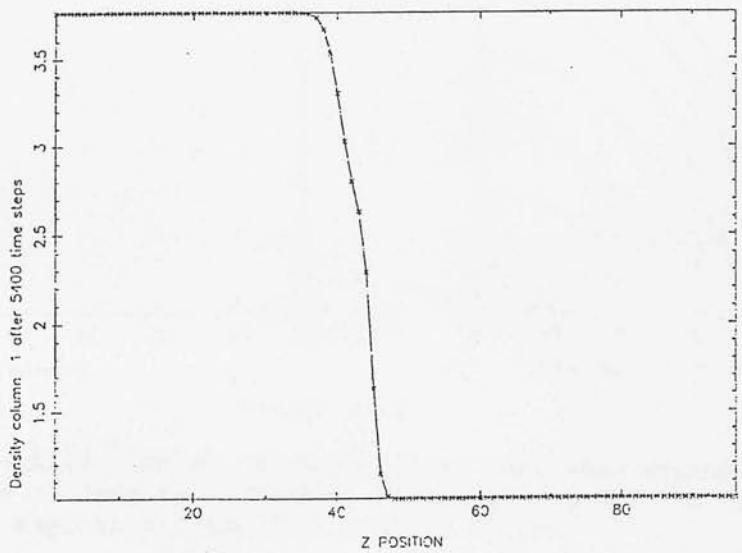

Figure A1.1
The propagation of a plane shock by the modified form of the FLIC code for a logarithmic spacing along the z axis.

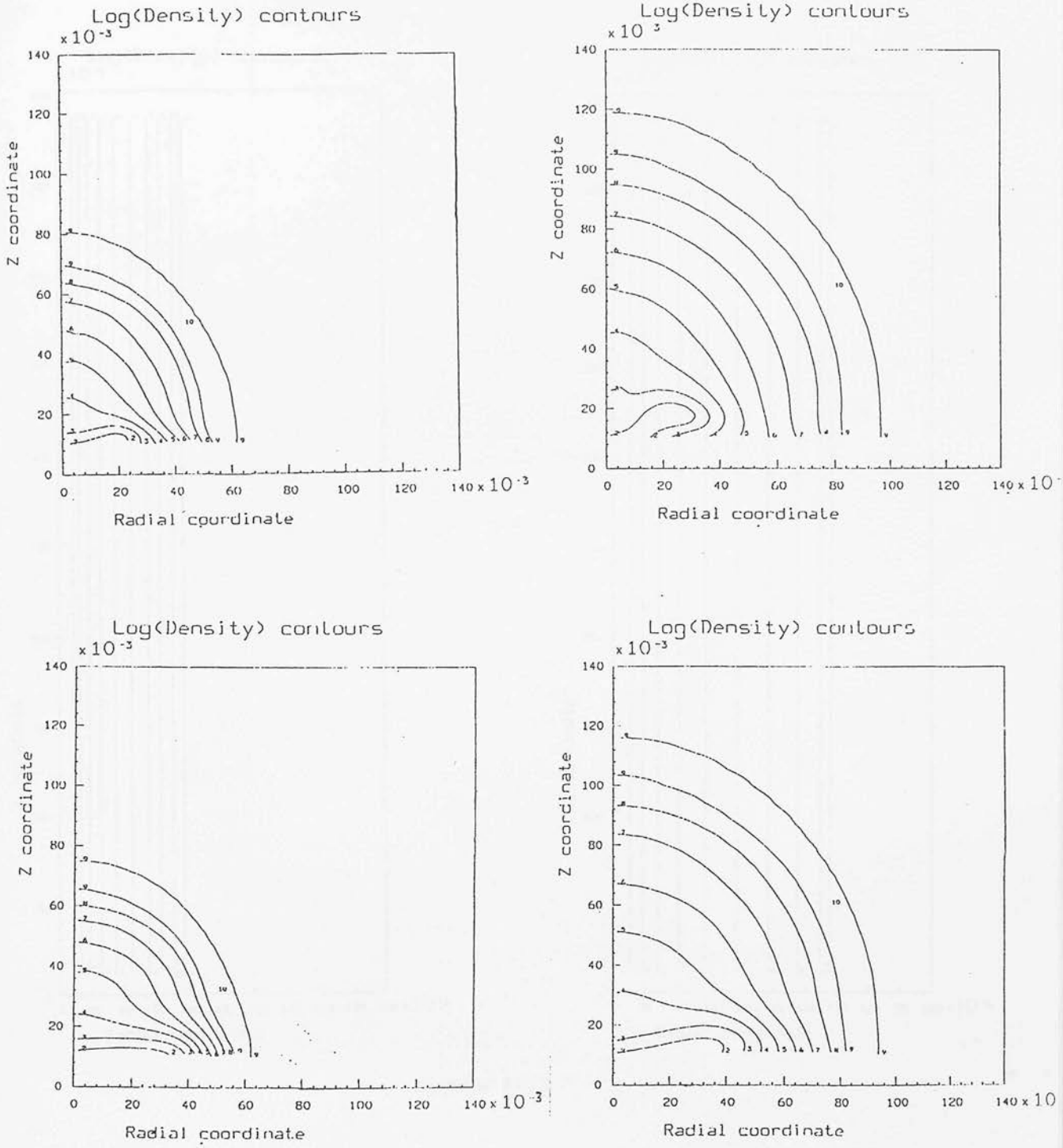

Figure A1.2

Figures A1.2 - A1.4 Point, line and plane explosion evolution are shown in terms of density contours. Figure A1.2 shows two different width 'point' explosions (see text section 3.2.3)

(i) Gaussian width 3 cells
(ii) Gaussian width 5 cells

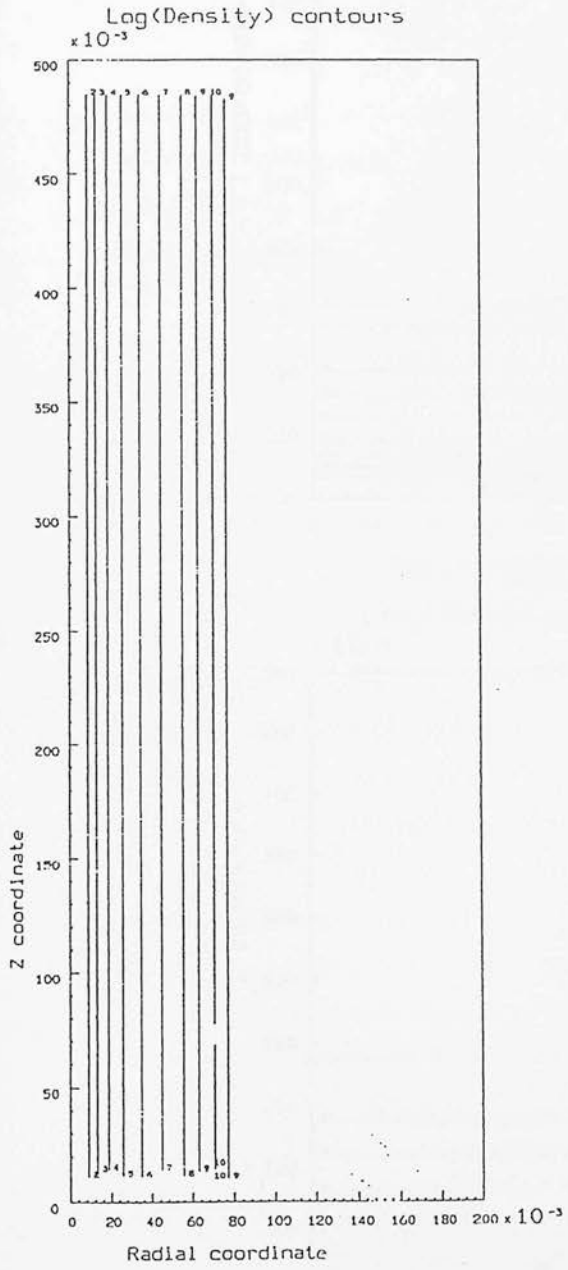
Log(Density) contours
x10⁻³
500
450
400
350
300
250
200
150
100
50
0
Z coordinate
0 20 40 60 80 100 120 140 160 180 200 x10⁻³
Radial coordinate

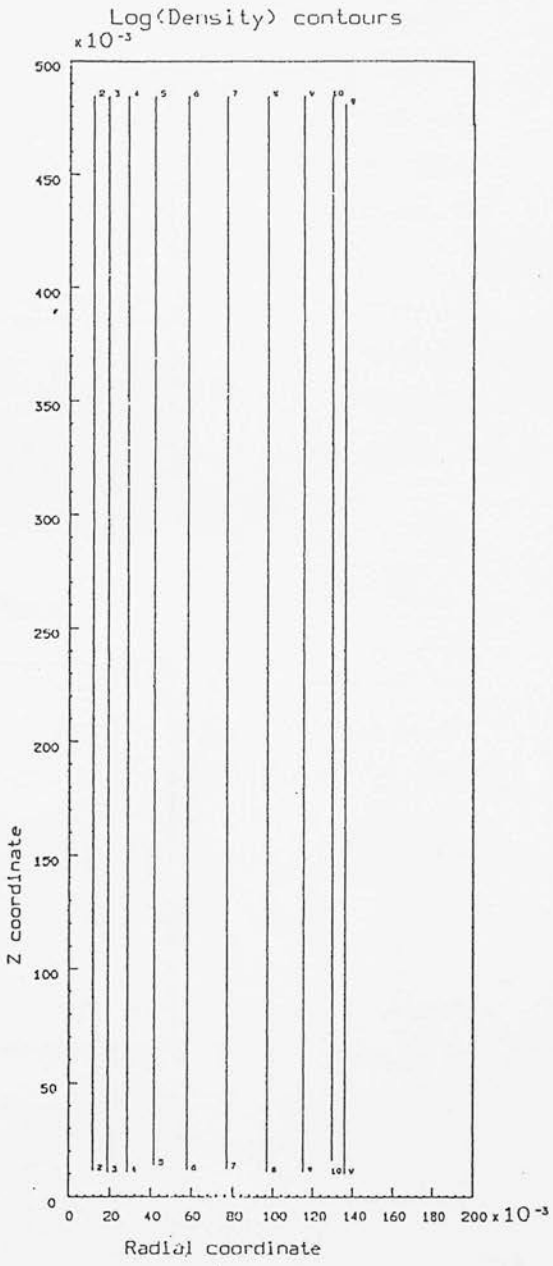
Log(Density) contours
x10⁻³
500
450
400
350
300
250
200
150
100
50
0
Z coordinate
0 20 40 60 80 100 120 140 160 180 200 x10⁻³
Radial coordinate

Figure A1.3

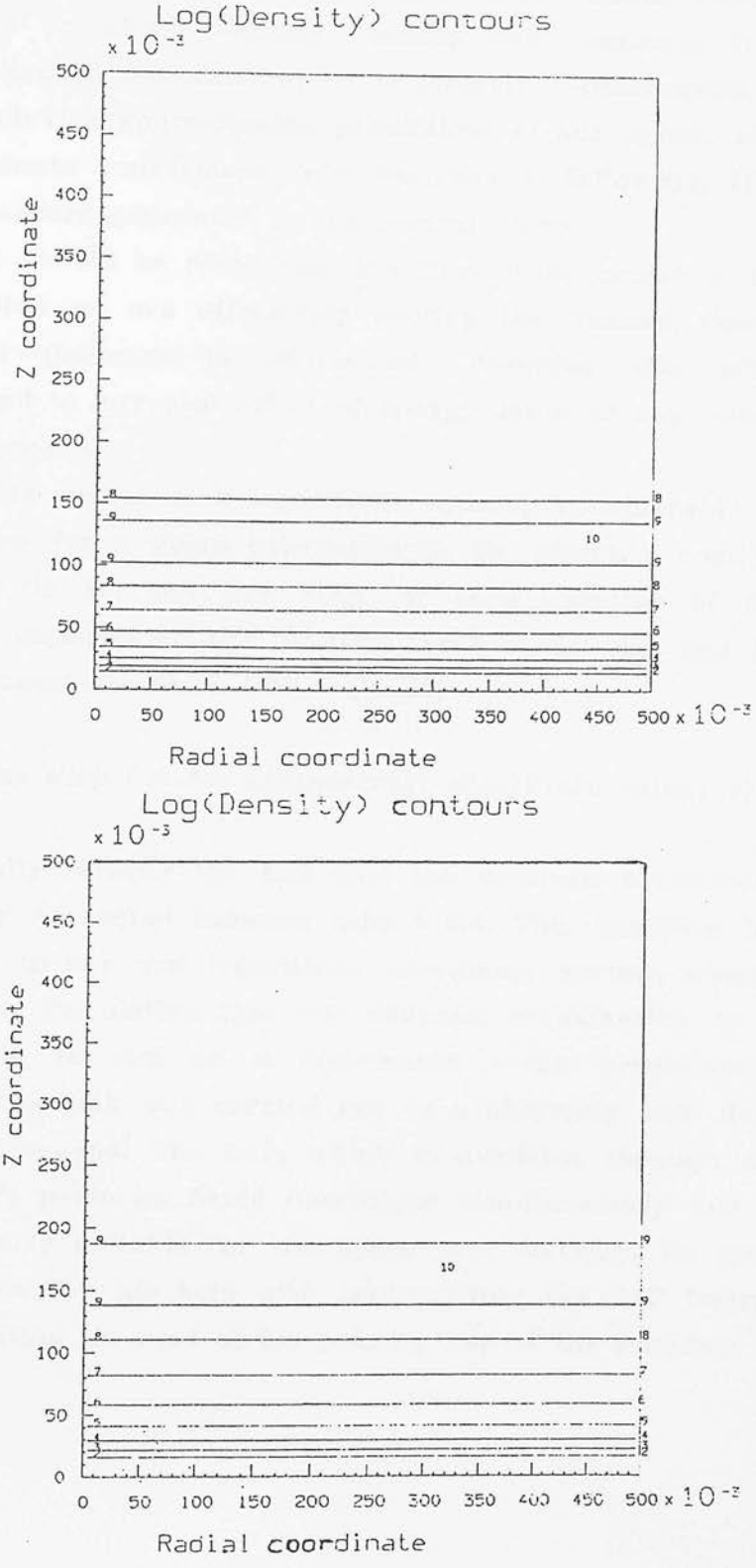
Log(Density) contours
x 10 -3
Z coordinate
Radial coordinate
Log(Density) contours
x 10 -3
Z coordinate
Radial coordinate

Figure A1.4

was checked quantitatively against simple shock theory predictions for the postshock velocity, density and pressure. In addition the pre-collapse behaviour, which is entirely 1-dimensional, should match the Zeldovich approximation predictions at any epoch. We also use the approximate expressions from Sunyaev & Zel'dovich (1972) to check the pressure generated in the central plane.

It should be noted that the first order nature of the solution is such that we are effectively solving the viscous flow problem and viscous pressure is introduced. Provided this effect is small compared to any real effect of energy input at the collapse epoch we can ignore it.

The choice of a logarithmic spacing considerably increases the CPU time for a given calculation as the stability condition employed by Flic to set the time step for each iteration of the difference scheme depends on the relation between cell size and fluid velocity. The Courant condition (GMD eq^{n}. 28)

$$\text{time step} < 0.4 \times \text{minimum}(\text{cell size}/\text{fluid velocity}) \quad (A1.13)$$

essentially reflects the fact that the maximum fractional size of any quantity convected between cells = 0.4. This condition is thus easily adapted to our new logarithmic coordinate system, where we convect $\hat{\rho}e^{-z}$ etc. Calculation time was reduced considerably by transferring the code to run on a distributed array processor (DAP). This non-trivial task was carried out in a charming and elegant way by Dr. A.F.Heavens! The DAP, which is available through a link to the E.R.C.C.*, performs 64x64 operations simultaneously and is obviously particularly suitable for the space grid solution. We are grateful to Dr A.Trew for his help with implementing the DAP fortran code and for granting us some of his priority use of the machine.

*Edinburgh Regional Computing Centre.

Appendix 2

Hydrodynamics results plots

The behaviour of density, pressure and temperature is illustrated for two different models.

Figure A2.1 $\epsilon = 10^{2}$, $z_c = 5$

Figure A2.2,A2.3 $\epsilon = 10^{-1.5}$, $z_c = 2$

For details see individual figure captions.

Figure A2.1
The behaviour of density, pressure and temperature following the input of explosion energy $\epsilon=10^2$ at $z_c=5$ (see text for details). The radial and 'z' coordinates are comoving values scaled to the pancake length 55.2 Mpc.

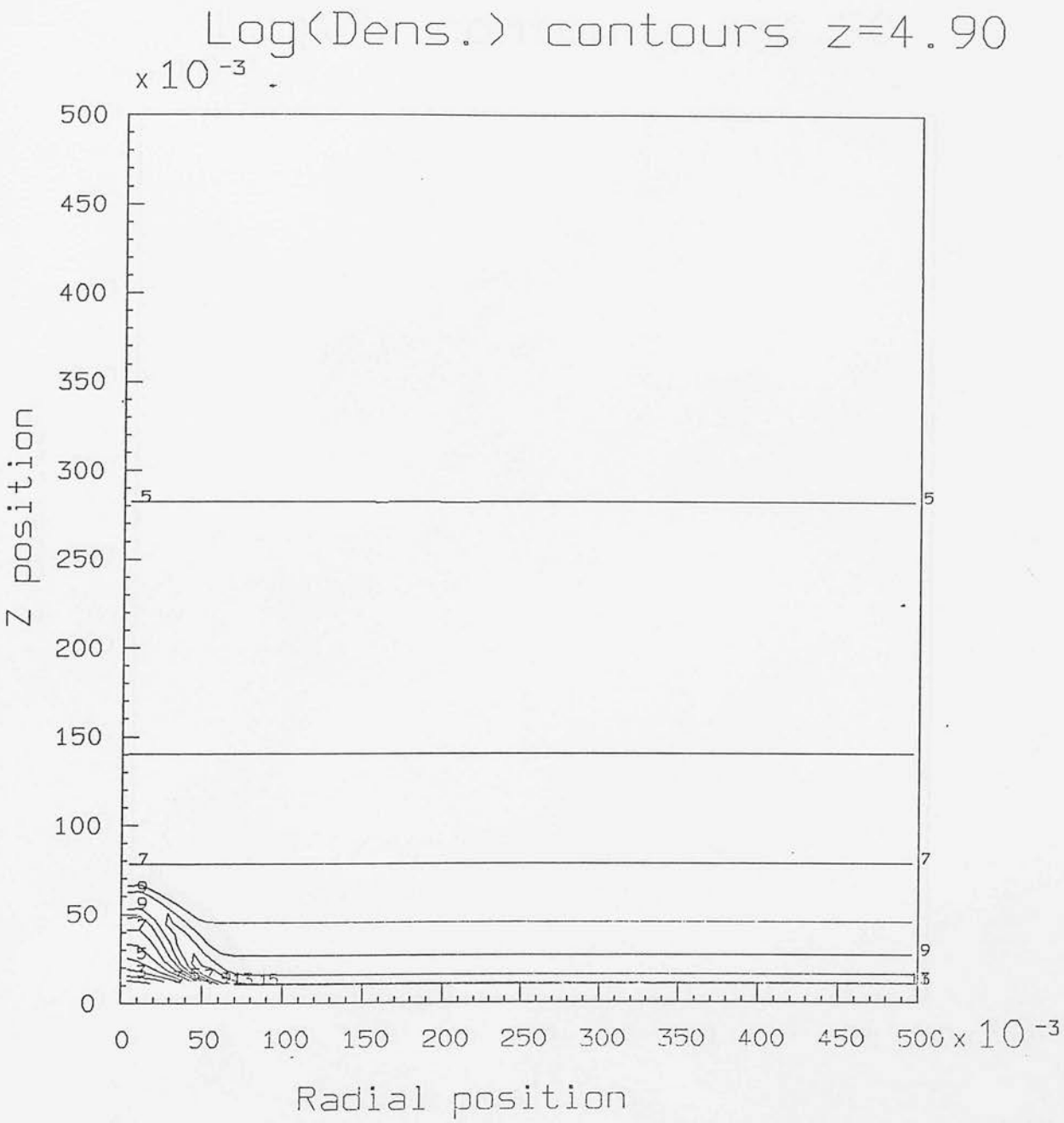

Contour No.	Contour level
1	-25.67
4	-25.25
7	-24.84
11	-24.28
15	-23.73

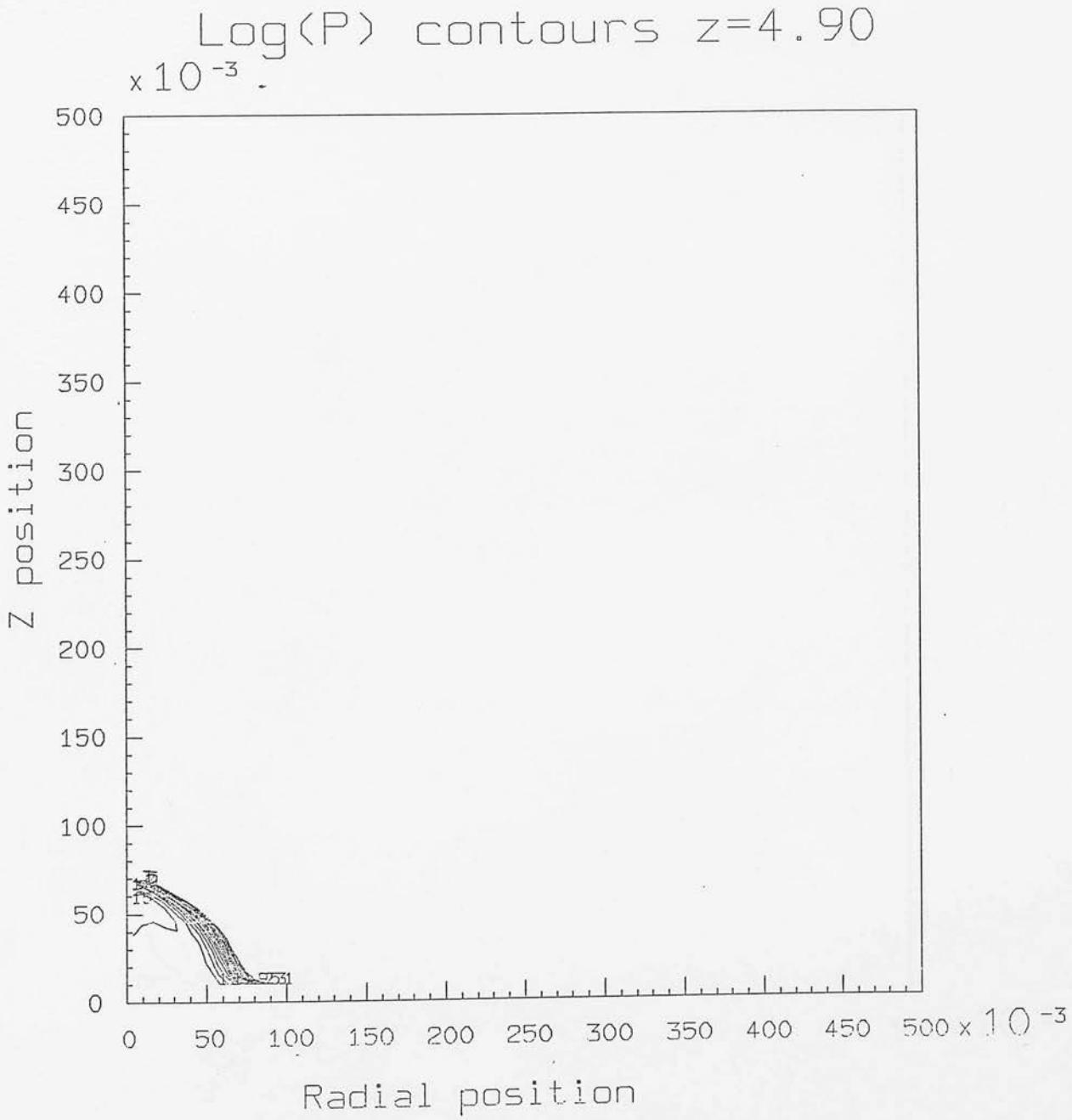

Contour No.	Contour level
1	-15.00
4	-14.10
7	-13.20
11	-12.00
15	-10.80

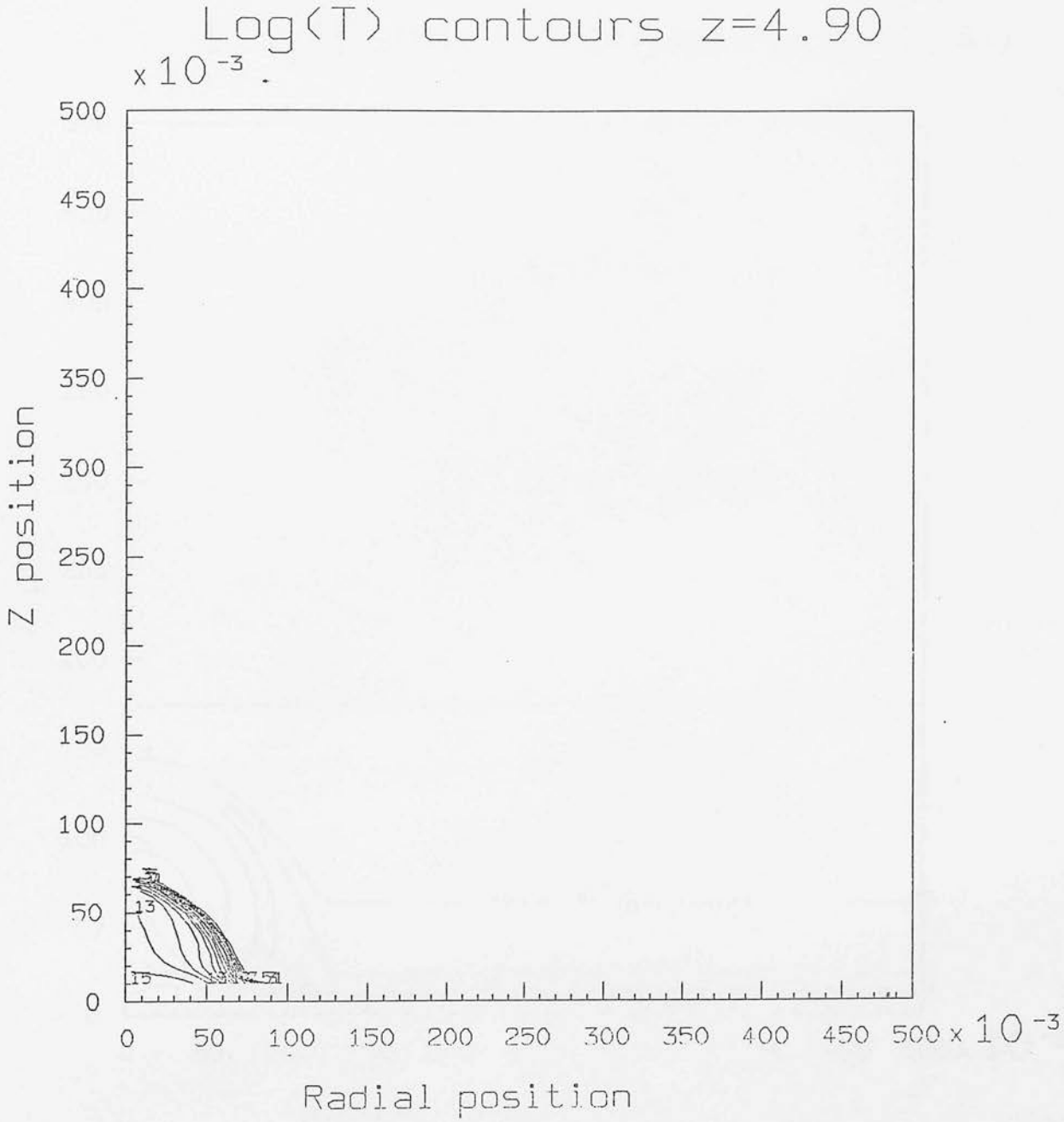

Contour No.	Contour level
1	5.50
4	6.51
7	7.52
11	8.87
15	10.22

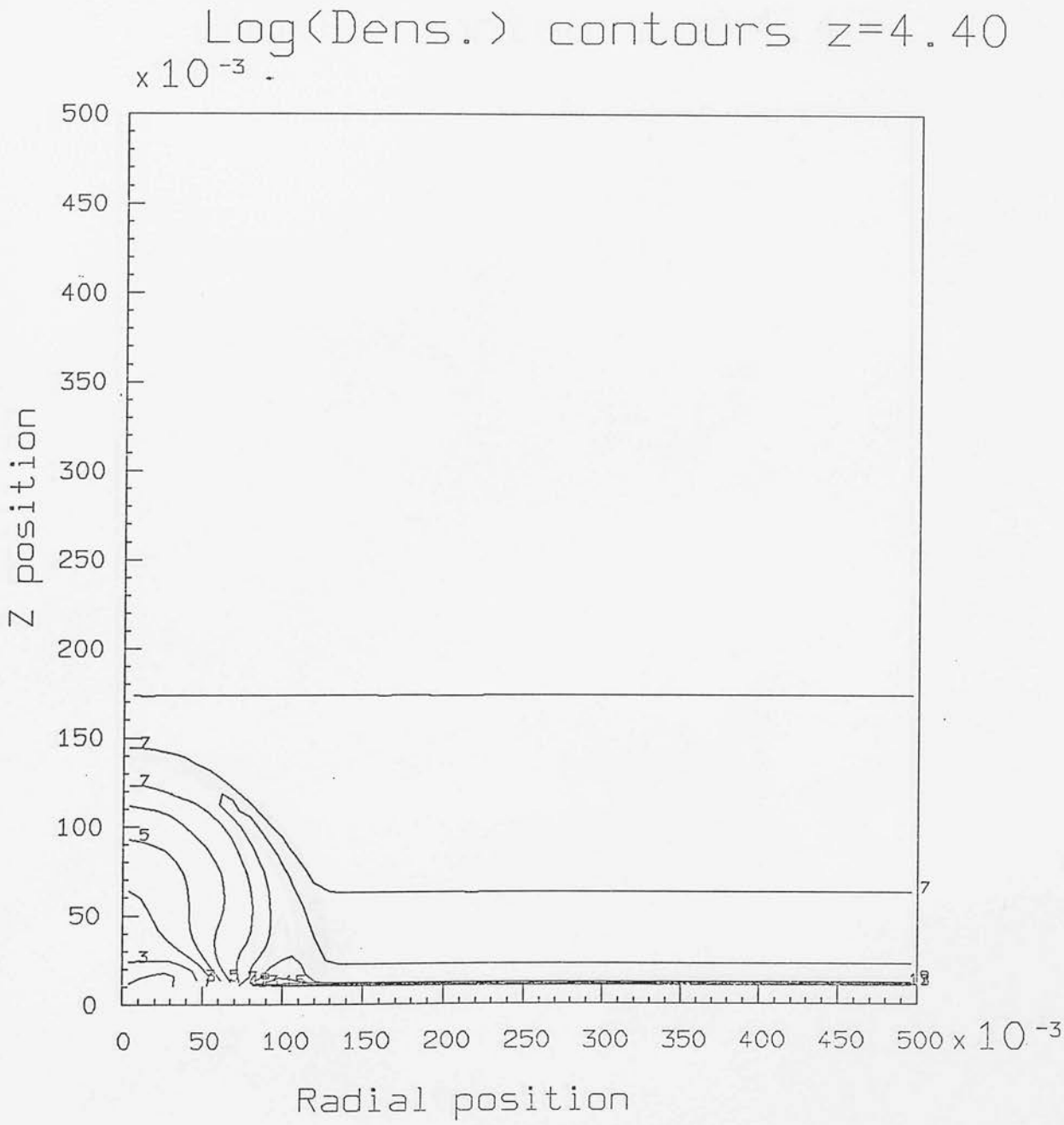

Contour No.	Contour level
1	-26.26
4	-25.61
7	-24.95
11	-24.07
15	-23.20

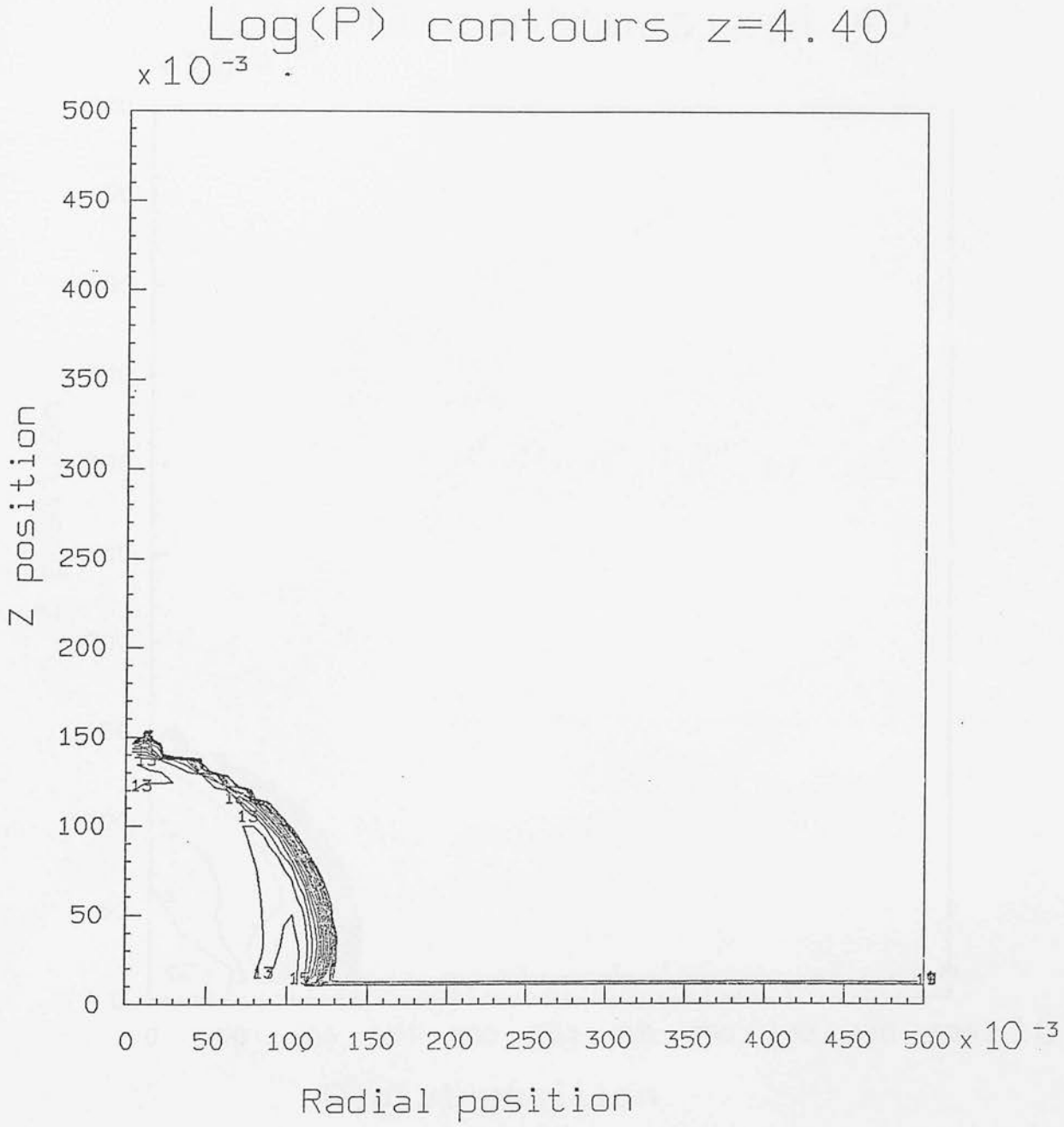

Contour No.	Contour level
1	-15.00
4	-14.31
7	-13.62
11	-12.70
15	-11.78

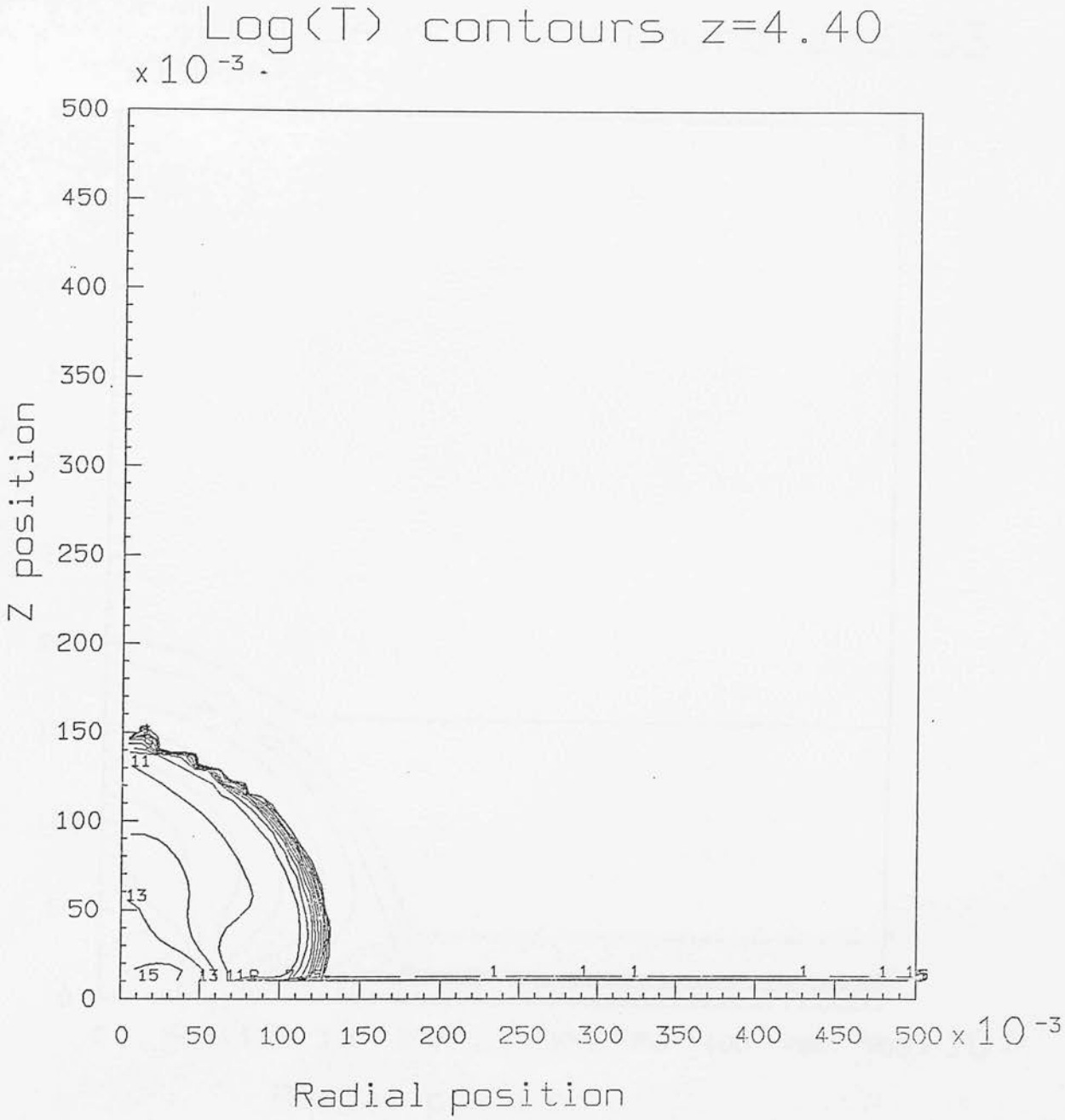

Contour No.	Contour level
1	5.50
4	6.40
7	7.31
11	8.51
15	9.72

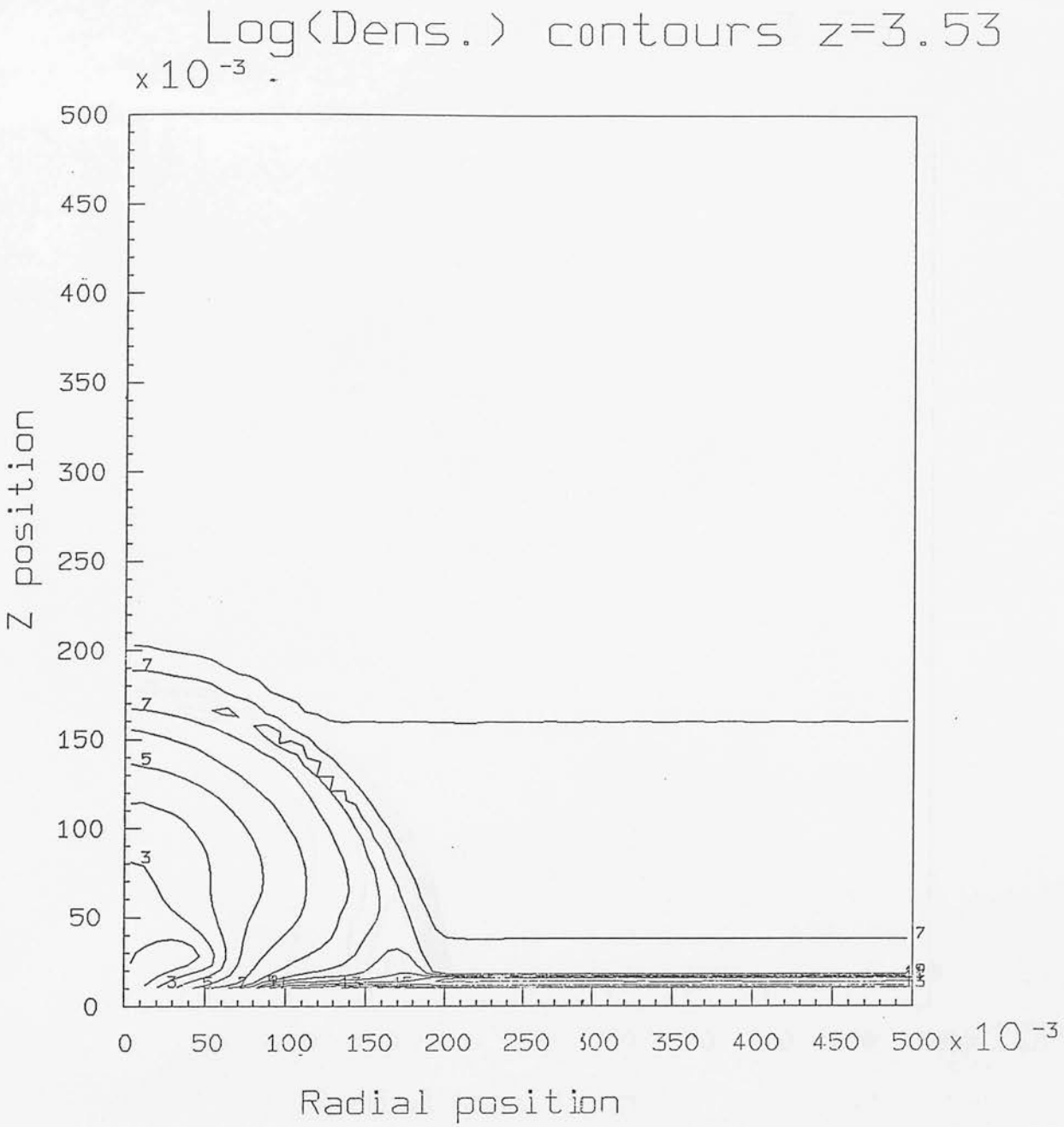

Contour No.	Contour level
1	-26.62
4	-25.91
7	-25.21
11	-24.26
15	-23.32

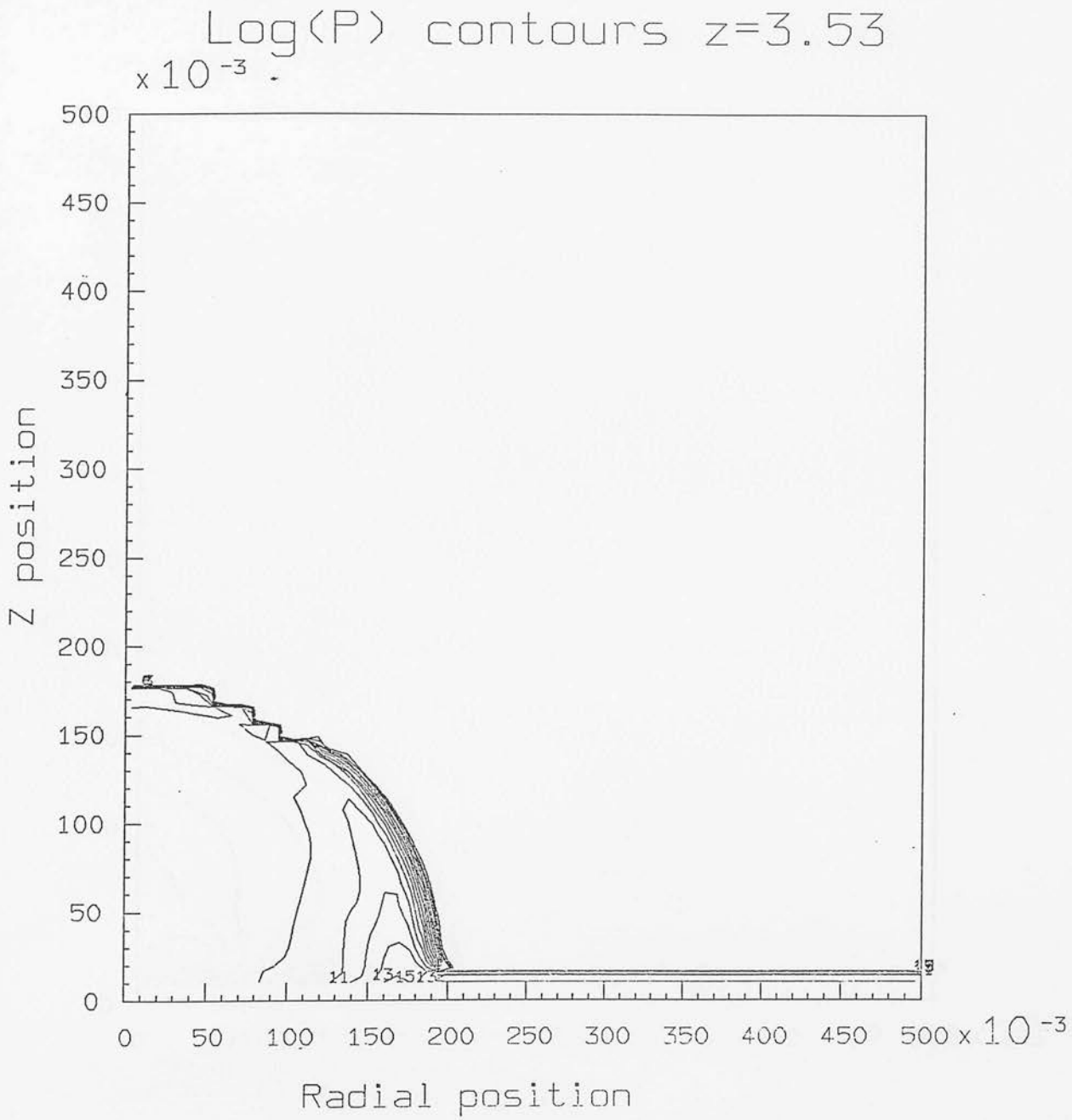

Contour No.	Contour level
1	-15.00
4	-14.39
7	-13.77
11	-12.95
15	-12.13

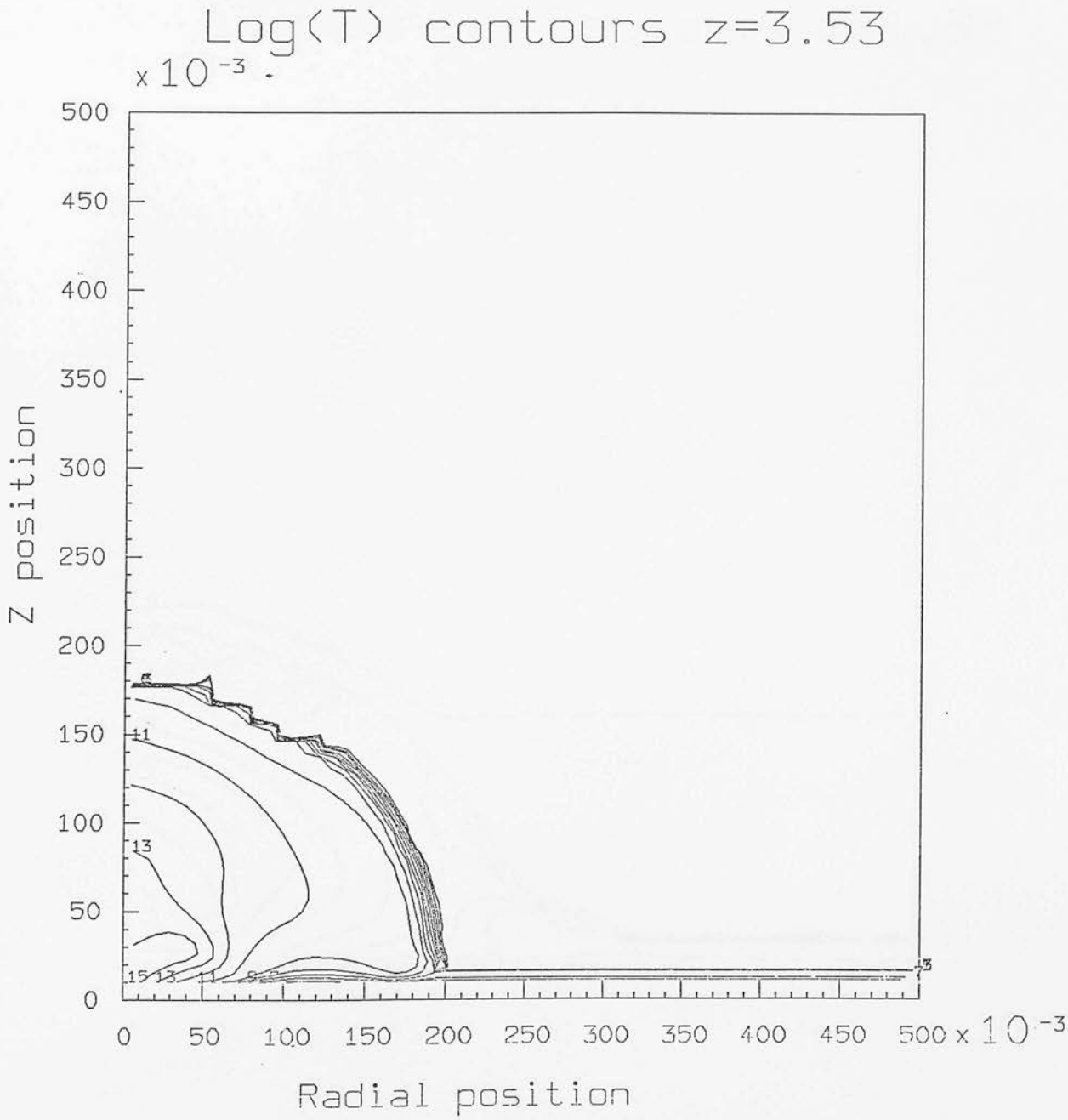

Contour No.	Contour level
1	5.50
4	6.29
7	7.09
11	8.14
15	9.20

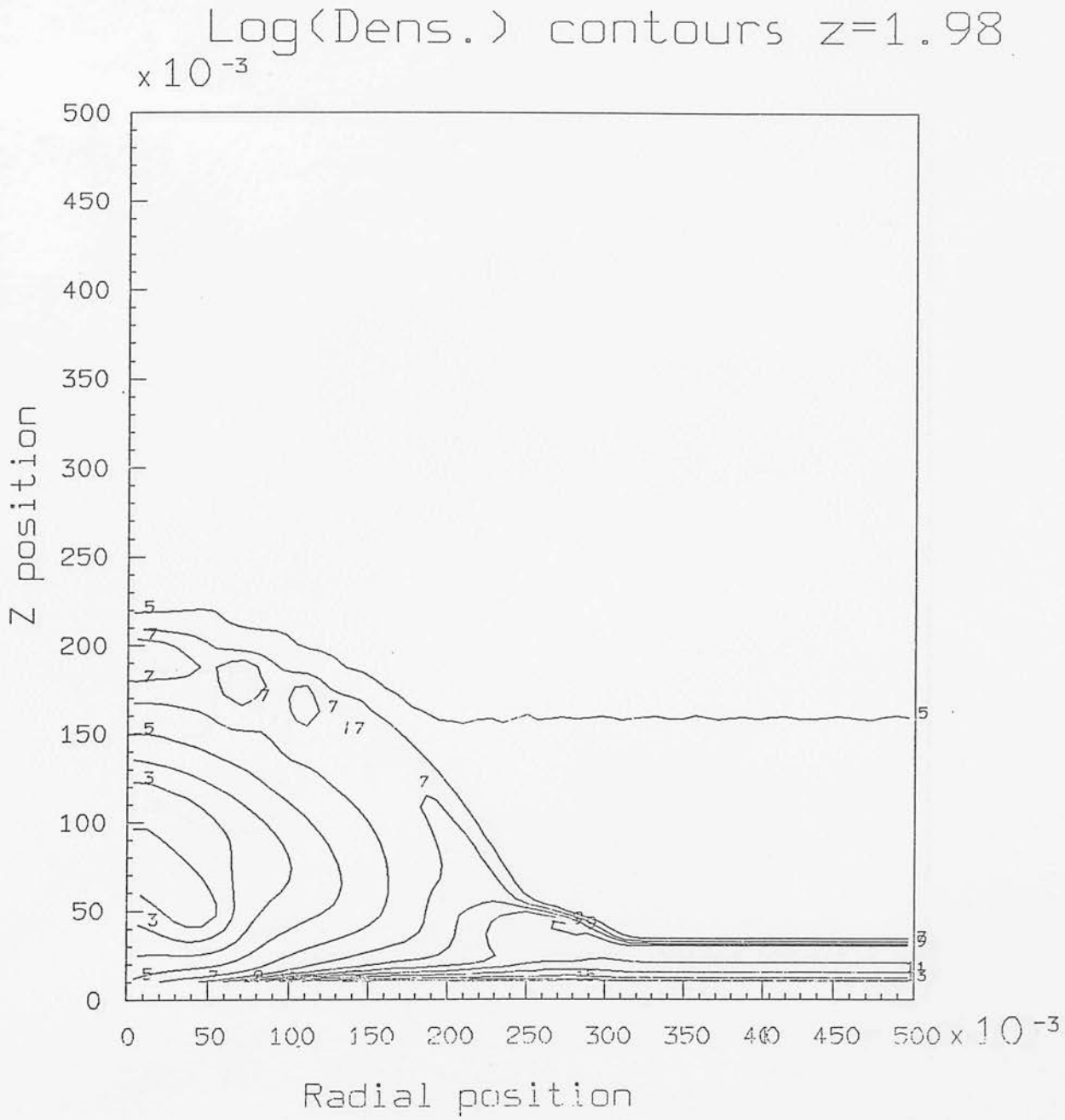

Contour No.	Contour level
1	-27.06
4	-26.37
7	-25.69
11	-24.78
15	-23.87

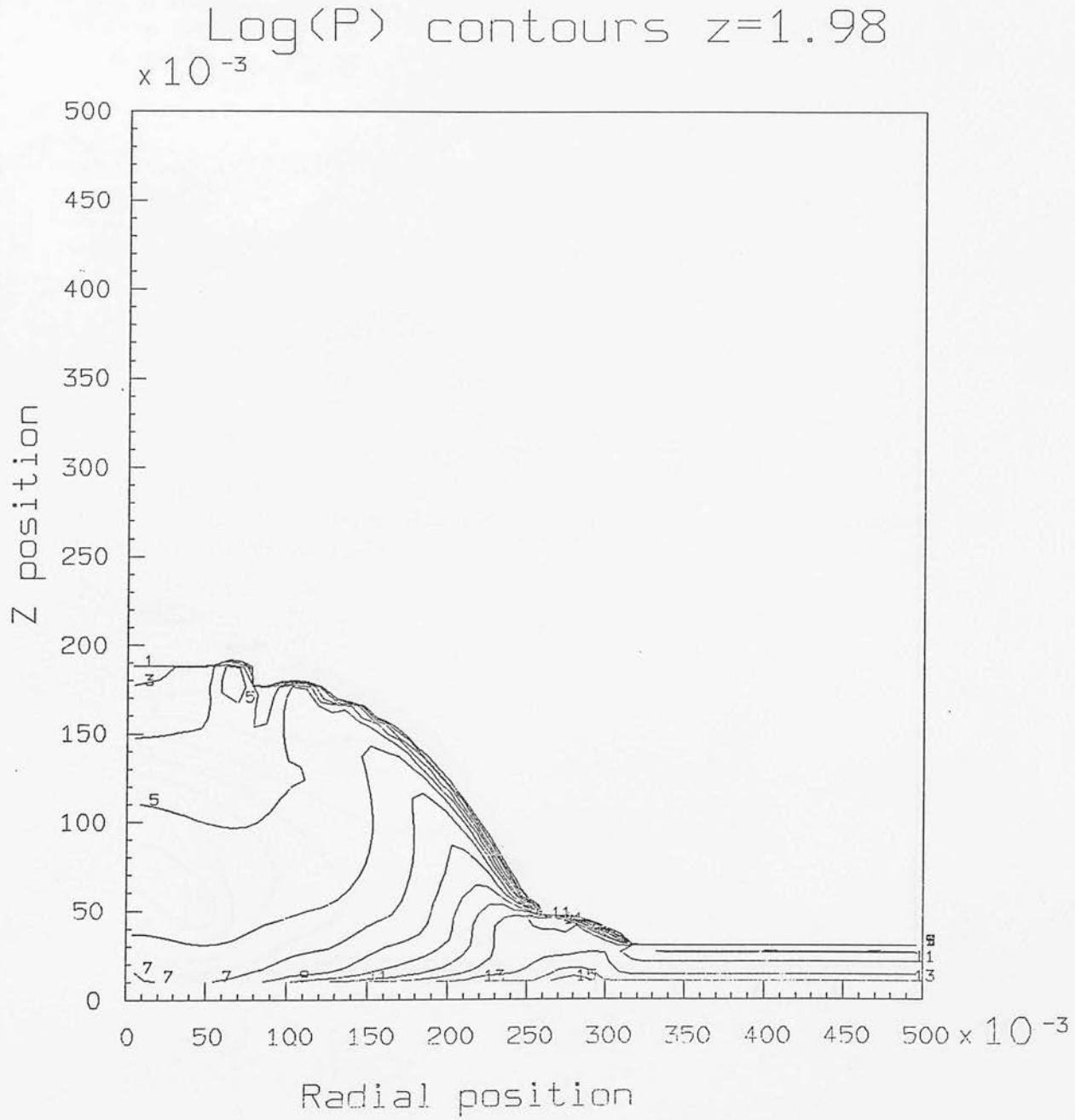

Contour No.	Contour level
1	-15.00
4	-14.58
7	-14.16
11	-13.59
15	-13.03

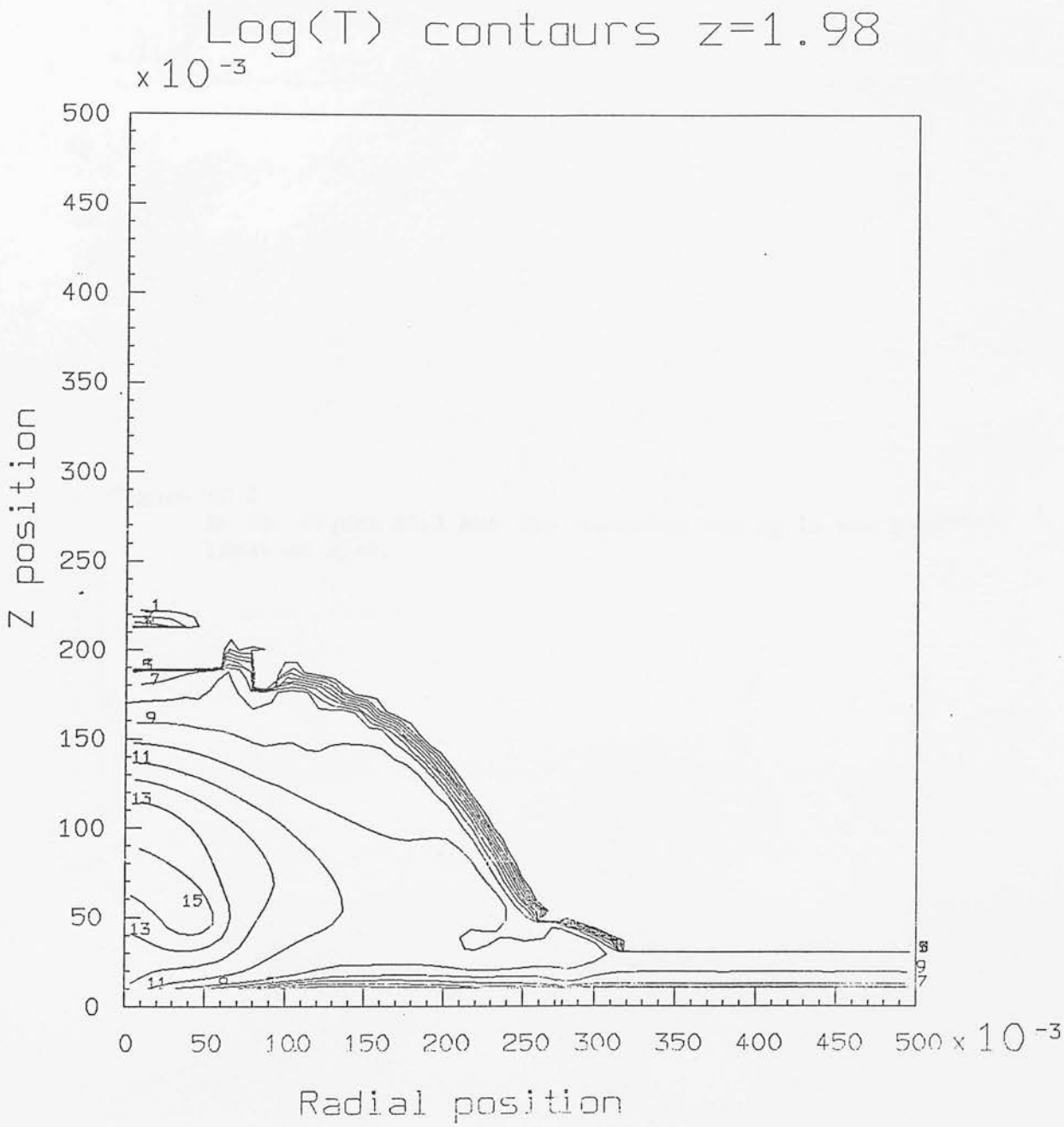

Contour No.	Contour level
1	5.50
4	6.15
7	6.80
11	7.67
15	8.54

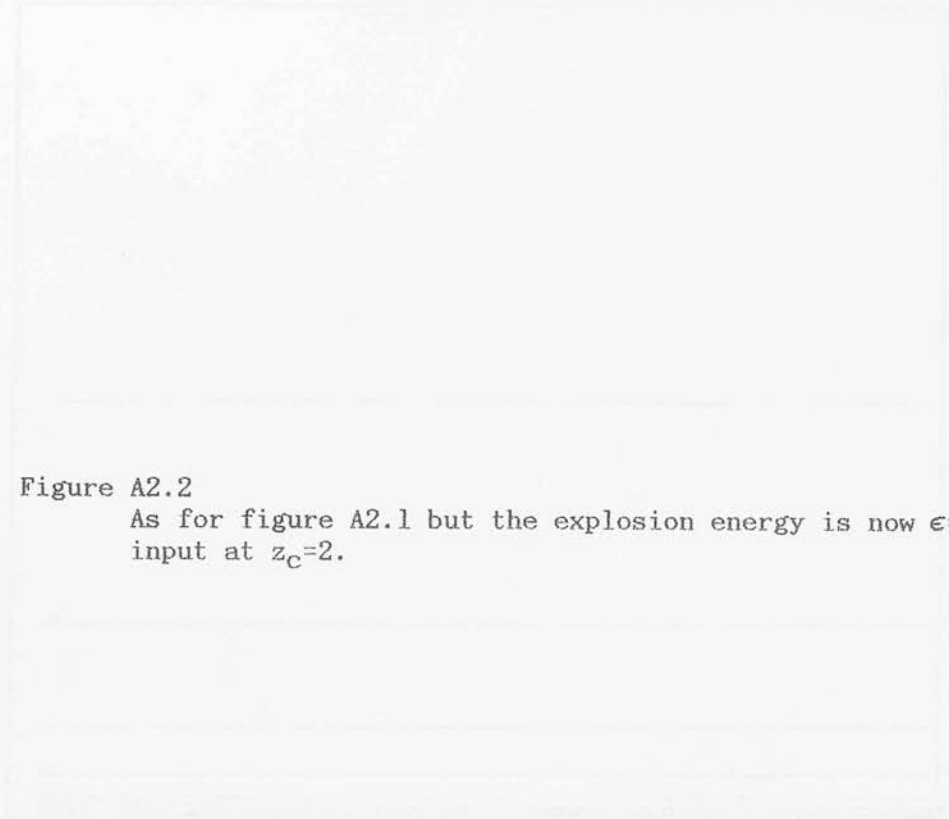

Figure A2.2
As for figure A2.1 but the explosion energy is now $\epsilon=10^{-1.5}$ input at $z_c=2$.

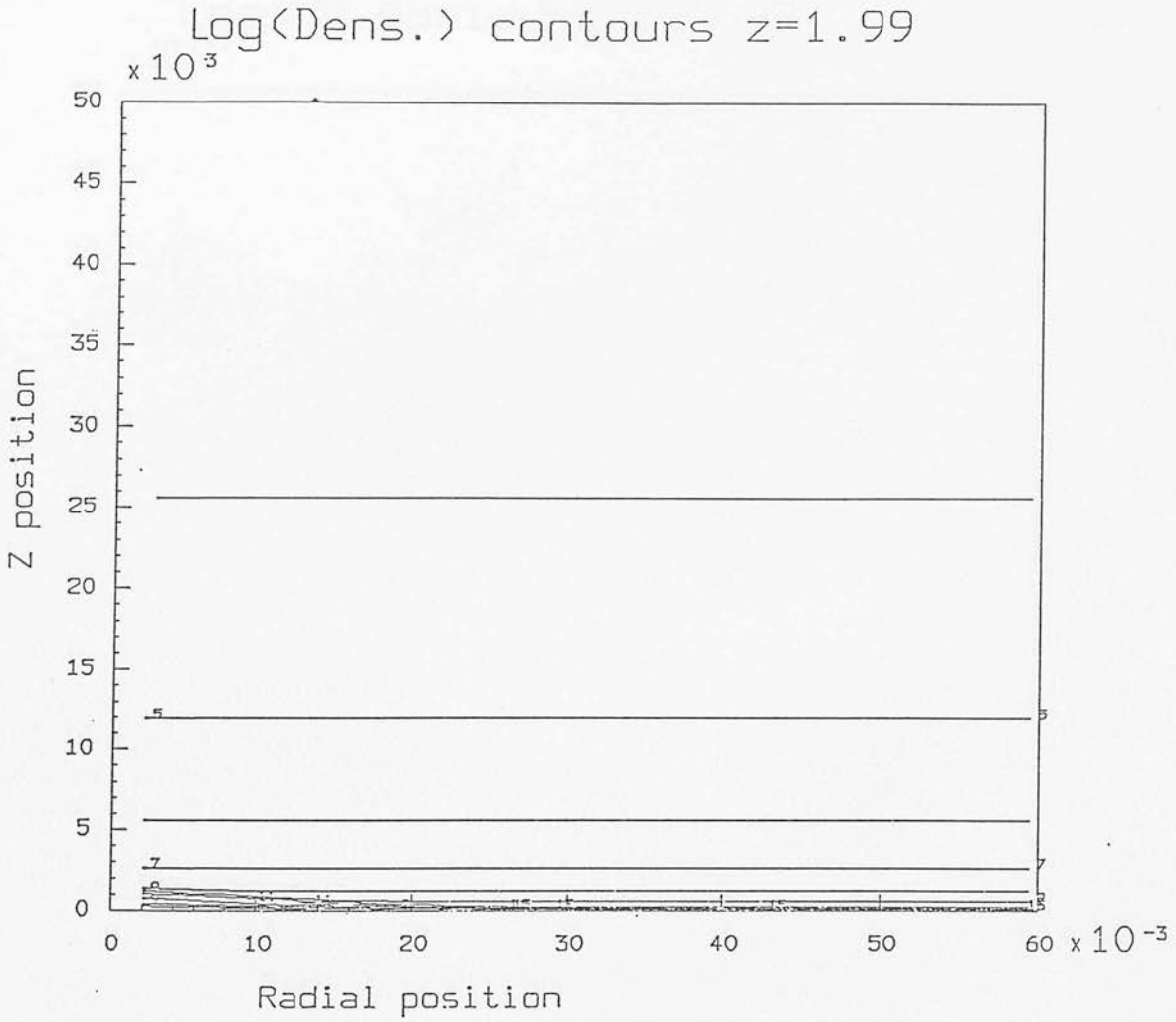

Contour No.	Contour level
1	-26.05
4	-25.42
7	-24.79
11	-23.95
15	-23.11

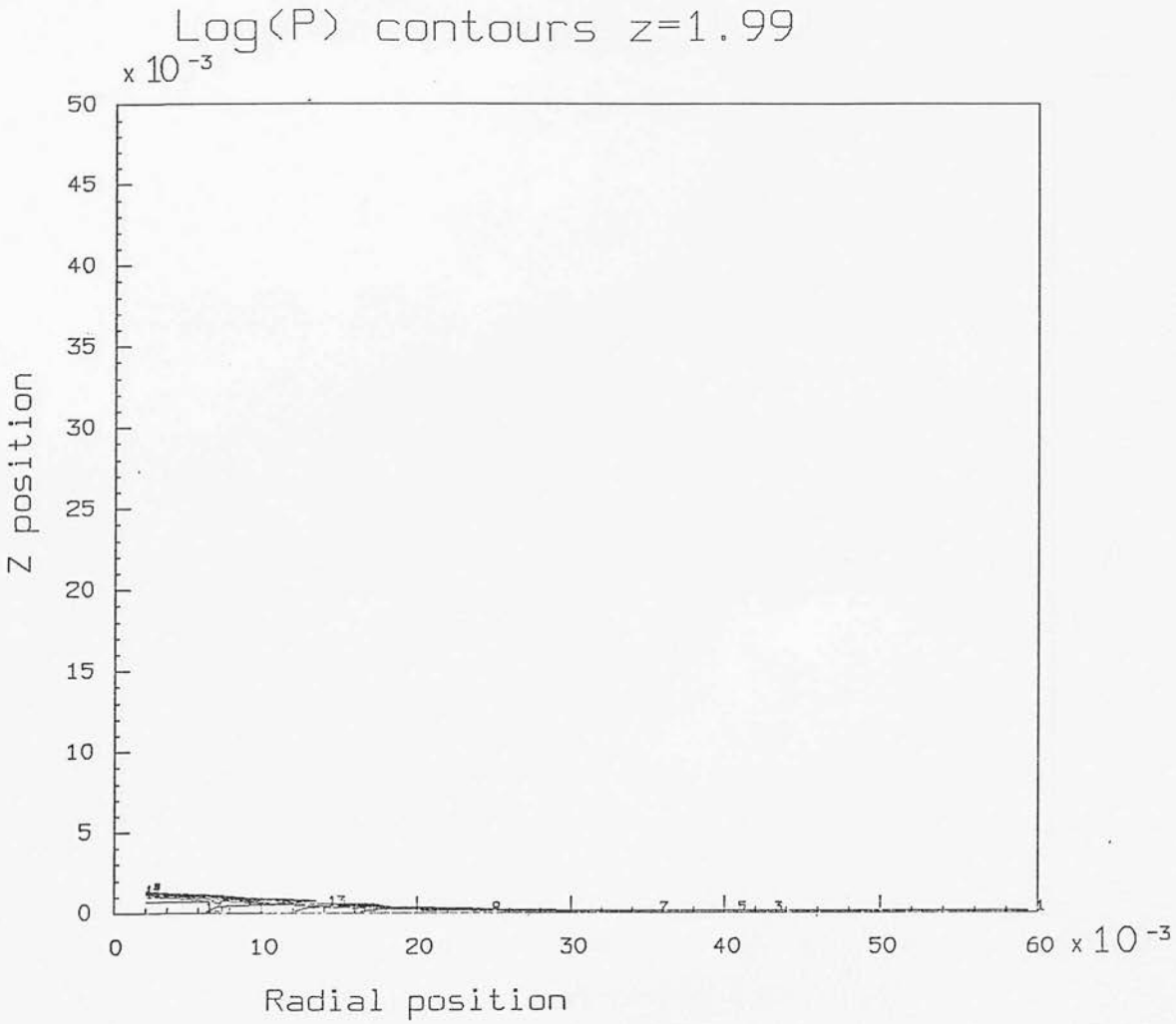

Contour No.	Contour level
1	-15.00
4	-14.43
7	-13.86
11	-13.10
15	-12.34

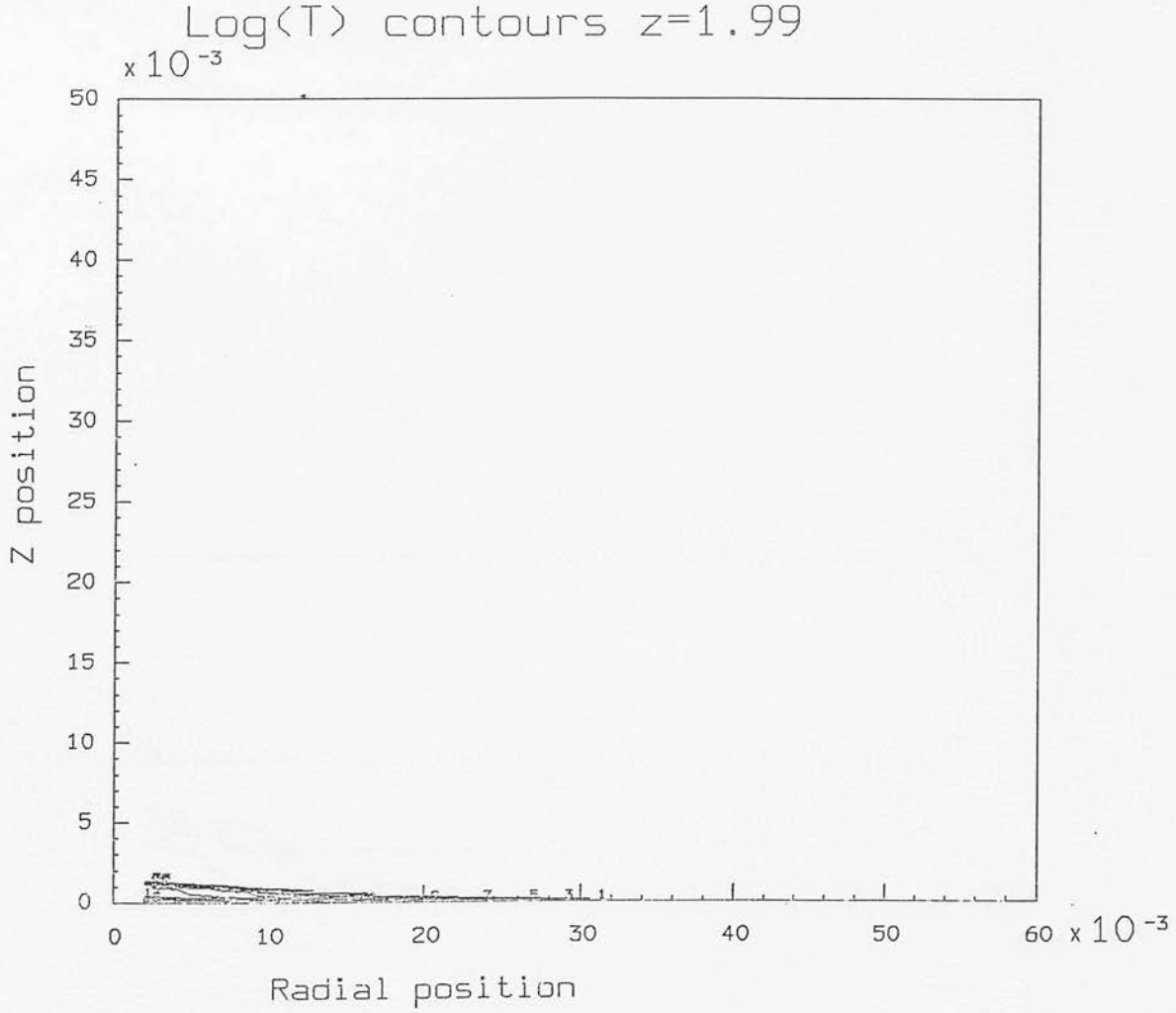

Contour No.	Contour level
1	5.50
4	6.03
7	6.57
11	7.28
15	7.99

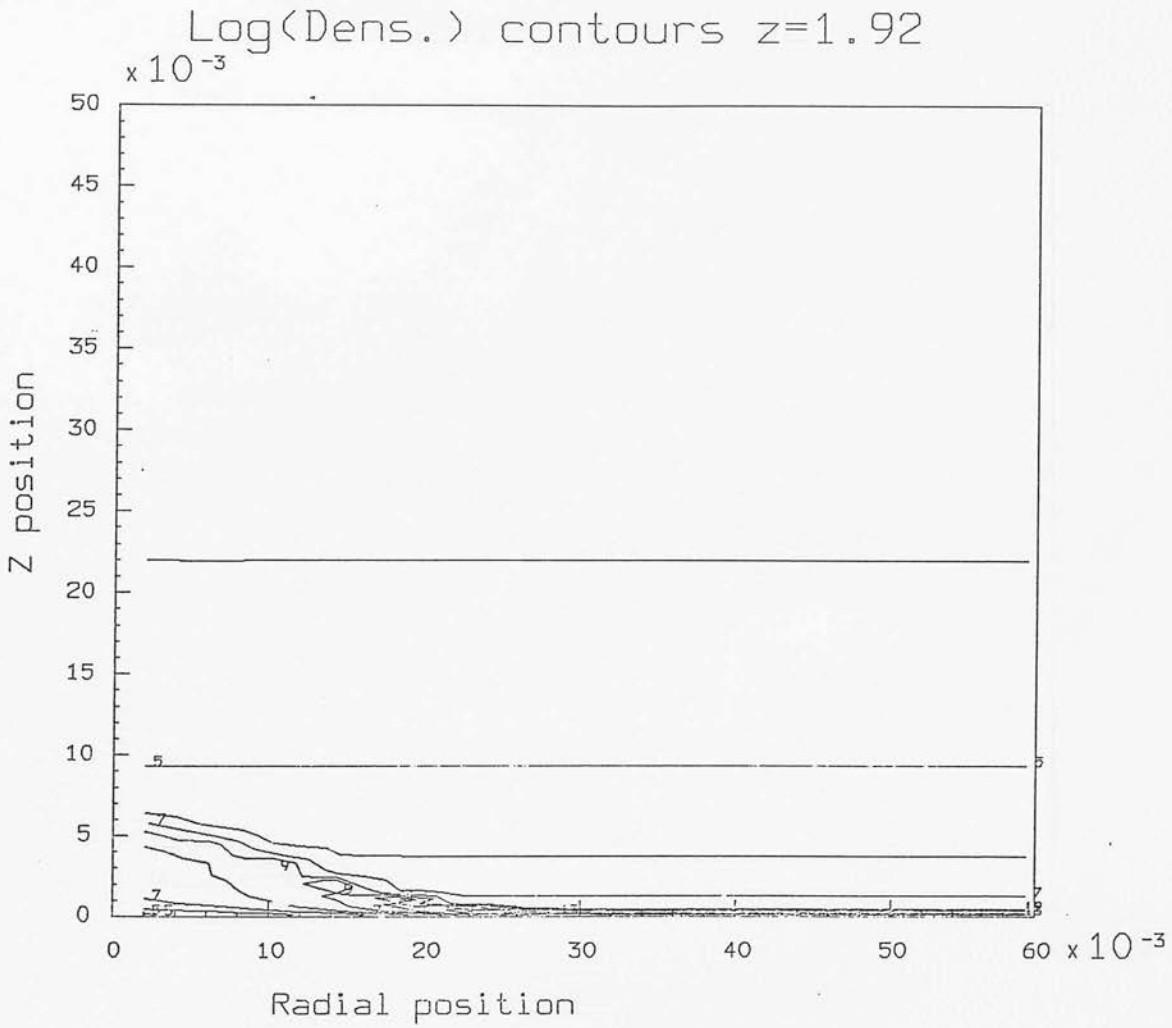

Contour No.	Contour level
1	-26.09
4	-25.44
7	-24.78
11	-23.91
15	-23.03

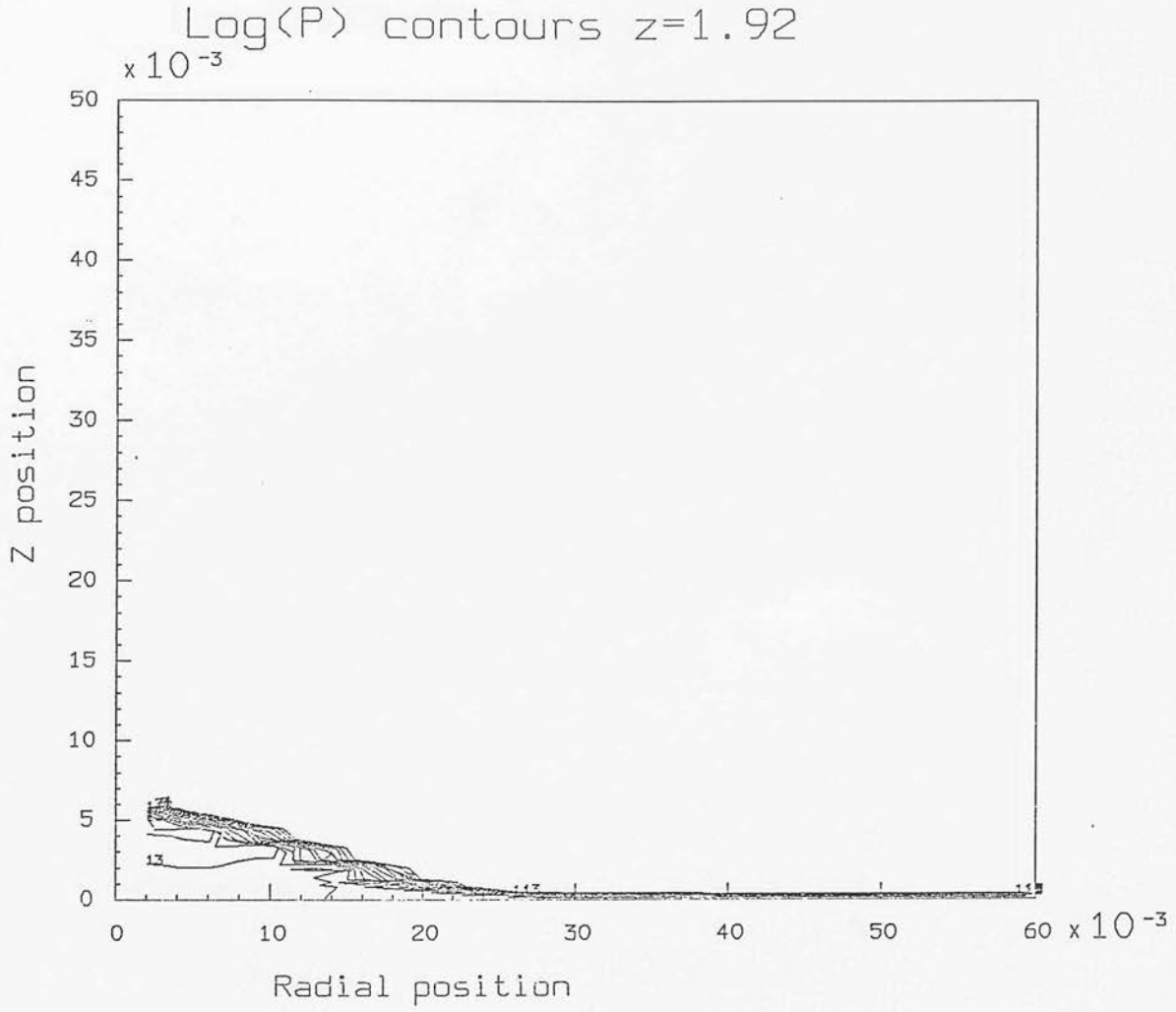

Contour No.	Contour level
1	-15.00
4	-14.59
7	-14.18
11	-13.64
15	-13.10

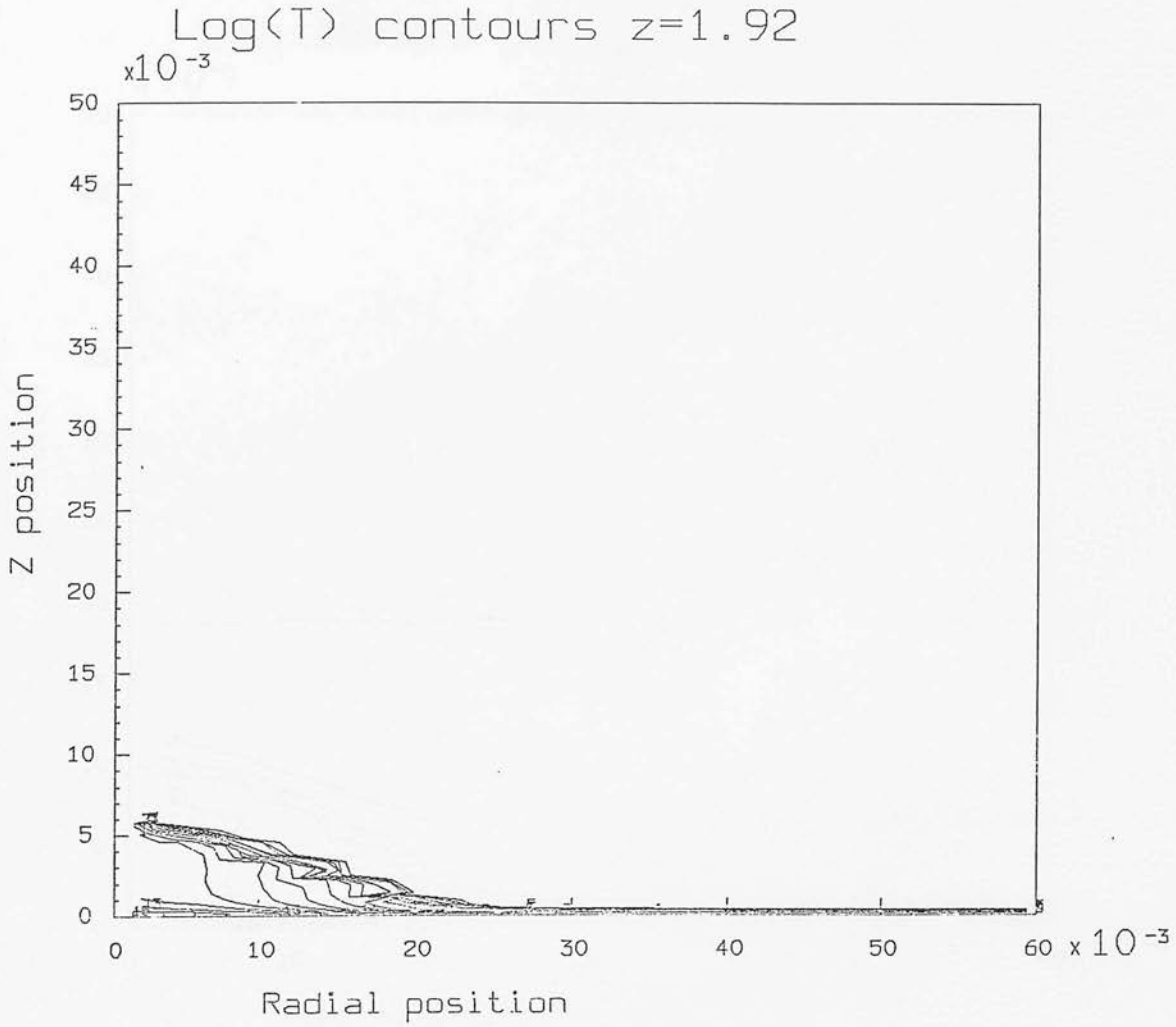

Contour No.	Contour level
1	5.50
4	5.97
7	6.44
11	7.07
15	7.69

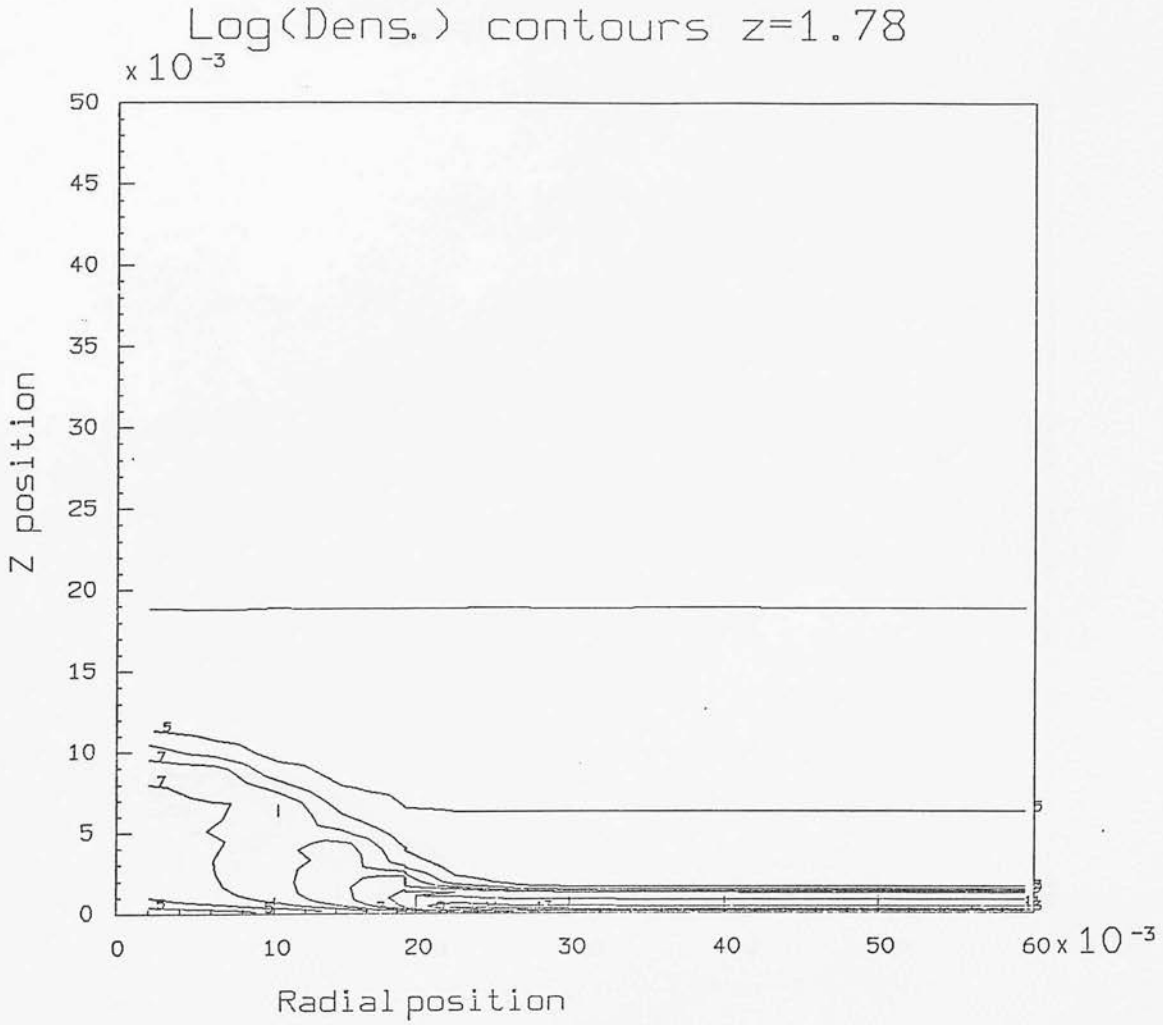

Contour No.	Contour level
1	-26.17
4	-25.52
7	-24.87
11	-24.00
15	-23.14

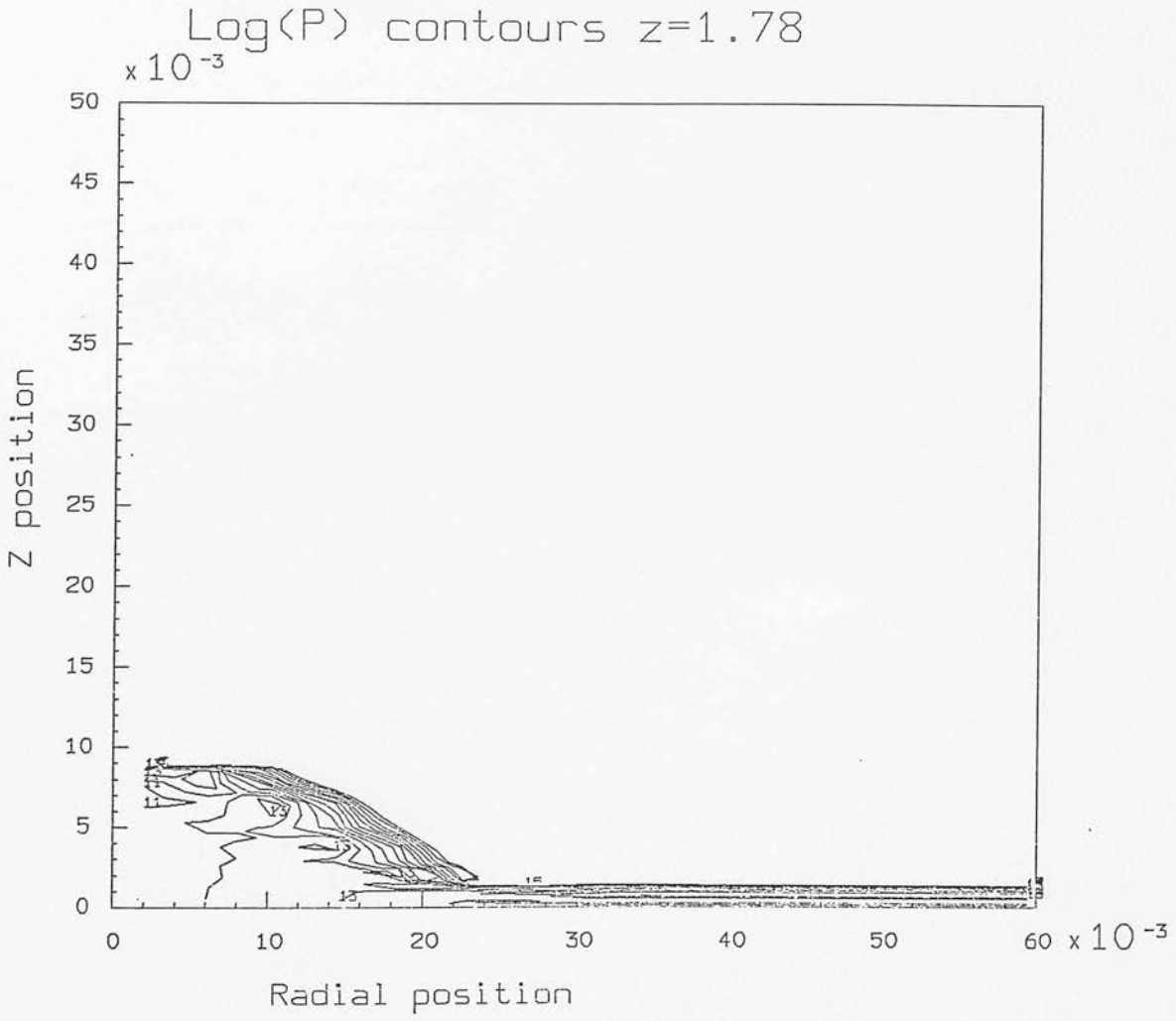

Contour No.	Contour level
1	-15.00
4	-14.67
7	-14.34
11	-13.90
15	-13.45

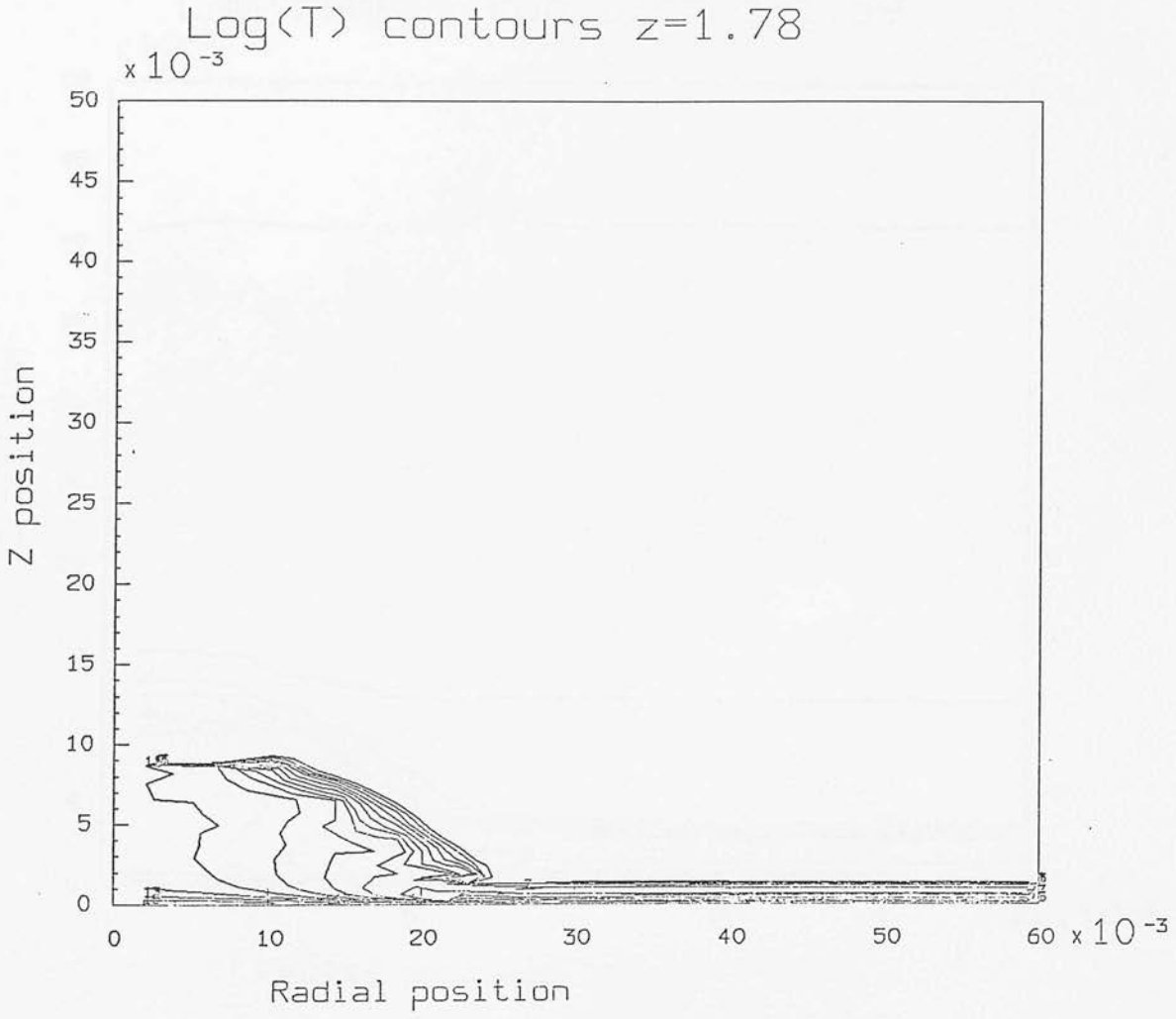

Contour No.	Contour level
1	5.50
4	5.93
7	6.36
11	6.94
15	7.52

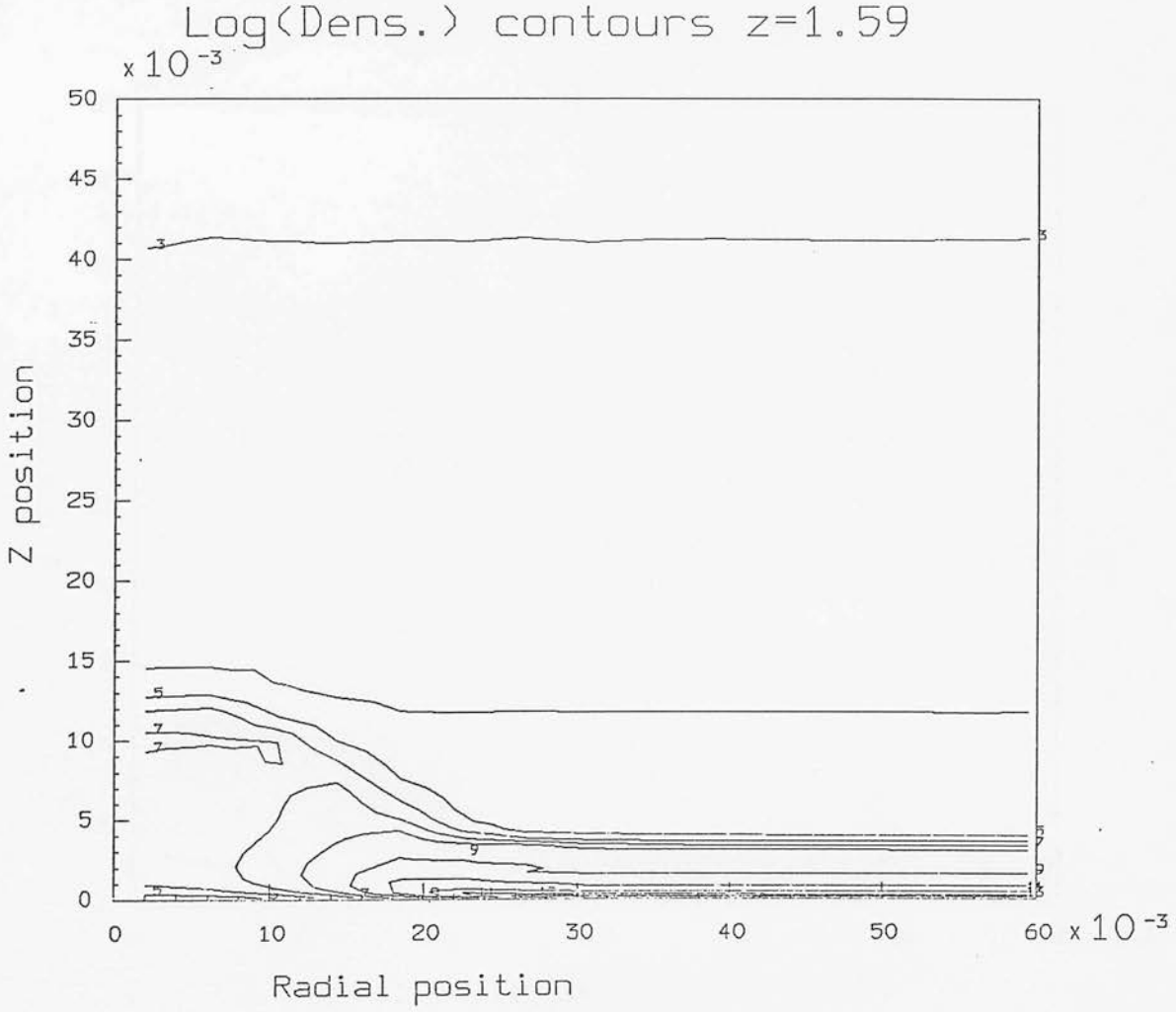

Contour No.	Contour level
1	-26.28
4	-25.63
7	-24.98
11	-24.11
15	-23.24

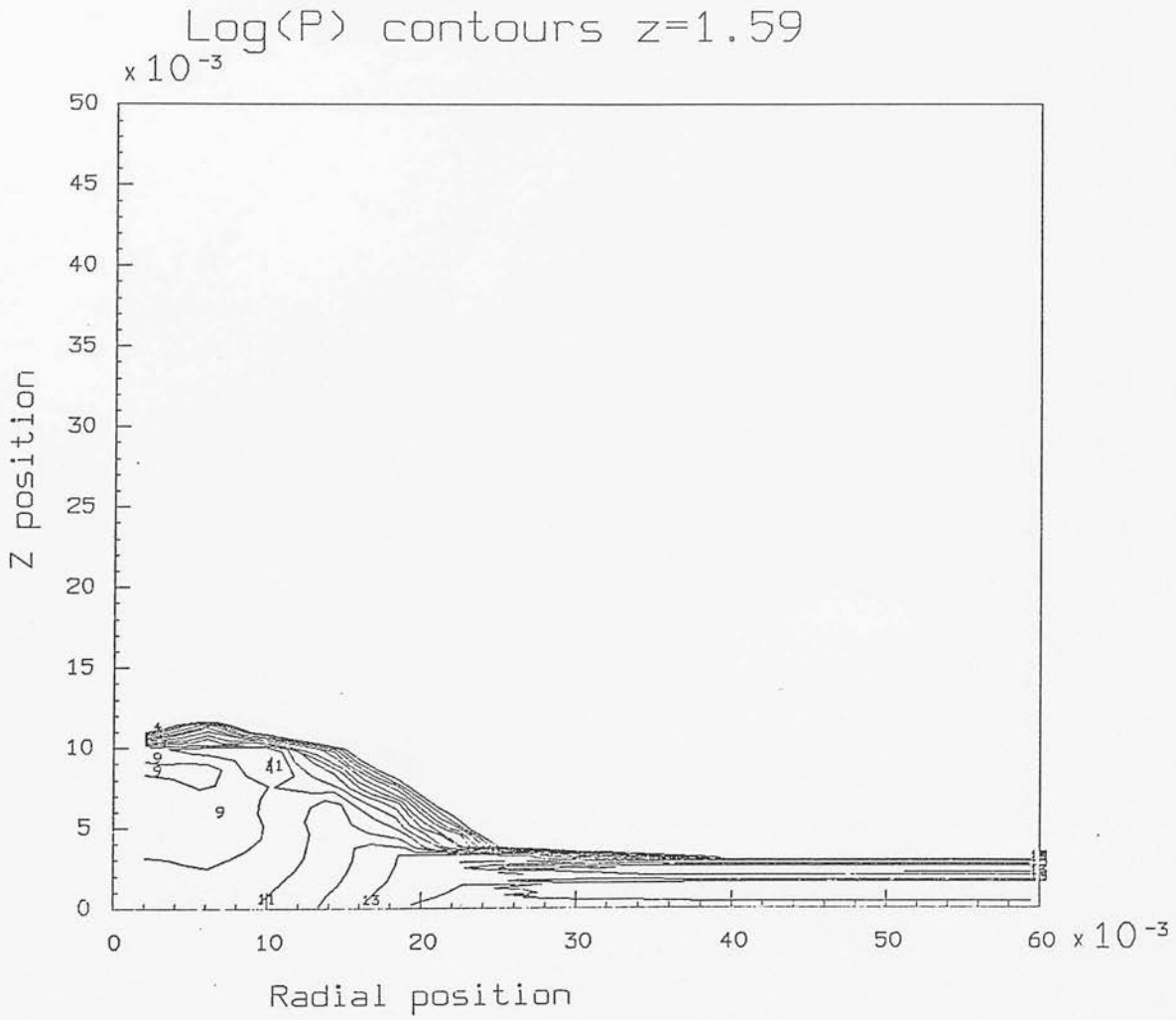

Contour No.	Contour level
1	-15.00
4	-14.69
7	-14.39
11	-13.98
15	-13.57

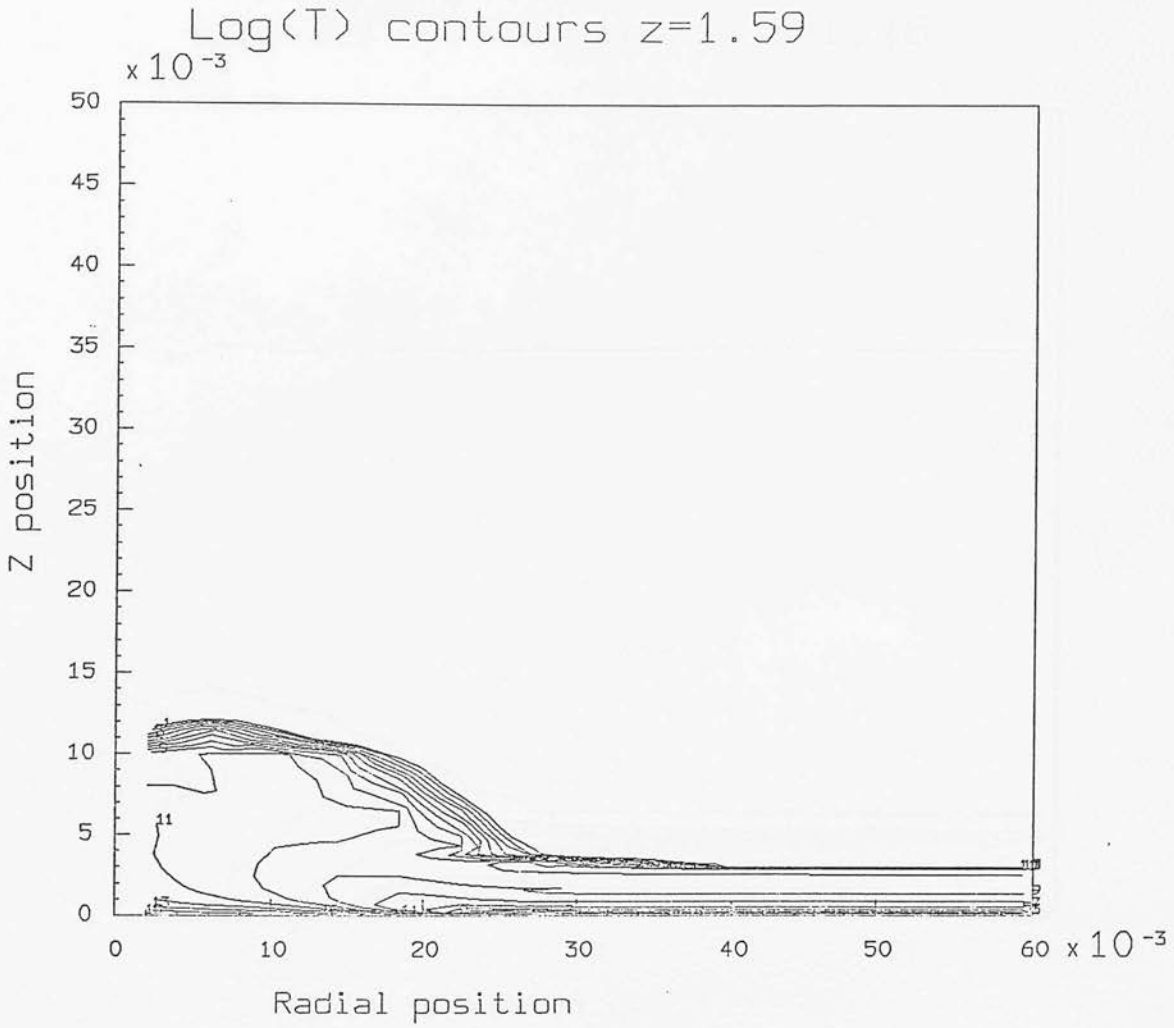

Contour No.	Contour level
1	5.50
4	5.92
7	6.33
11	6.89
15	7.44

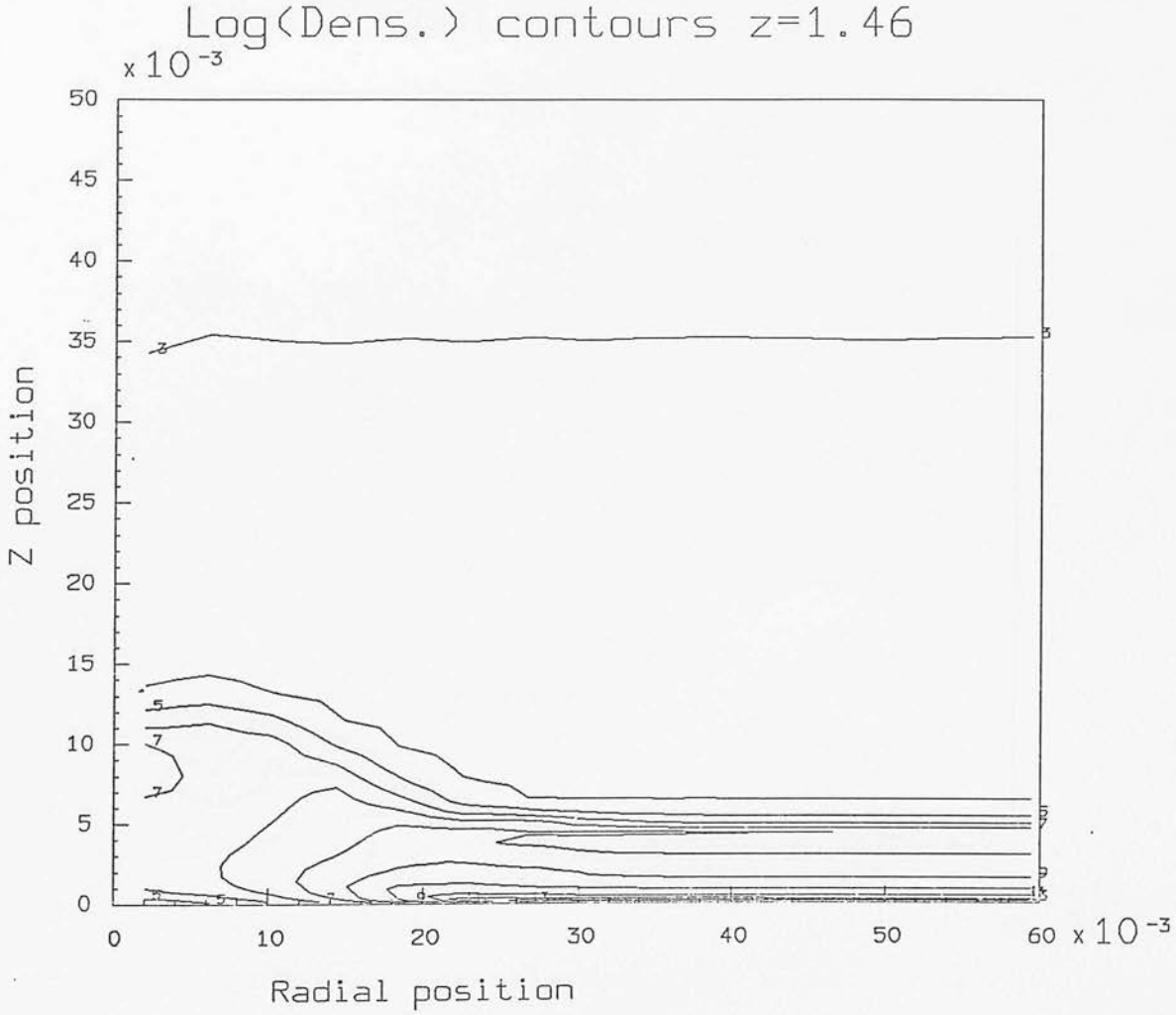

Contour No.	Contour level
1	-26.35
4	-25.70
7	-25.04
11	-24.17
15	-23.29

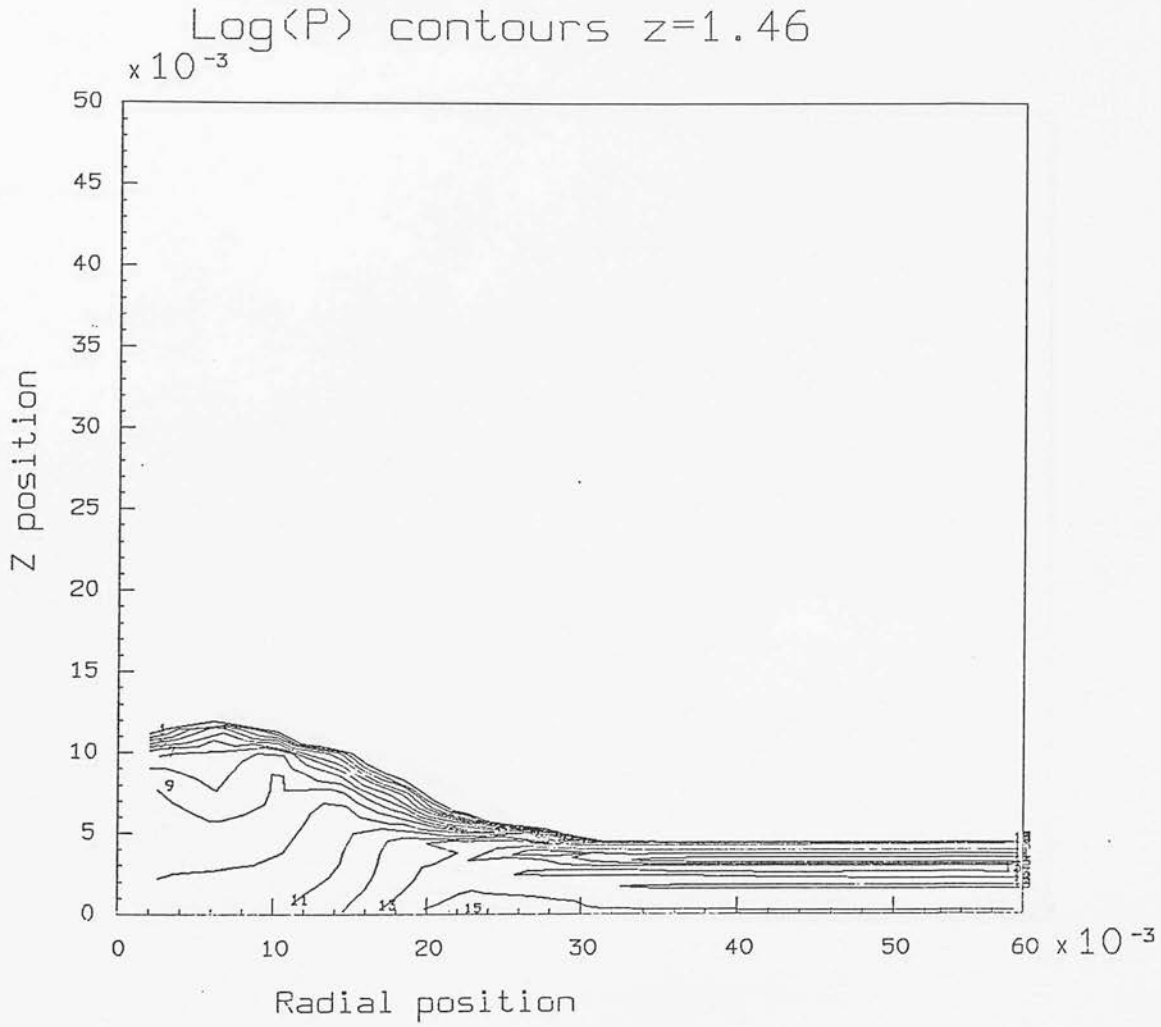

Contour No.	Contour level
1	-15.00
4	-14.71
7	-14.41
11	-14.02
15	-13.63

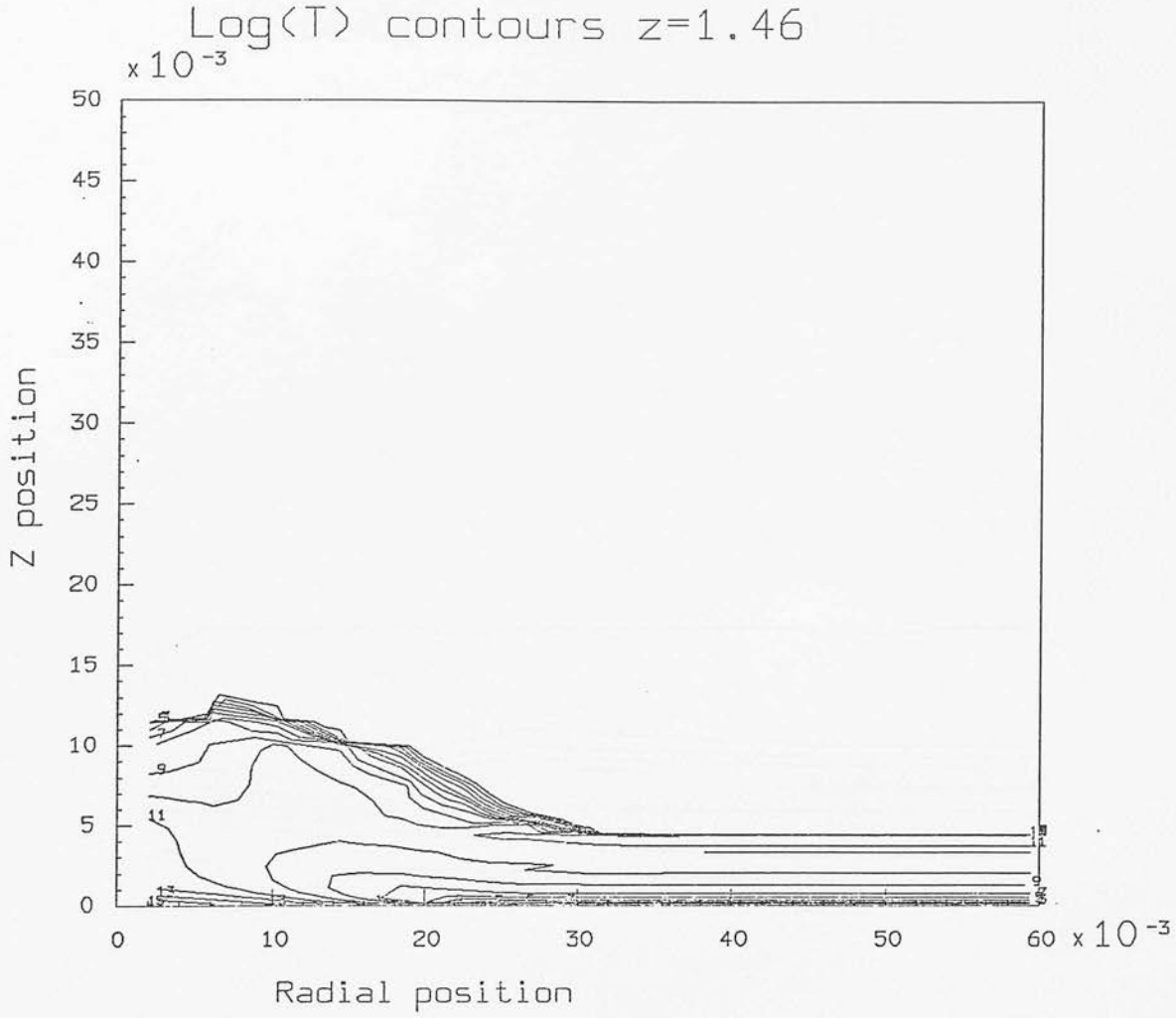

Contour No.	Contour level
1	5.50
4	5.90
7	6.31
11	6.84
15	7.38

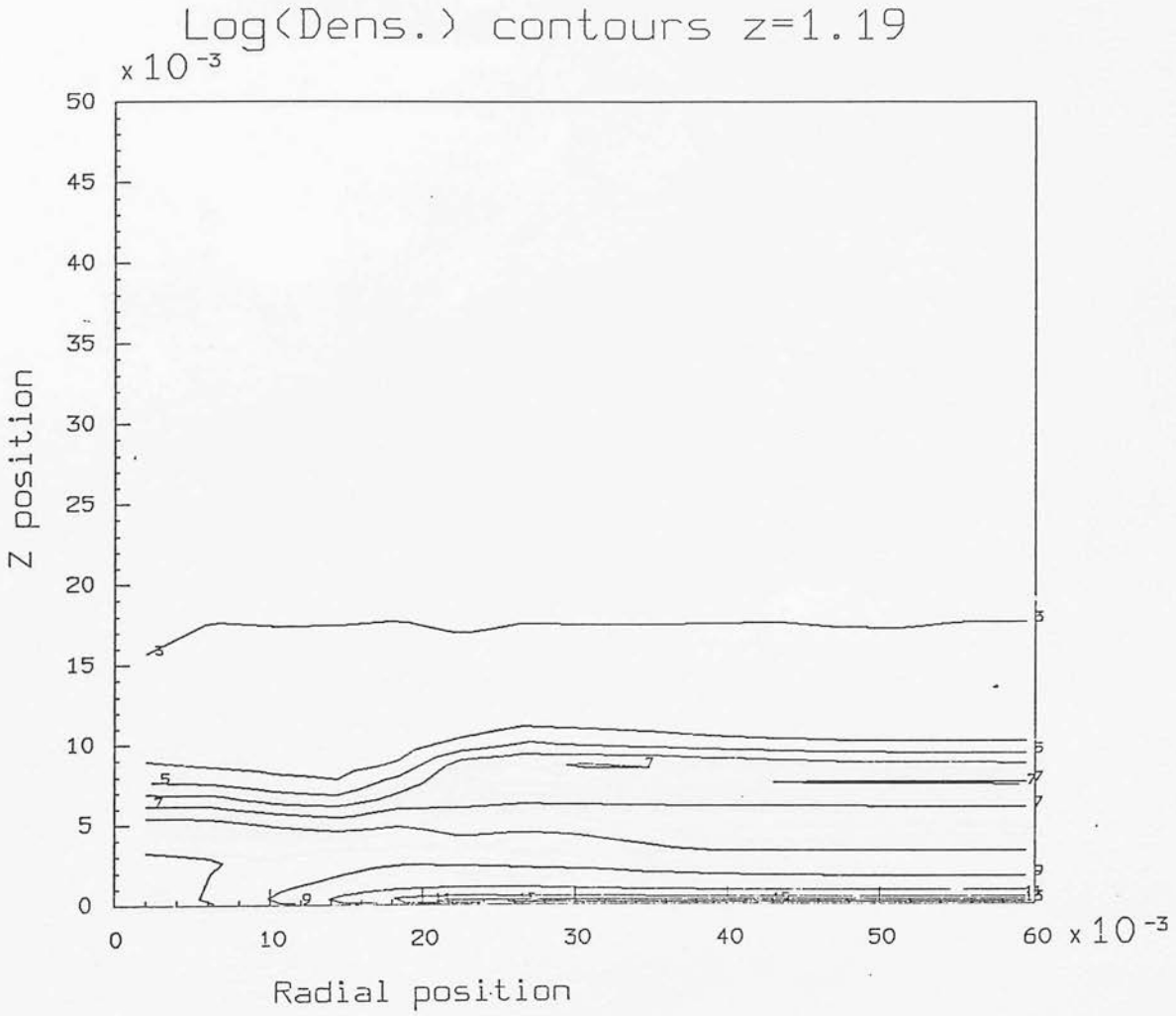

Contour No.	Contour level
1	-26.54
4	-25.87
7	-25.21
11	-24.31
15	-23.42

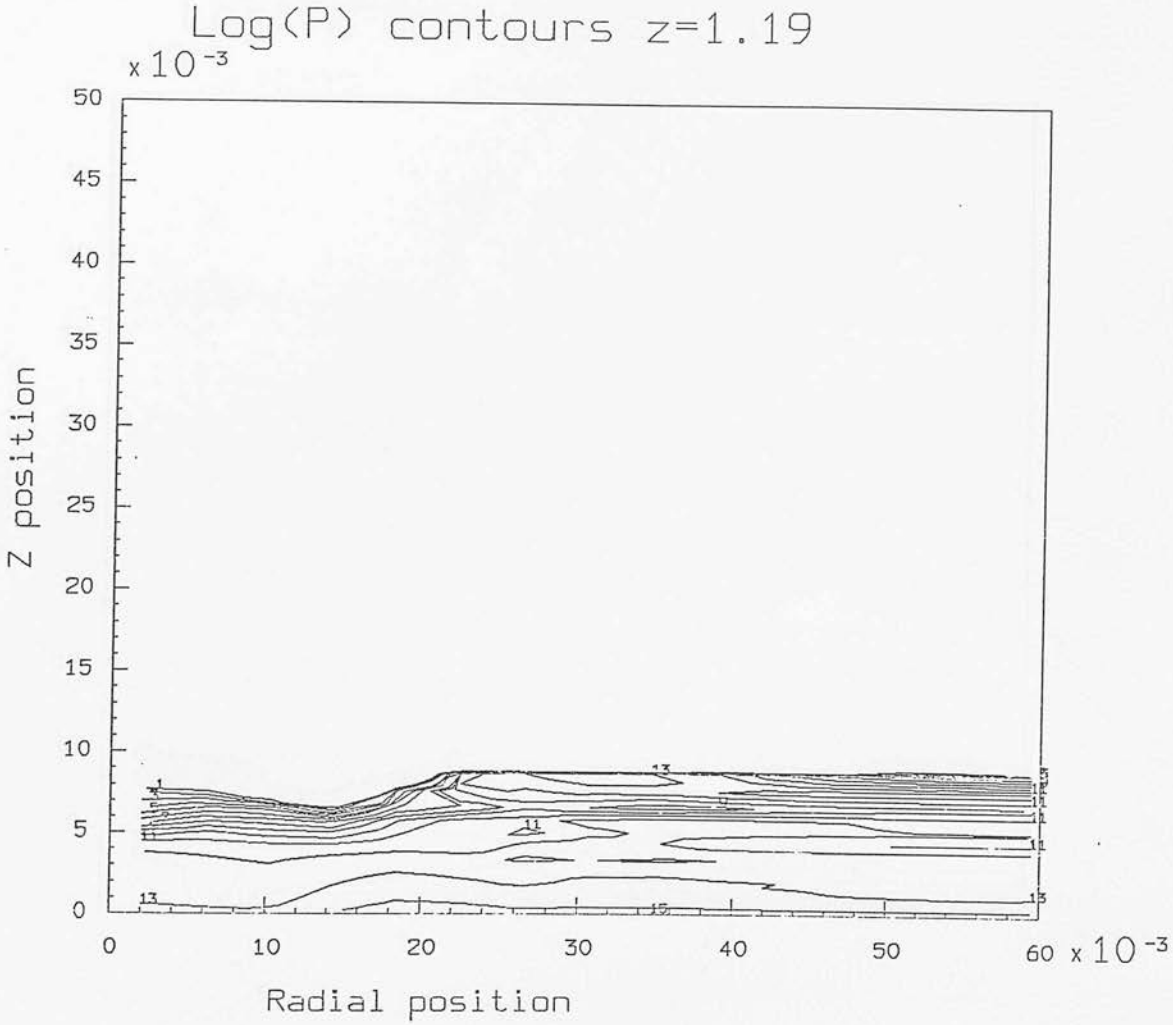

Contour No.	Contour level
1	-15.00
4	-14.74
7	-14.48
11	-14.13
15	-13.78

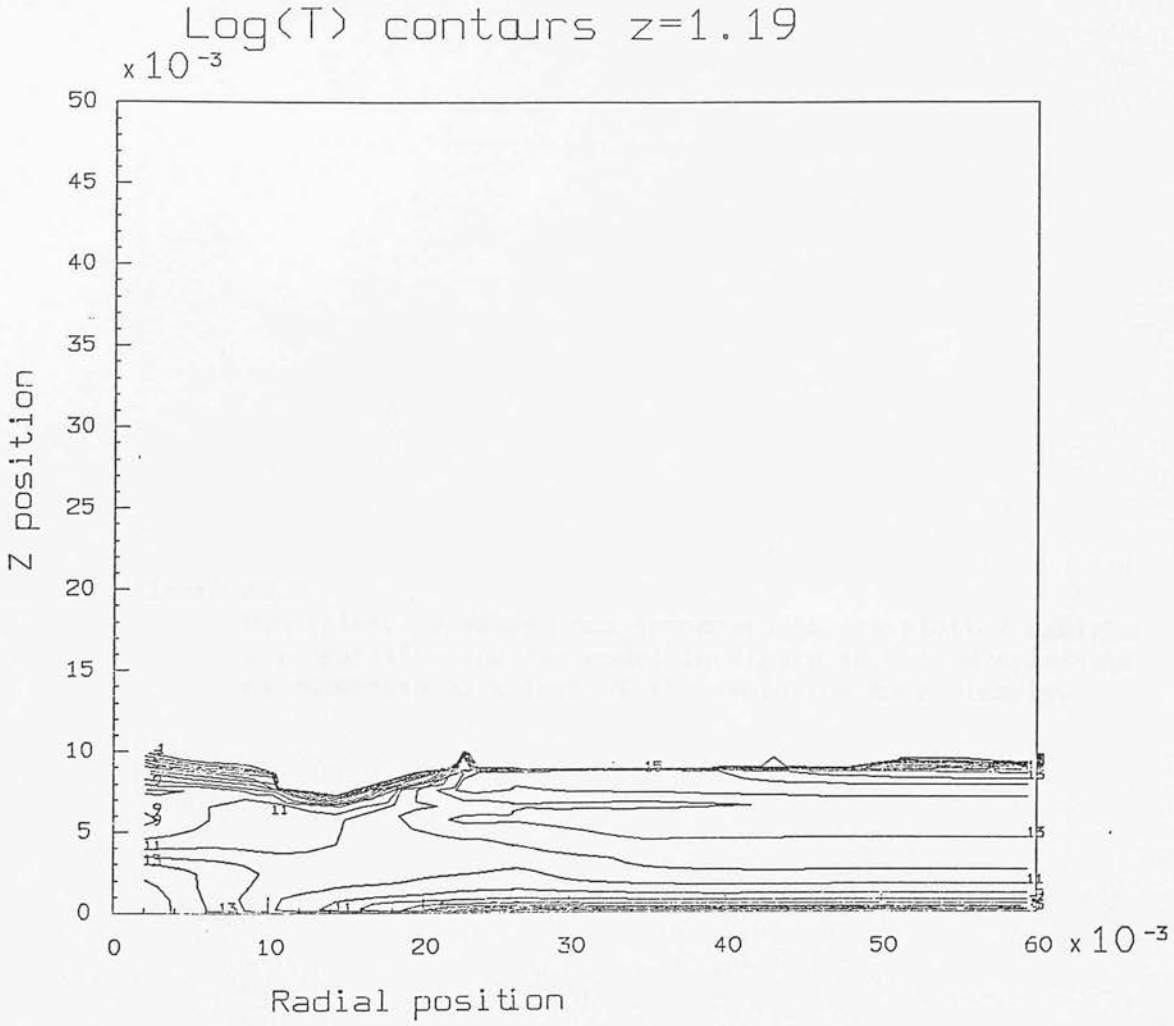

Contour No.	Contour level
1	5.50
4	5.84
7	6.18
11	6.64
15	7.10

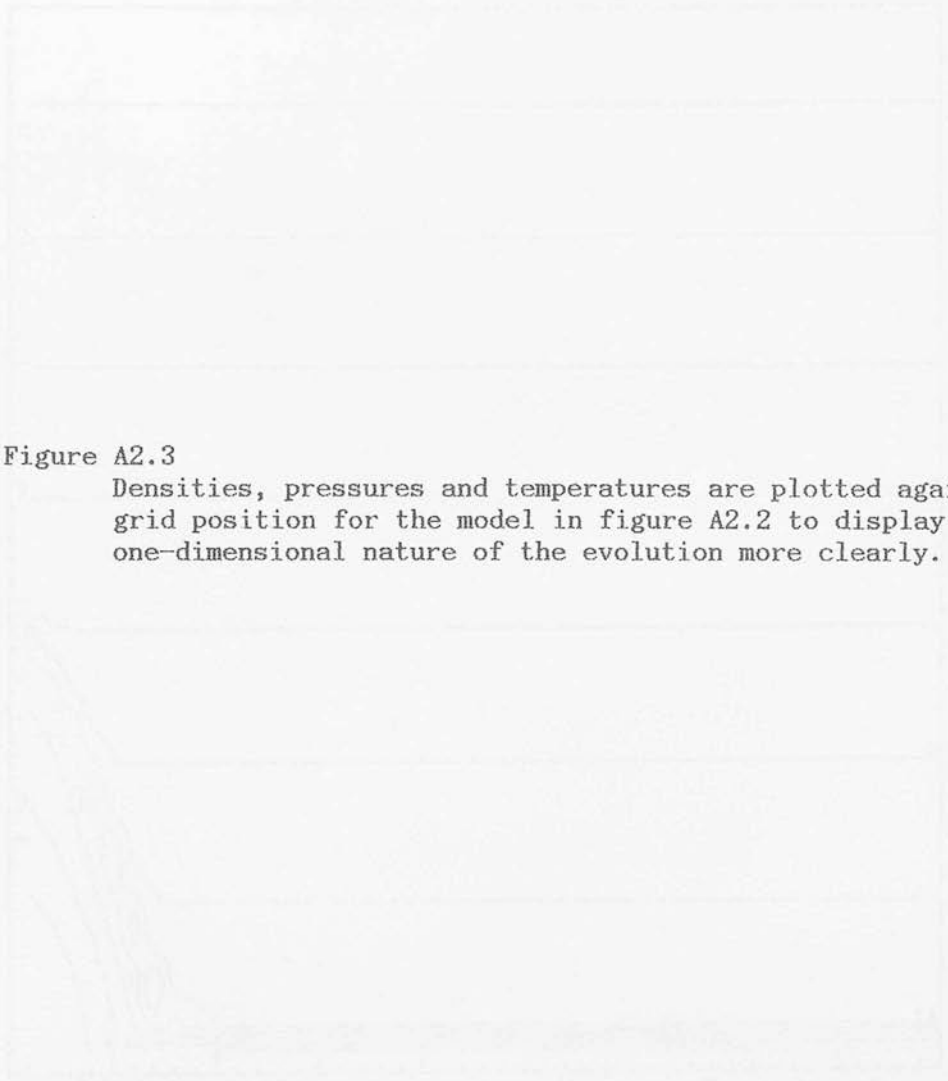

Figure A2.3
Densities, pressures and temperatures are plotted against grid position for the model in figure A2.2 to display the one-dimensional nature of the evolution more clearly.

Log(Dens.) contours z=1.99

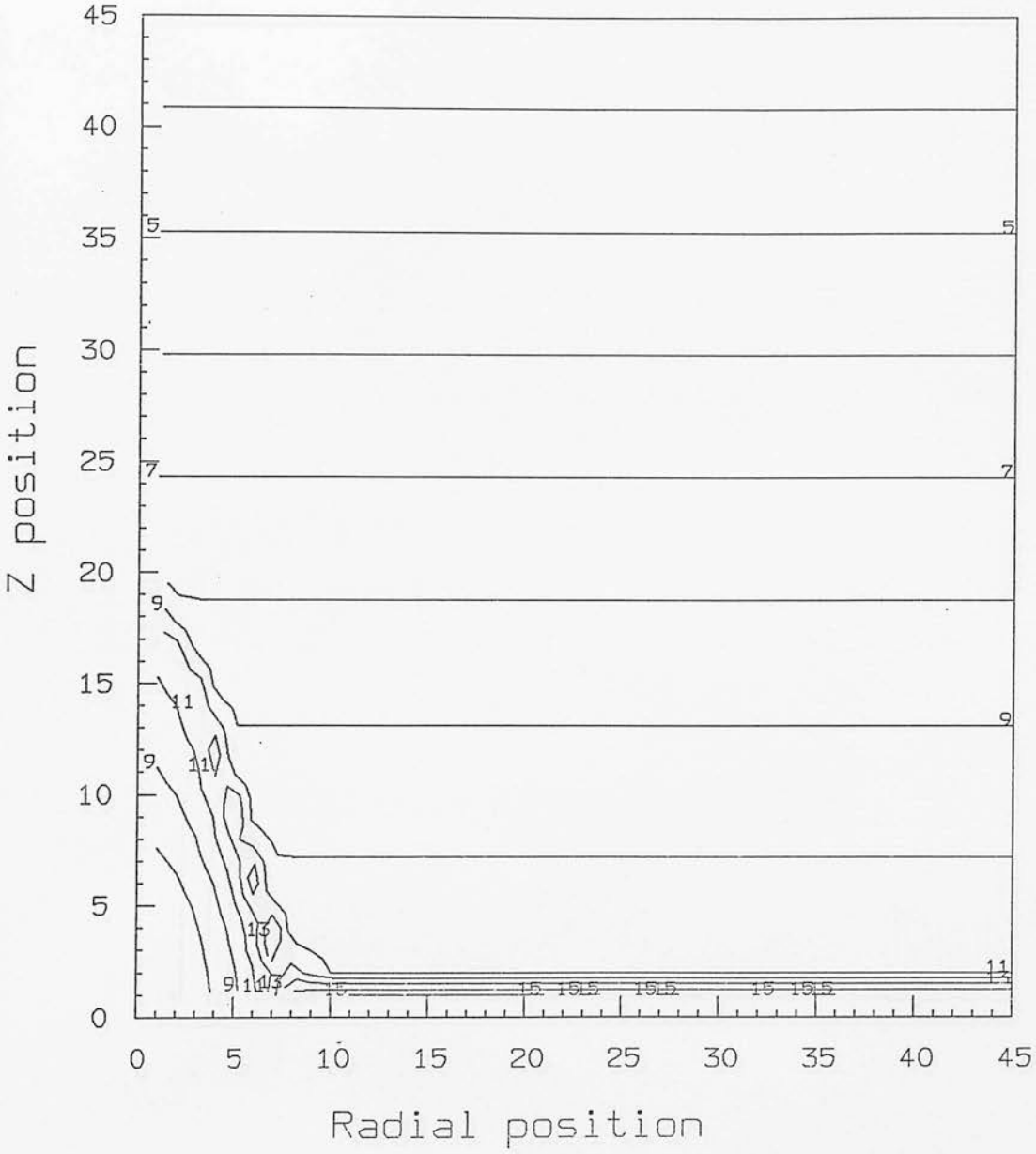

Contour No.	Contour level
1	-26.05
4	-25.42
7	-24.79
11	-23.95
15	-23.11

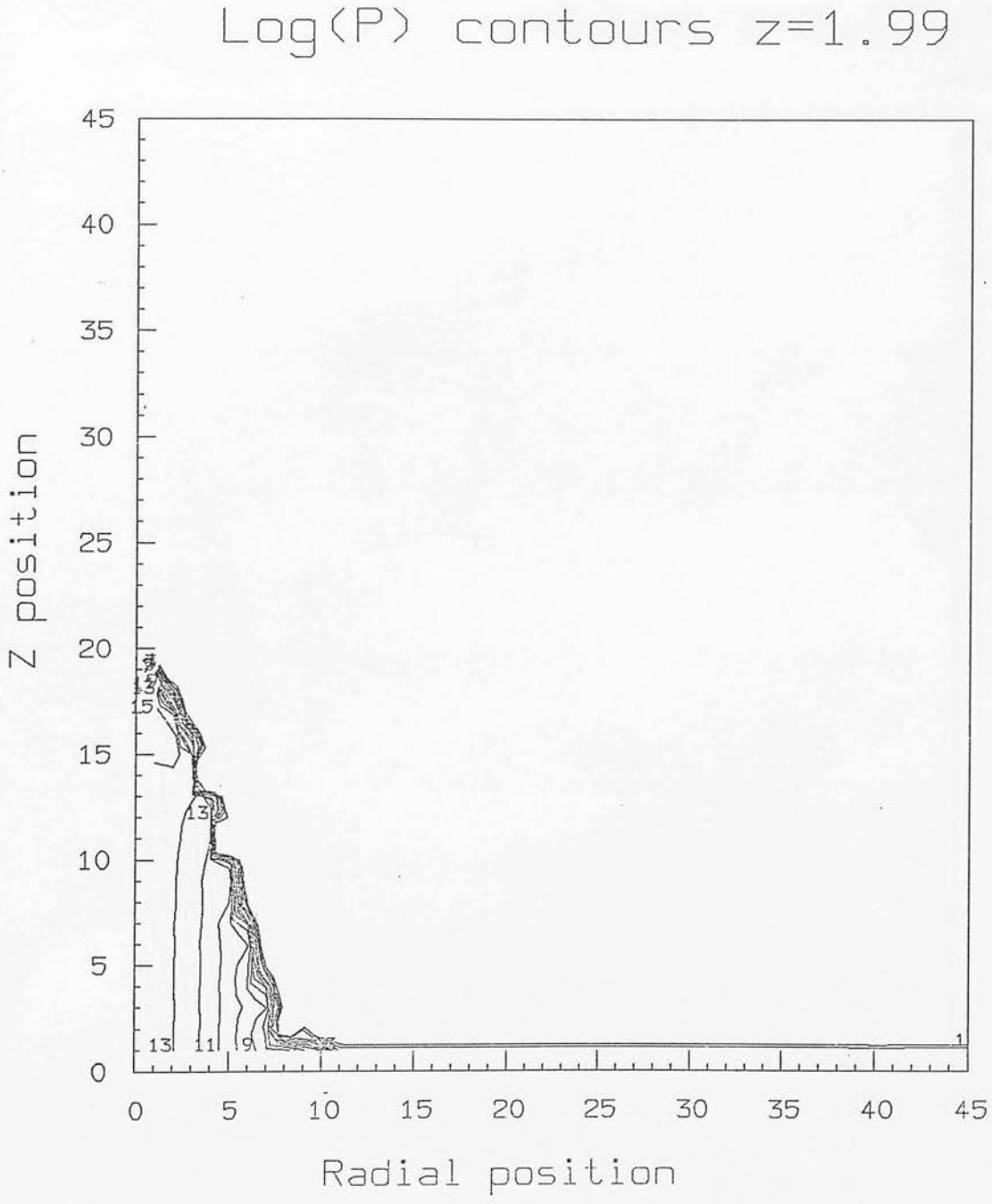

Contour No.	Contour level
1	5.50
4	6.03
7	6.57
11	7.28
15	7.99

Log(T) contours z=1.99

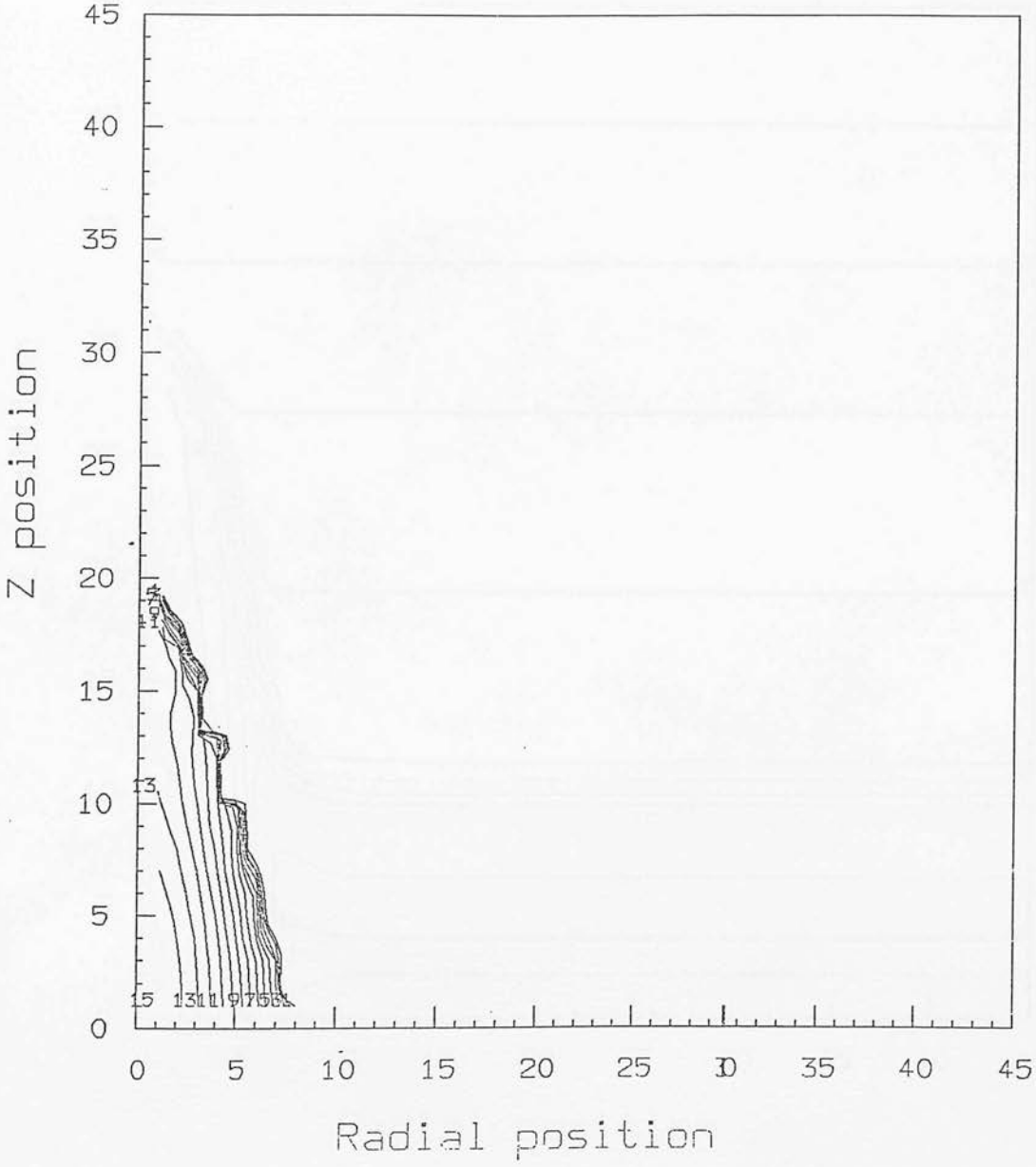

Contour No.	Contour level
1	-15.00
4	-14.43
7	-13.86
11	-13.10
15	-12.34

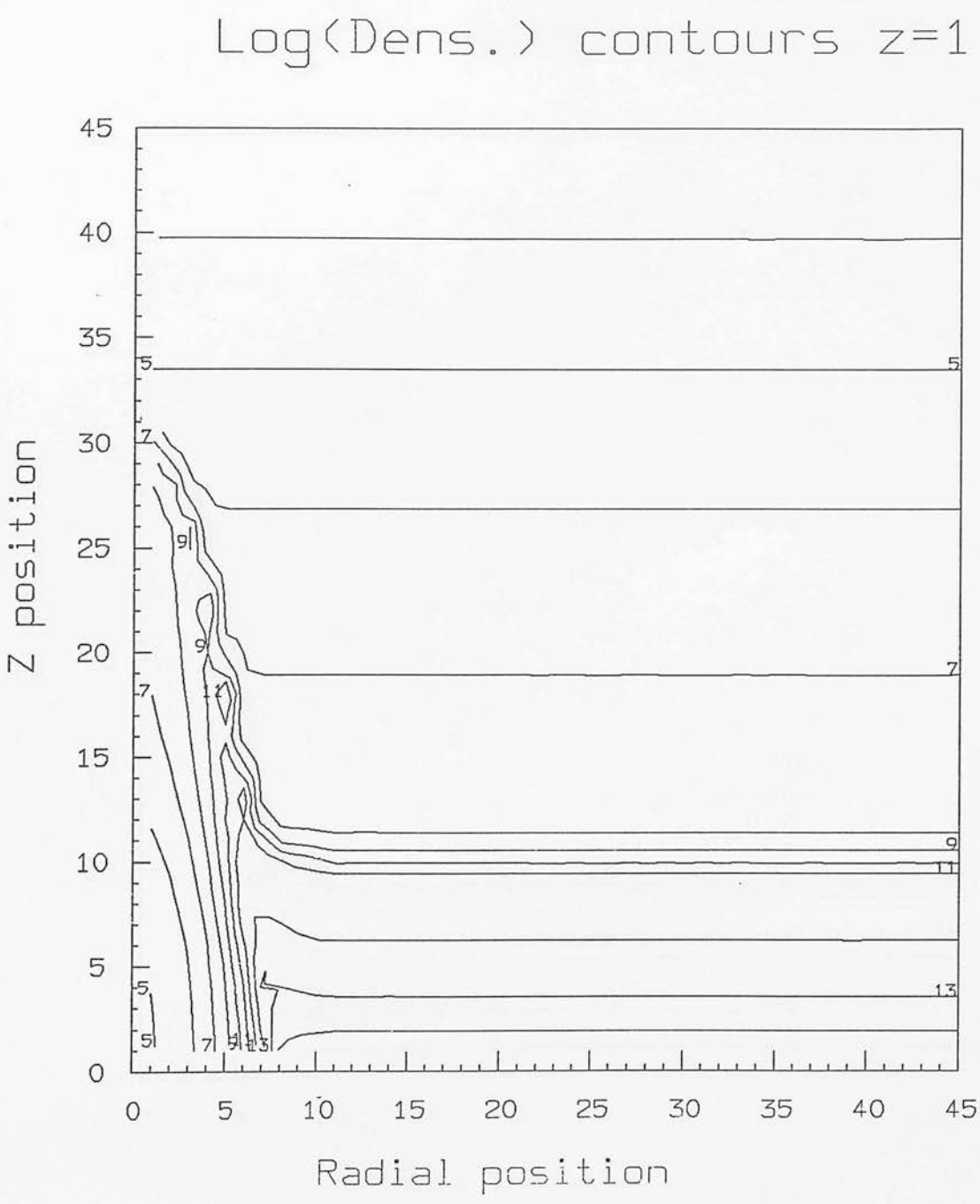

Contour No.	Contour level
1	-26.09
4	-25.44
7	-24.78
11	-23.91
15	-23.03

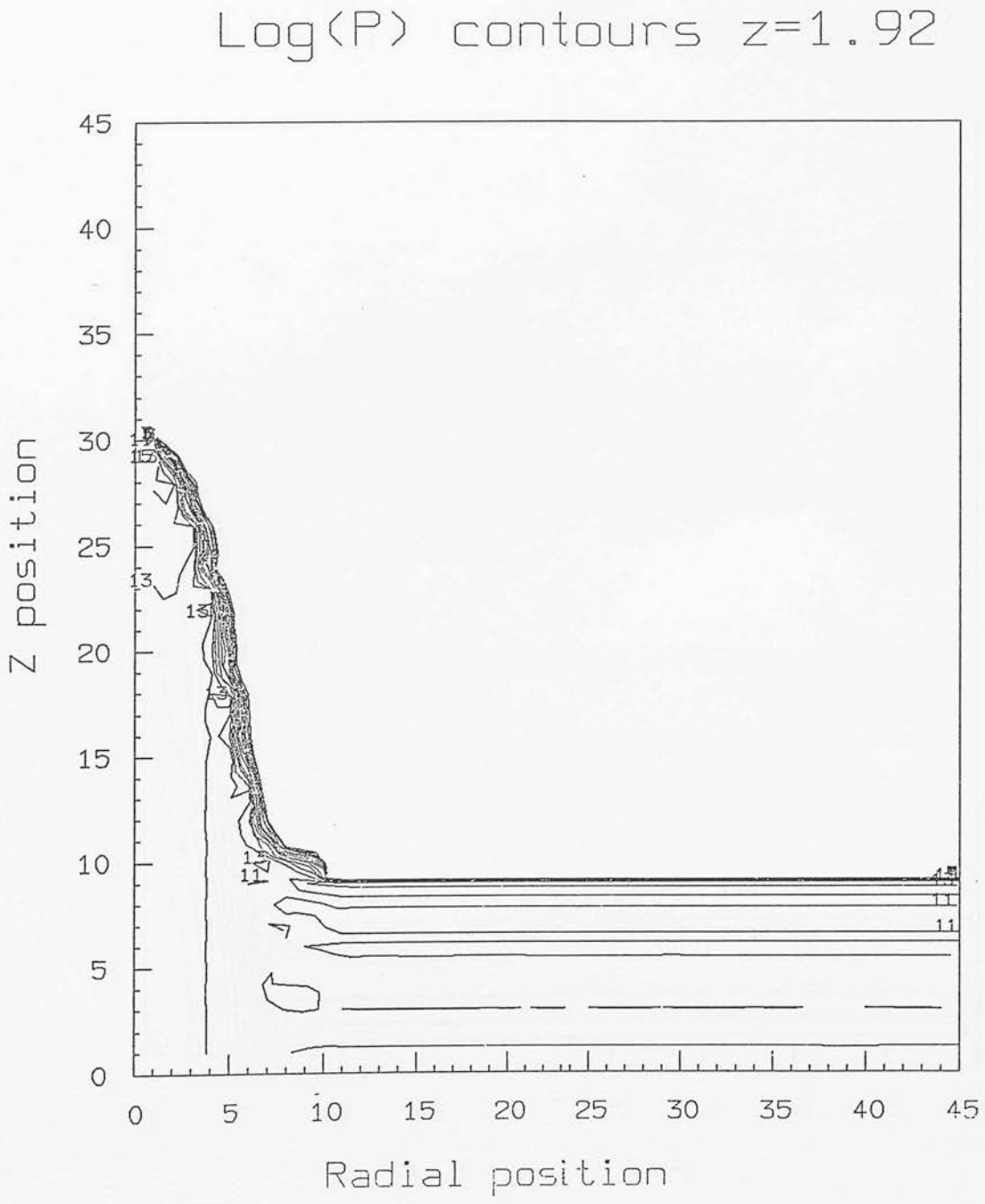

Contour No.	Contour level
1	-15.00
4	-14.59
7	-14.18
11	-13.64
15	-13.10

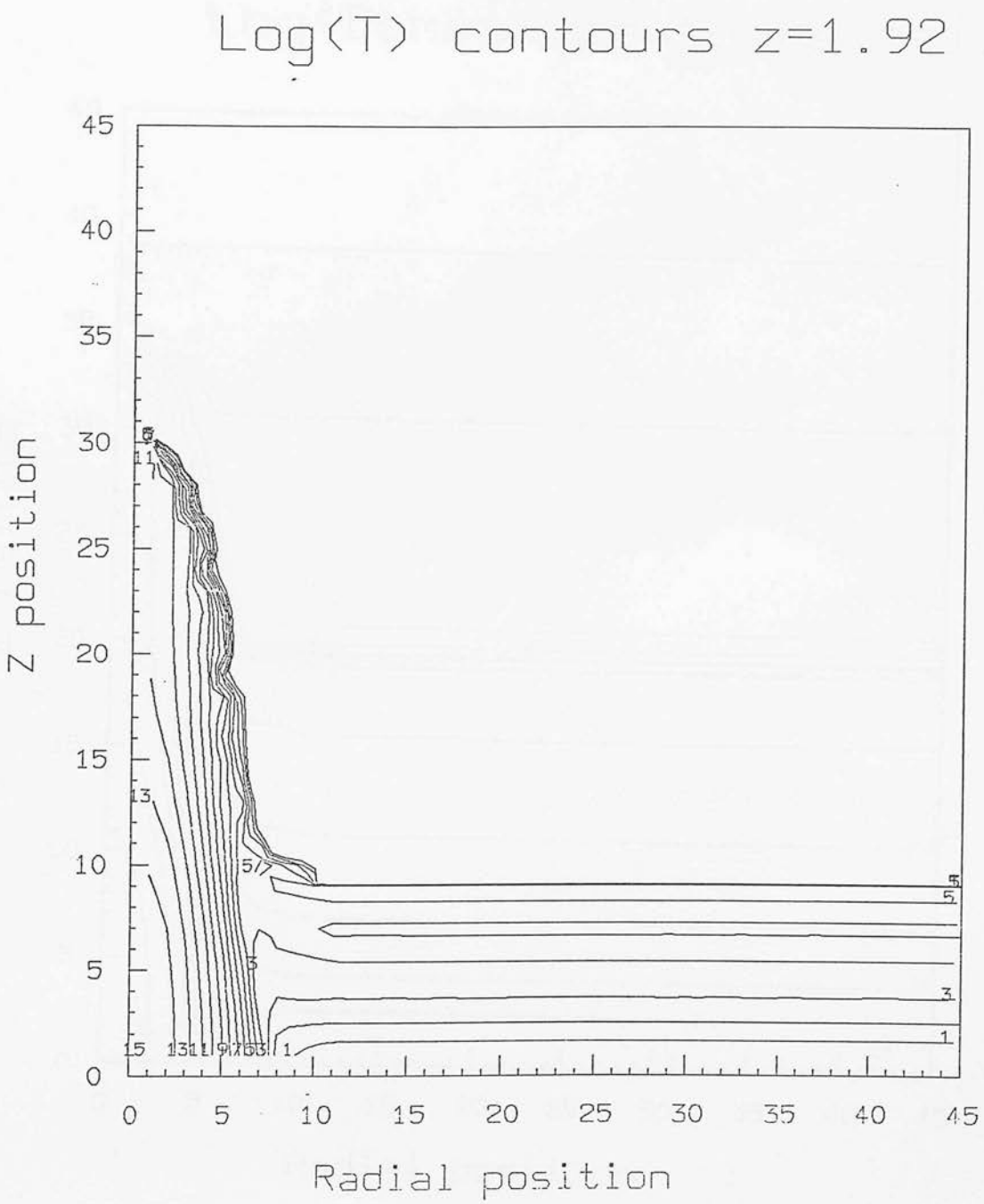

Contour No.	Contour level
1	5.50
4	5.97
7	6.44
11	7.07
15	7.69

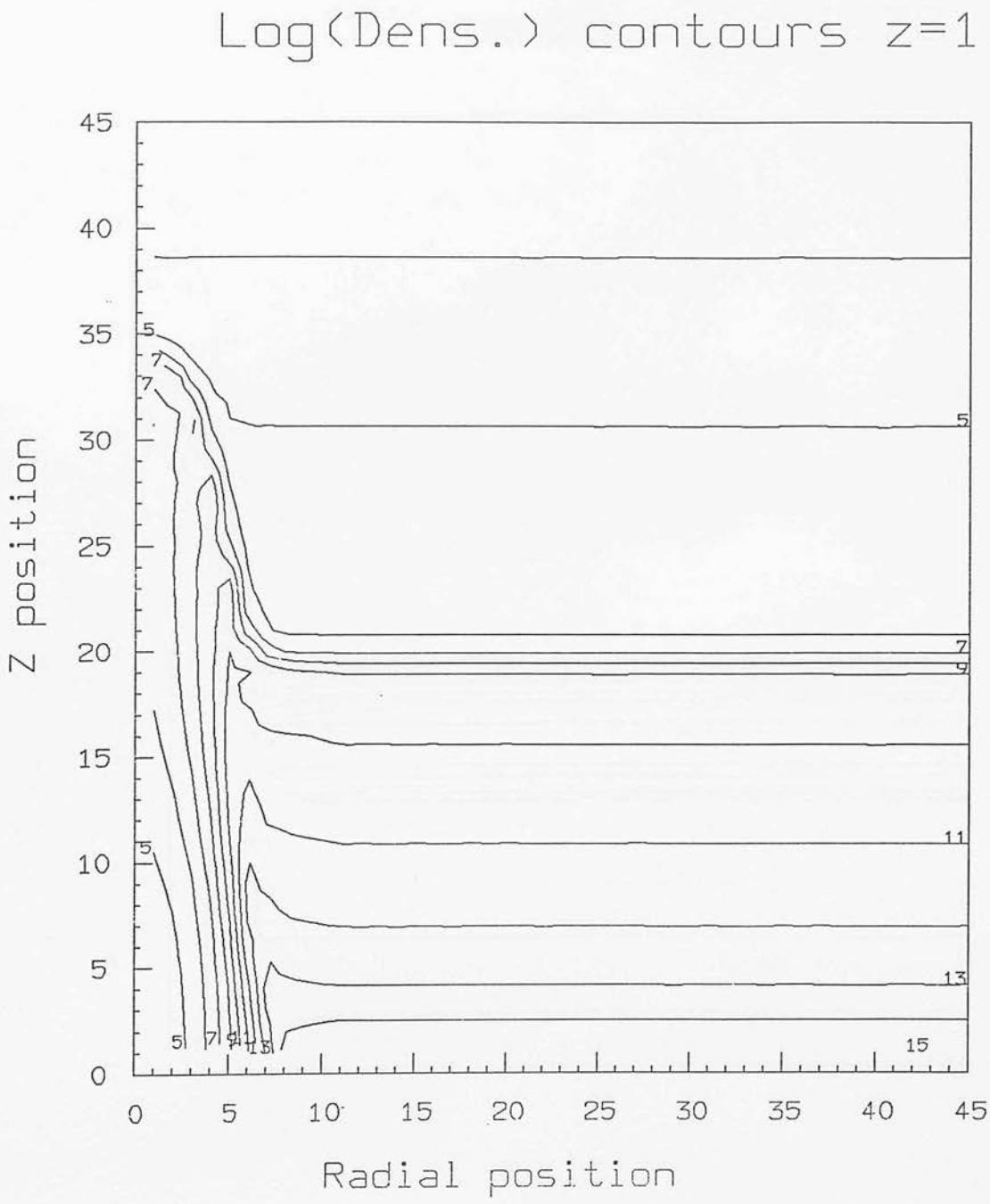

Contour No.	Contour level
1	-26.17
4	-25.52
7	-24.87
11	-24.00
15	-23.14

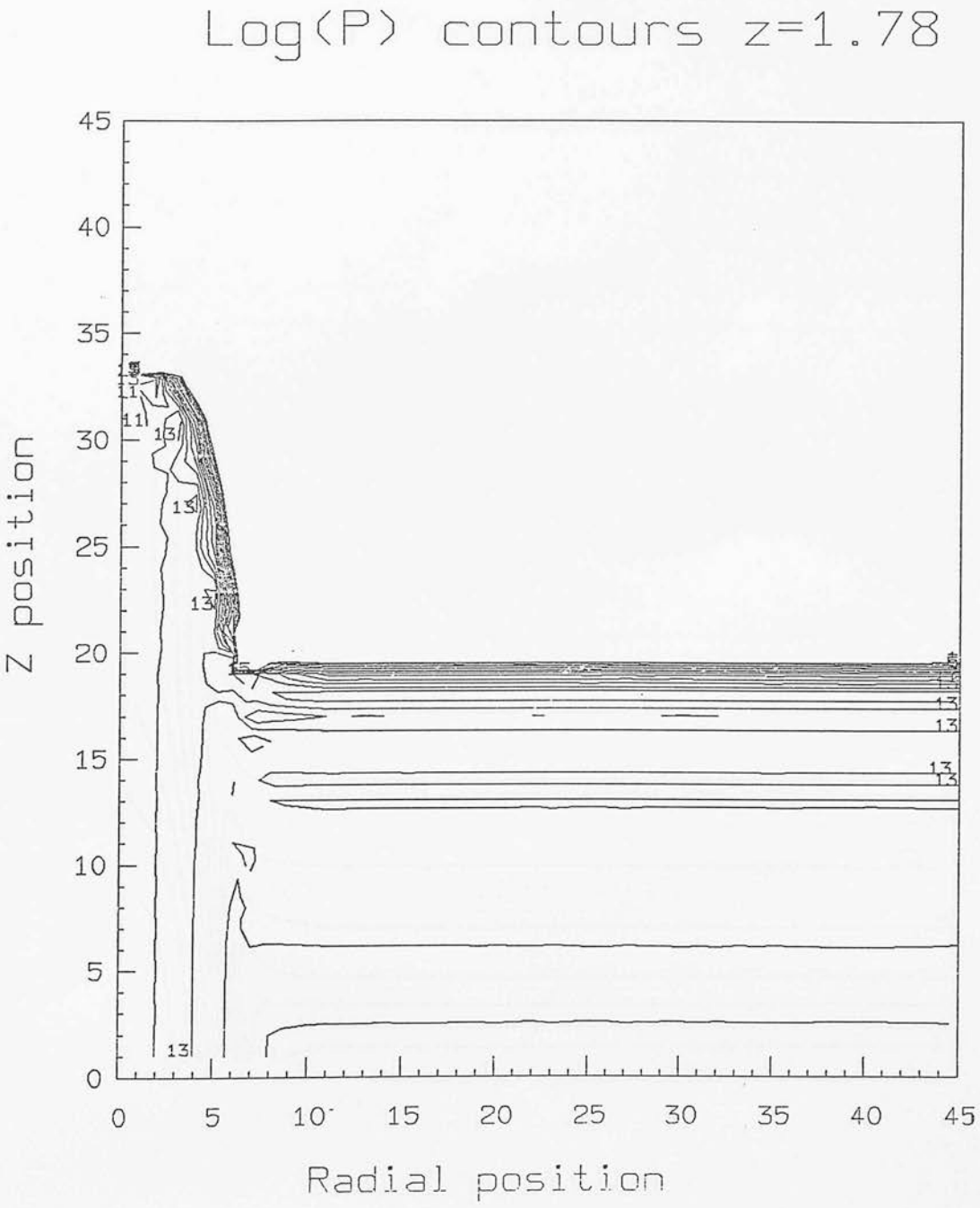

Contour No.	Contour level
1	-15.00
4	-14.67
7	-14.34
11	-13.90
15	-13.45

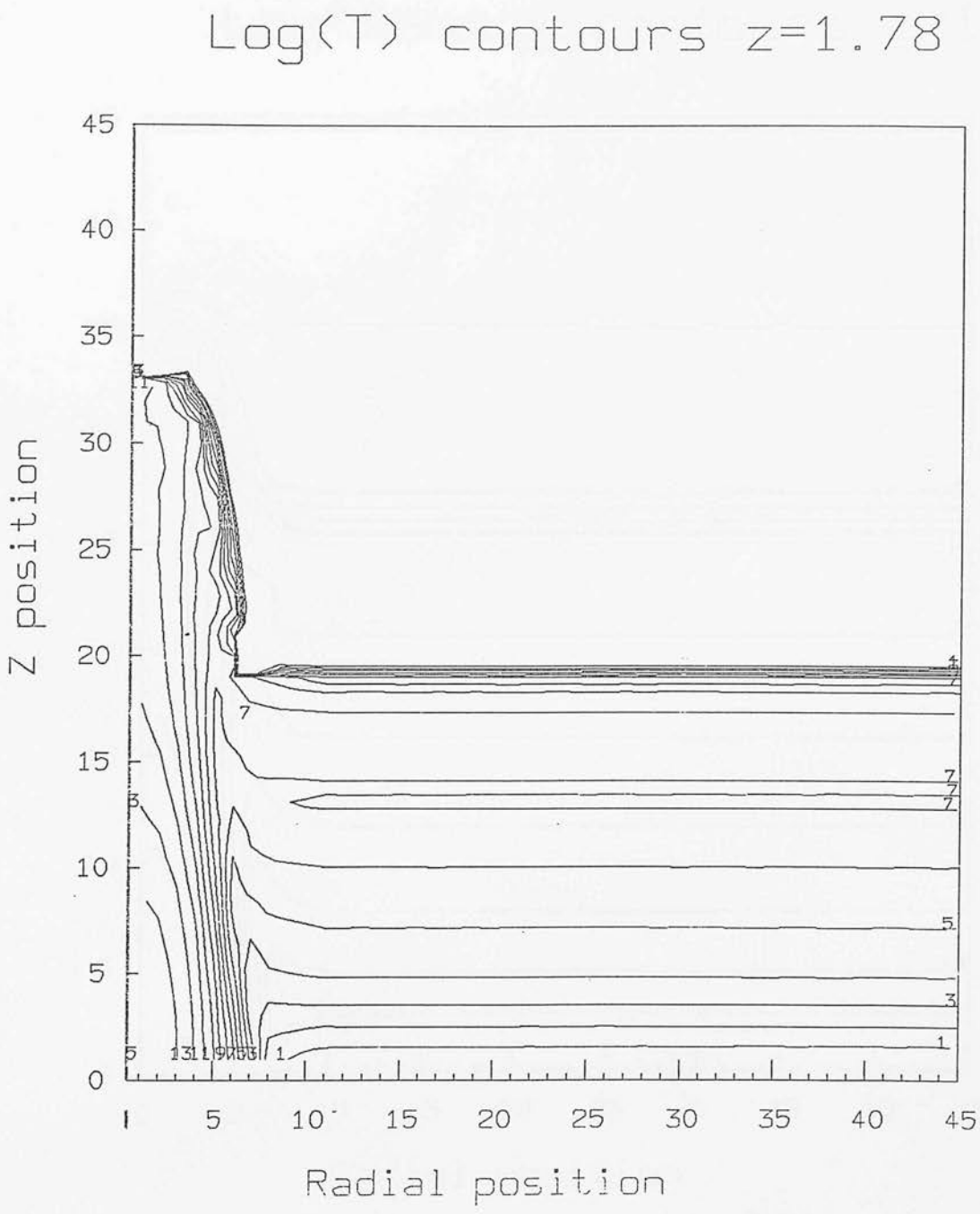

Contour No.	Contour level
1	5.50
4	5.93
7	6.36
11	6.94
15	7.52

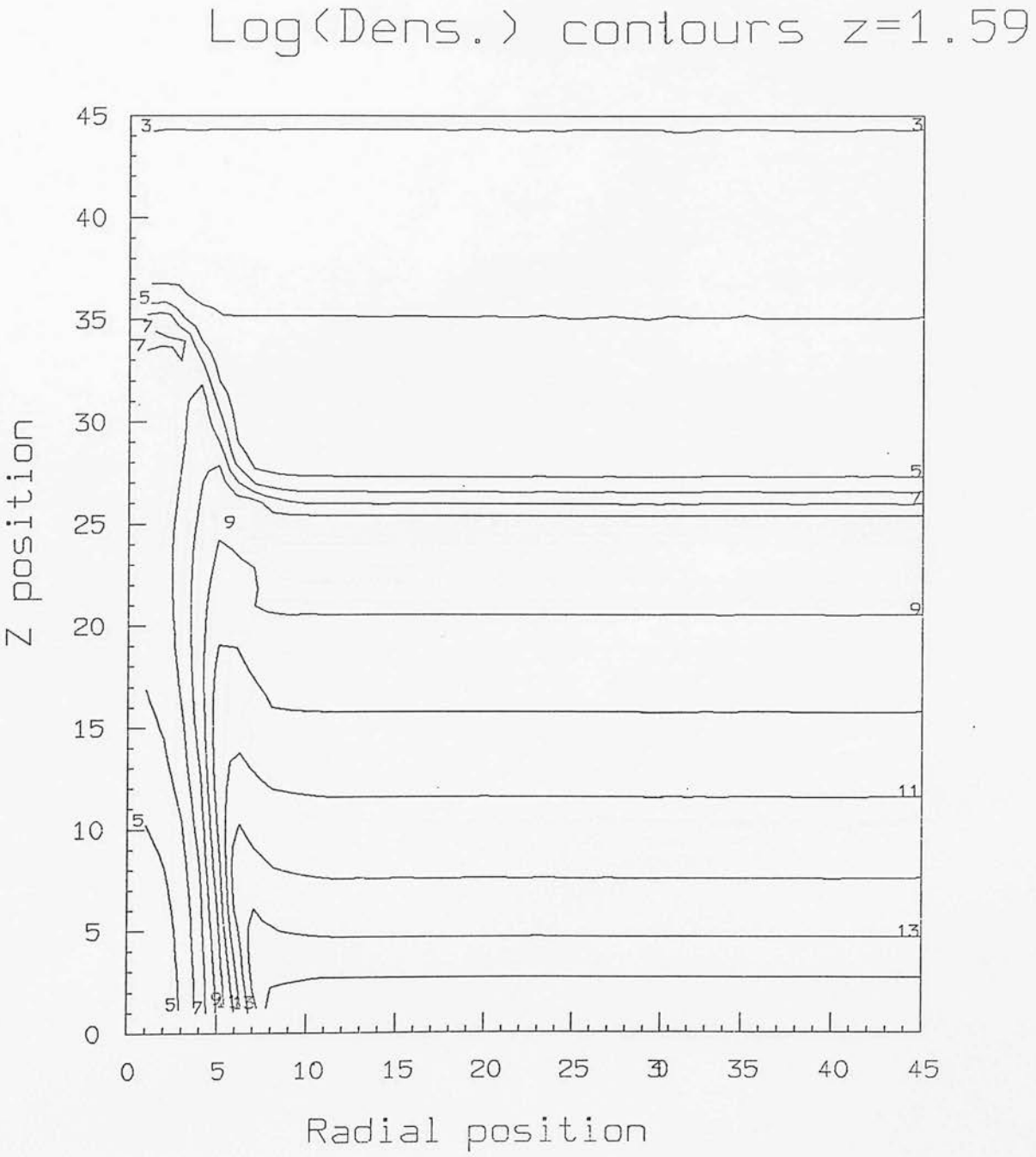

Contour No.	Contour level
1	-26.28
4	-25.63
7	-24.98
11	-24.11
15	-23.24

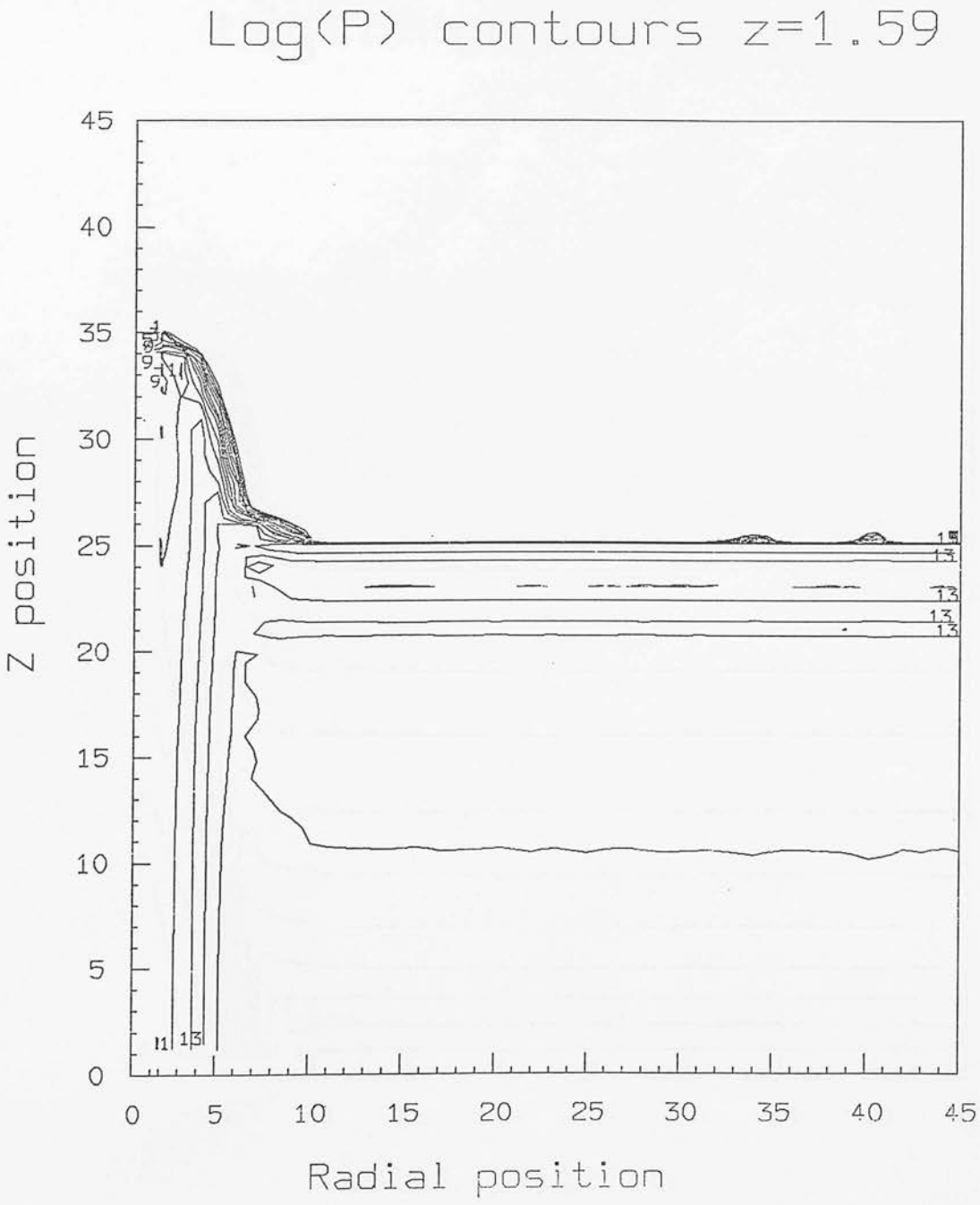

Contour No.	Contour level
1	-15.00
4	-14.69
7	-14.39
11	-13.98
15	-13.57

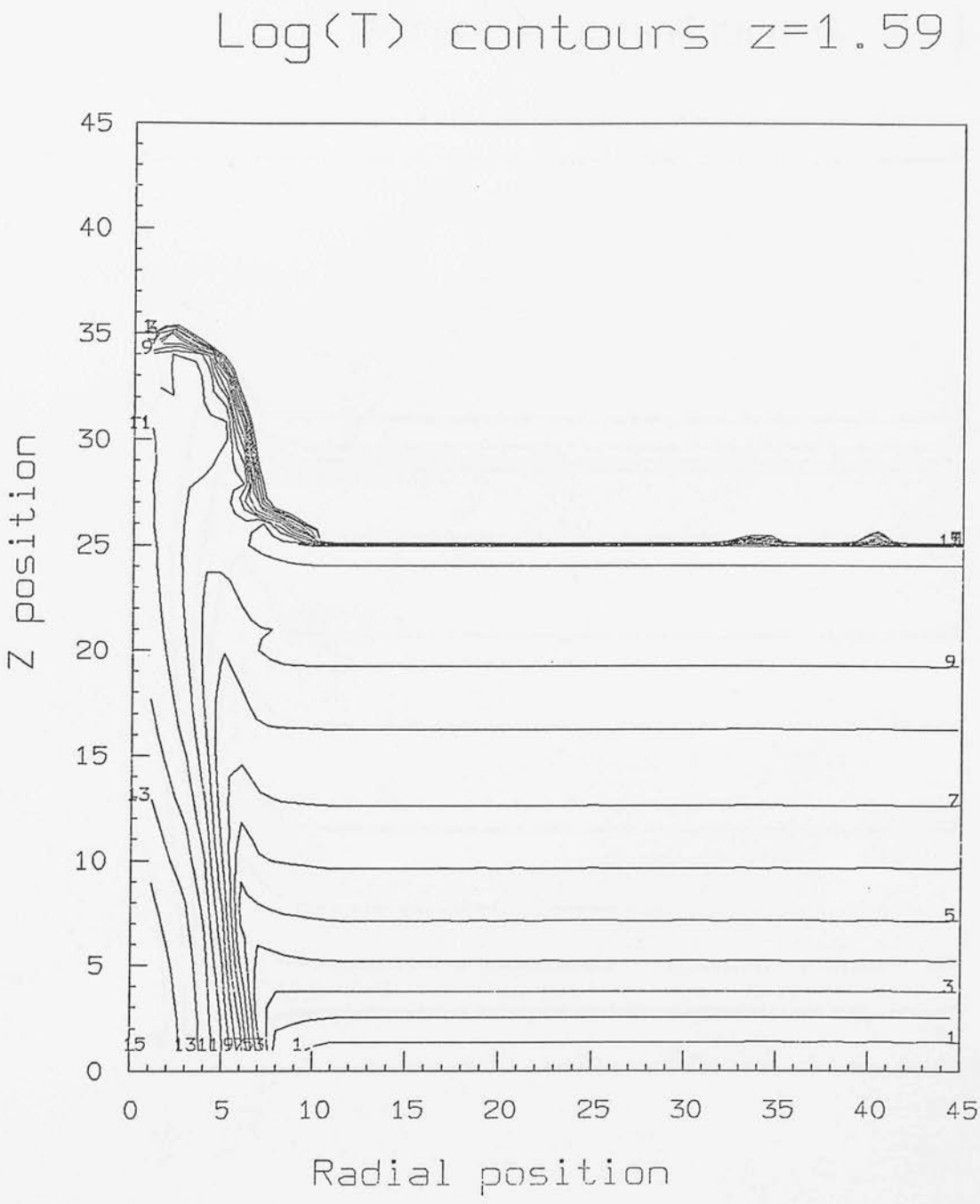

Contour No.	Contour level
1	5.50
4	5.92
7	6.33
11	6.89
15	7.44

Log(Dens.) contours z=1.46

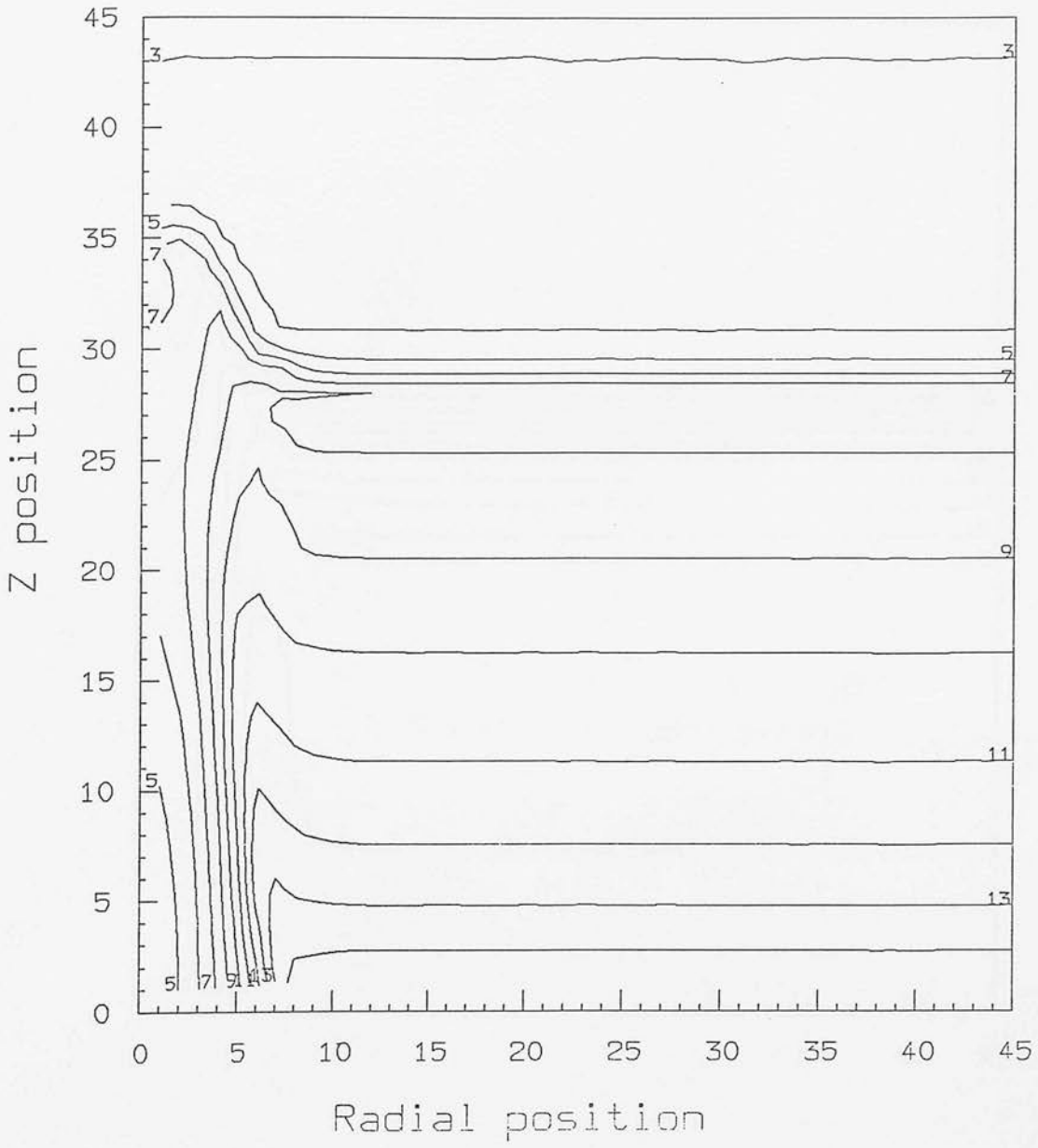

Contour No.	Contour level
1	-26.35
4	-25.70
7	-25.04
11	-24.17
15	-23.29

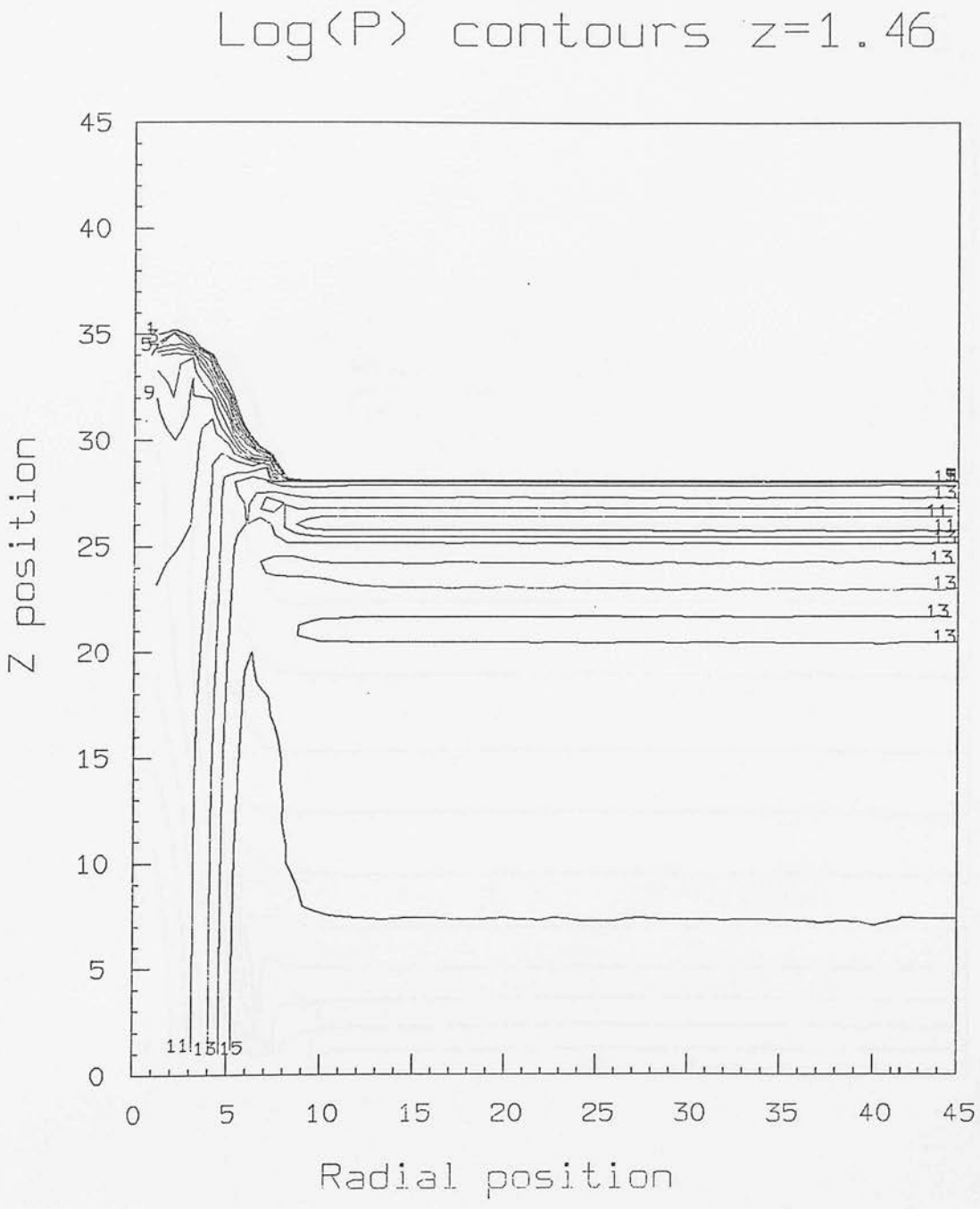

Contour No.	Contour level
1	-15.00
4	-14.71
7	-14.41
11	-14.02
15	-13.63

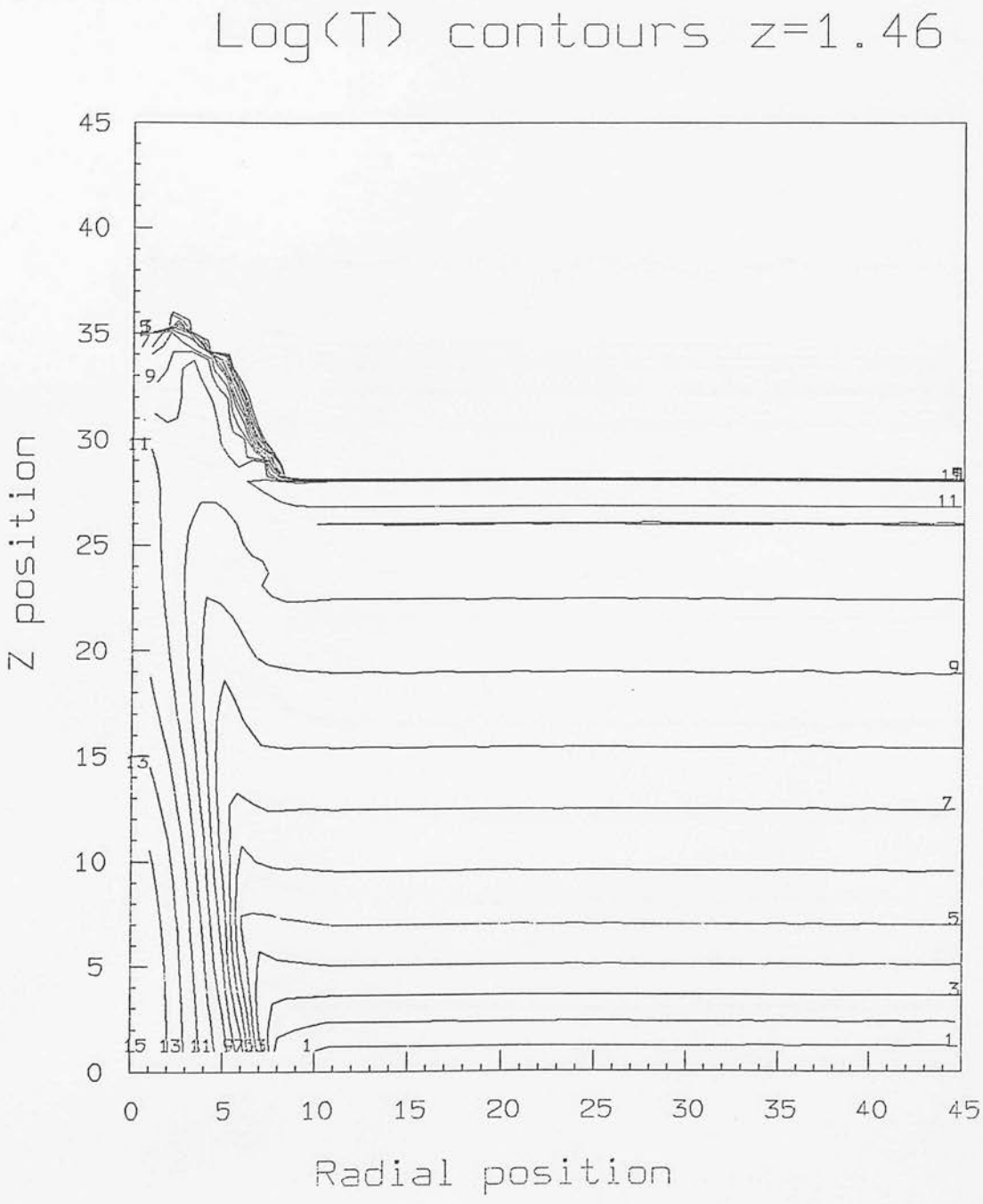

Contour No.	Contour level
1	5.50
4	5.90
7	6.31
11	6.84
15	7.38

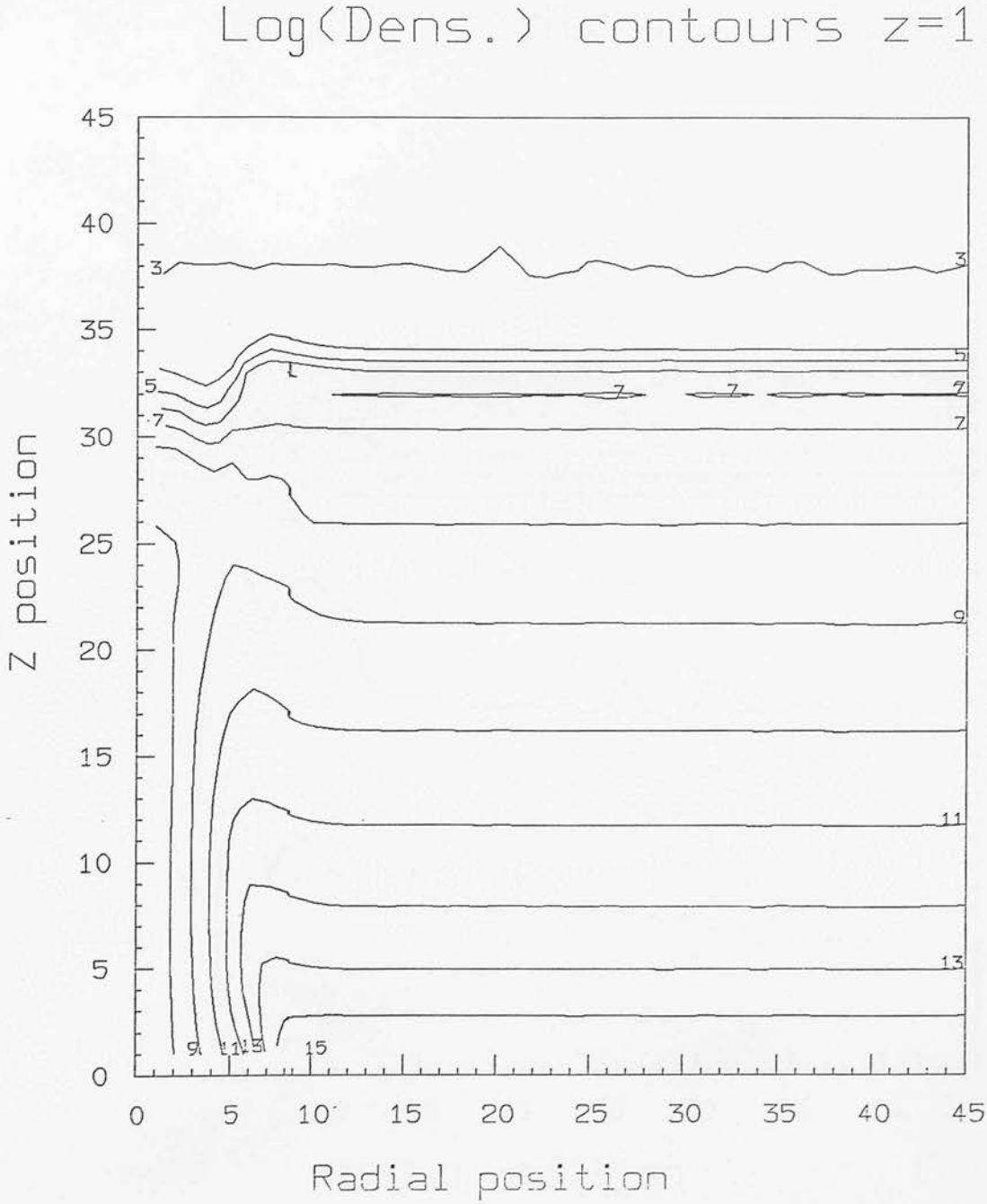

Contour No.	Contour level
1	-26.54
4	-25.87
7	-25.21
11	-24.31
15	-23.42

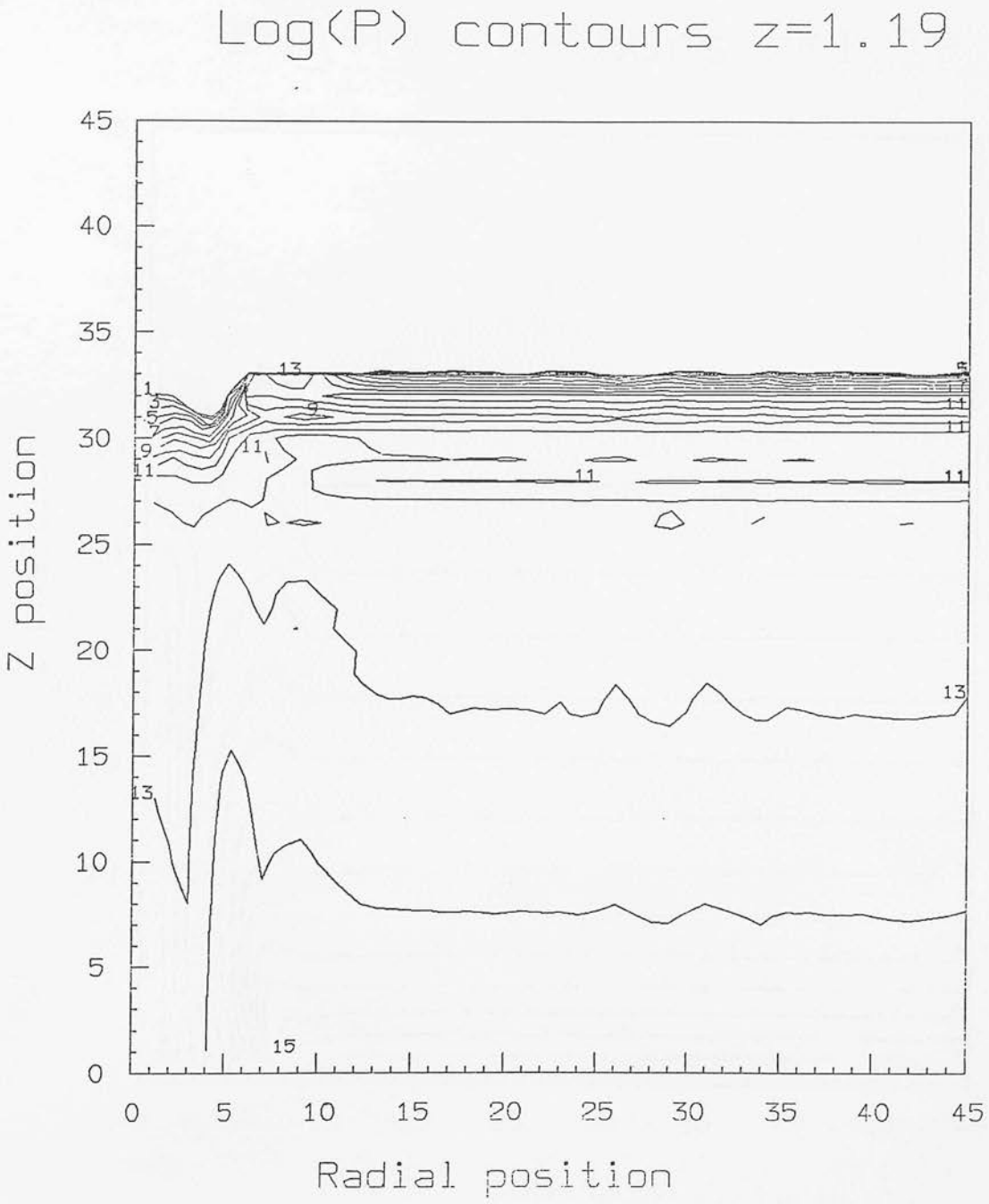

Contour No.	Contour level
1	-15.00
4	-14.74
7	-14.48
11	-14.13
15	-13.78

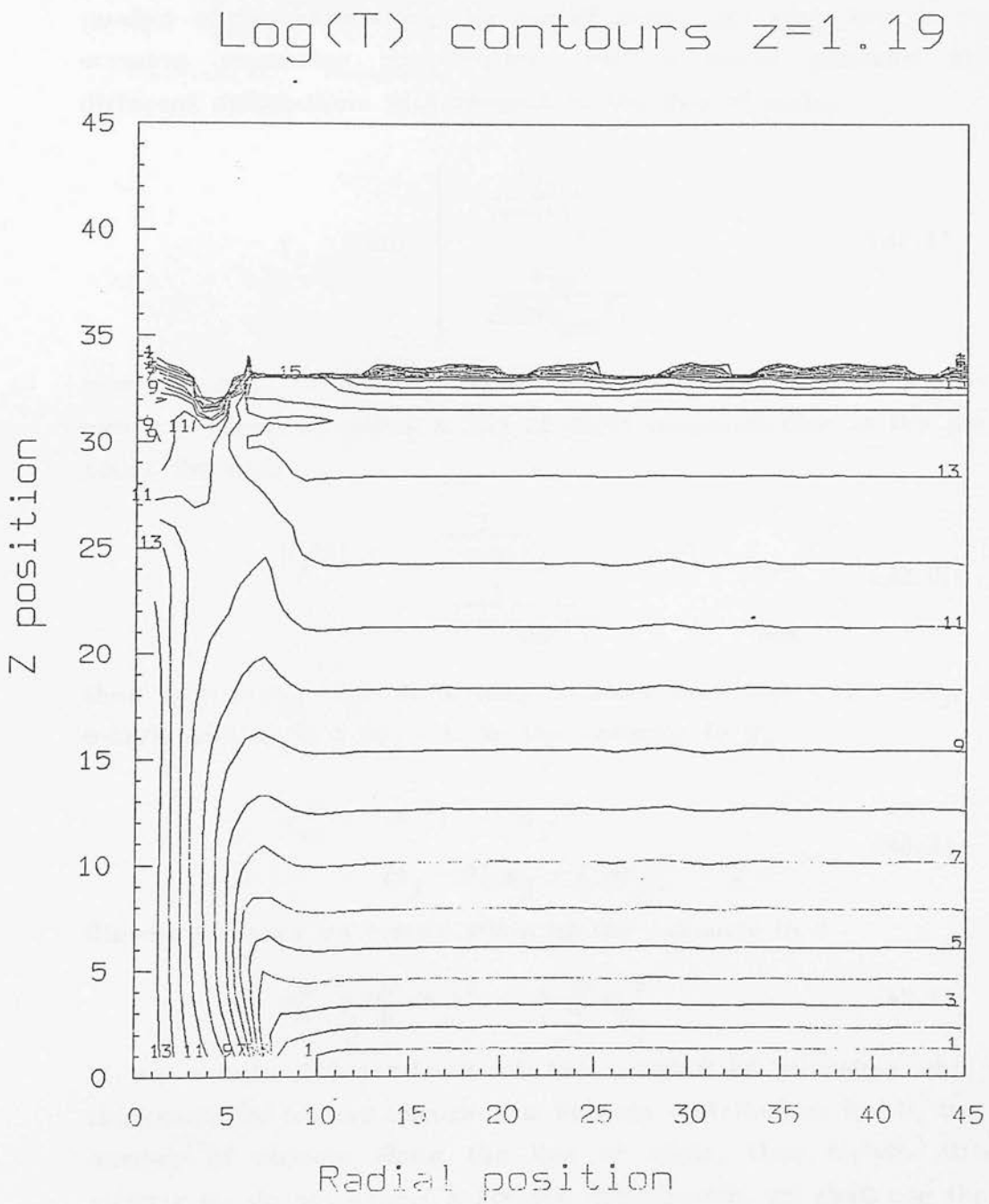

Contour No.	Contour level
1	5.50
4	5.84
7	6.18
11	6.64
15	7.10

Appendix 3

Microwave Distortions

The variation in $\Delta \equiv dT/T$ is composed of variations in N, the number of pancakes along the line of sight, and variations in y_j, the compton parameter contribution from a given pancake due to different orientations with respect to the line of sight.

$$y_j = \min \left\{ \begin{array}{l} \dfrac{y_{\perp j}}{(\cos i)_j} \\ \\ \dfrac{y_{\perp j}}{(\cos i_{max})_j} \end{array} \right. \qquad \text{(A3.1)}$$

where $\cos i_{max} = l_j/\lambda$. l_j is the pancake thickness and $y_{\perp j}$ is the compton parameter along a line of sight perpendicular to the pancake plane. Defining

$$S_j(i) = \begin{array}{ll} \dfrac{1}{(\cos i)_j} & i < i_{max} \\ \\ \dfrac{1}{(\cos i_{max})_j} & i > i_{max} \end{array} \qquad \text{(A3.2)}$$

then $\langle y_j \rangle = y_{\perp j} \langle S_j \rangle$. It is easy to show that $\langle S_j \rangle = 1 + \ln\Phi_j$, where $\Phi_j = \lambda/l_j$ and $\langle S_j^2 \rangle = 2\Phi_j - 1$. So the variance in S_j

$$\begin{aligned} \sigma_{sj}^2 &= \langle S_j^2 \rangle - \langle S_j \rangle^2 \\ &= 2\Phi_j - 2\ln\Phi_j - (\ln\Phi_j)^2 - 2 \end{aligned} \qquad \text{(A3.3)}$$

Standard theory on errors gives us the variance in Δ

$$\sigma_\Delta^2 = \sigma_N^2 \langle \Delta_j \rangle^2 + 4 \sum_j \sigma_{y_j}^2 \qquad \text{(A3.4)}$$

If we assume independence of the number of pancakes and their thickness i.e. we are assuming a Poisson distribution for N, the total number of objects along the line of sight, then $\sigma_N^2 = N$. Although strictly we do not expect a Poisson distribution, we shall see that the result is not sensitive to this assumption. Also $\sigma_{yj}^2 = y_{\perp j}^2 \sigma_{sj}^2$ and with a little algebra

$$\sigma_\Delta = \langle \Delta \rangle \left[\frac{1}{\langle N \rangle} + \frac{\sum_j y_{\perp j}^2 \sigma_{Sj}^2}{(\sum_j y_{\perp j} \langle S_j \rangle)^2} \right]^{1/2} \qquad \text{(A3.5)}$$

where $\langle \Delta \rangle = -2 \sum_{j=1}^{N} y_{\perp j} \langle S_j \rangle$

So given $y_{\perp j}$ and $\Phi_j (=\lambda/l_j)$ i.e given the compton parameter along a line of sight perpendicular to the plane and the pancake thickness we can calculate the desired variance in Δ. We estimate the variance by distributing pancakes evenly in comoving distance out to the formation epoch z_c.

Appendix 4

Published Papers

The research papers to which I have contributed are enclosed:

1) The gravitational collapse of triaxial protoclusters.
James G. More, Alan F. Heavens & John. A. Peacock.
Mon. Not. R. astr. Soc. 220,189,1986.

2) Explosions in pancake models of galaxy formation.
J.G. More, A.F. Heavens, M.J. Wilson & A.S. Trew.
I.A.U. Symp. 130., 1988. Large Scale Structures of
the Universe, ed. Audouze, Pelletan & Szalay.

Mon. Not. R. astr. Soc. (1986) **220,** 189–202

The gravitational collapse of triaxial protoclusters

James G. More and Alan F. Heavens *Department of Astronomy, University of Edinburgh, Blackford Hill, Edinburgh EH9 3HJ*

John A. Peacock *Royal Observatory, Blackford Hill, Edinburgh EH9 3HJ*

Accepted 1985 November 27. Received 1985 November 8; in original form 1985 September 27

Summary. The gravitational collapse of non-rotating, homogeneous, triaxial ellipsoids is followed through and beyond the formation of a two-dimensional caustic surface ('pancake'). In previous work on this problem, 'filaments' (one-dimensional structures) correspond only to the degenerate case of collapsing prolate spheroids; all other shapes, except spheres, collapse to pancakes. In this work, we find that, assuming dissipation or relaxation processes keep the surface relatively thin after formation, pancakes undergo further anisotropic collapse in their planes, forming either filamentary structures or more isotropic configurations which we call clusters. Filaments thus do not correspond to a degenerate case, but arise naturally from this secondary collapse phase. Some pancakes may nevertheless persist indefinitely, never undergoing the secondary collapse to a filament. However, if we compare the initial shapes required for this behaviour with the initial shape distribution expected for maxima in three-dimensional Gaussian noise, we find that long-lived pancakes should be rare, particularly for high Ω_0 values. In addition we find a very simple yet powerful result on the collapse epoch of objects of a given overdensity with different initial shapes.

1 Introduction

Since the pioneering work of Lin, Mestel & Shu (1965), it has been well known that the anisotropic gravitational field of a uniform density ellipsoid leads to accentuation of asphericity with time. As the collapse proceeds, a two-dimensional elliptical caustic surface is produced, with infinite density. Only in the degenerate case of an ellipsoid with two equal short axes will collapse lead to a one-dimensional filament. Spherically symmetric collapse to a point occurs only if all three axes are equal.

Doroshkevich (1970) discussed the nature of constant overdensity surfaces for random density perturbations in the context of the Zel'dovich formalism; high-density regions may be

approximated by homogeneous ellipsoids and the shapes of the constant overdensity surfaces thus give the initial axes of these ellipsoids. He showed that these surfaces are generally aspherical, and the probability that two principal axes (of the deformation tensor) are equal is particularly low, so it might seem that filament and point structures should be very rare. However, let us consider the evolution of an homogeneous ellipsoid beyond its collapse to a two-dimensional pancake. If the formation of such a caustic surface results in dissipation of the motion perpendicular to the surface, then the anisotropic gravitational and velocity fields will lead to further growth of anisotropy, in the sense that the eccentricity of the elliptical pancake increases with time.

In the adiabatic theory of galaxy formation (for a recent review, see Efstathiou & Silk 1983), fluctuations in density are damped below a mass scale $M_{\rm D}\simeq 1.3\times10^{12}(\Omega_0 h^2)^{-3/2}M_\odot$, or $4\times10^{15}(m_\nu/30\,{\rm eV})^{-2}M_\odot(h=H_0/100\,{\rm km\,s^{-1}\,Mpc^{-1}})$ if the mass of the Universe is dominated by one light neutrino of mass m_ν. In these cases, the identification of ellipsoids with supercluster-scale regions of higher-than-average density is not too unrealistic. In this picture, as collapse proceeds any new layers of gas which accrete onto the pancake have most of their kinetic energy transformed into heat by a pair of shock waves set up in the baryon fluid either side of the caustic surface (Sunyaev & Zel'dovich 1972). This heat can then be dissipated in the dense central region by radiative cooling which is more rapid than the dynamical time-scales characterizing the flow and so a thin dense layer persists. If the Universe is dominated by light collisionless particles, then we expect dissipative pancakes to form by baryons falling into the potential wells of the large-scale dissipationless material. This has been confirmed by Shapiro & Struck-Marcell (1984). Their detailed hydrodynamical calculations of the coupled growth of such baryon/collisionless particle pancakes show that not only do baryons cool and compress into a dense central layer on short time-scales but the distribution of collisionless particles also remains highly flattened for some time after the caustic surface forms. Indeed, the presence of the baryon component serves to decrease the scale-height of the collisionless particle distribution further. This confirms the argument of Dekel (1983), who considered an adiabatic invariant treatment of non-dissipative pancakes which are expanding in their planes and demonstrated that, although the pancake thickness grows as it expands, it becomes relatively flatter in time. It seems justifiable then to neglect motions perpendicular to the plane and assume a planar velocity field within the pancake since this approximation is valid as long as the thickness of the pancake remains smaller than the two principal axes.

The procedure for this calculation splits into two parts: first (Section 2) we follow the collapse of ellipsoids to the formation of a caustic surface, in the spirit of White & Silk (1979), hereafter WS (see also Barrow & Silk 1981). We take this opportunity to vary some of the simplifying assumptions and starting conditions of WS, to test the sensitivity of their results to different simplifications. Secondly, we follow the subsequent collapse of pancakes in their planes (Section 3). At the instant of formation of the pancake, the short axis is expanding less quickly than the long axis, as our calculations demonstrate. The short axis, or indeed both axes, may be contracting, depending on the initial axial ratios of the ellipsoid when the overdensity of the ellipsoid $\delta\varrho/\varrho$ is much less than unity.

2 Pre-pancaking evolution

2.1 THE MODEL

The evolution of regions of overdensity in an expanding universe is, in general, extremely complicated. It is possible, however, to gain some insight into the behaviour using a simplified approach following the methods developed by Lin *et al.* (1965) and WS on the collapse of homogeneous ellipsoids. This is the most general three-dimensional problem which can be

handled exactly by current analytic means. One of the main difficulties with this method is how to treat the gravitational effect of the material outside the ellipsoid. WS assumed it remained uniform at the average universal density. This requires matter to fall continuously into the surroundings of the ellipsoid. Alternatively, we may instead allow the external density to differ from the average density of the universe as a whole. The justification for this is as follows; if space is populated by these ellipsoids, then neighbouring objects will on average prevent the infall of matter needed to keep the surrounding density high. We make what is in essence an opposite assumption: we assume that there is no infall from outside a sphere of comoving radius r equal to the initial semi-major axis of the ellipsoid, a. Mass inside r is conserved, with average density equal to the average density of the universe (so the ellipsoid is surrounded by an underdense region). We could, of course, generalize this approach by assuming there is no infall from outside some general radius $r \geqslant a$. WS's approximation amounts to $r \rightarrow \infty$, hence the two approximations can be thought of as the opposite extremes of this method. A further minor alteration to WS's method is that we follow a pure growing mode, so include a velocity perturbation in the initial conditions. This will be appropriate if perturbations have been able to grow before recombination, when we start our calculation; this is the case for perturbations in a high-density universe dominated by 'hot' collisionless particles. Including the growing mode is almost exactly equivalent to reducing the initial overdensity by a factor 5/3 in the problem solved by WS, whose initial condition on velocity was pure Hubble flow. Now Peebles' (1980) calculation of the growing and decaying velocity modes is valid for the matter dominated regime. Our calculation, which assumes only the growing mode at recombination, therefore accurately represents the behaviour of a fluctuation in high-density universes where matter domination occurs before recombination and the decaying mode has had time to die out. For lower-density universes where recombination and matter domination occur more or less simultaneously, there will be in addition a decaying mode. We ignore all other tidal forces and magnetic fields.

Given a quadratic form for the potential, the basic requirement for evolution through a series of homogeneous ellipsoids is that the initial velocity perturbations should be in proportion to the axial ratios (Lin *et al.* 1965). This can be demonstrated for the growing-mode perturbation as follows:

The large-scale peculiar velocity field associated with large-scale irregularity in density is given in proper coordinates (Peebles 1980, p. 65) by

$$\mathbf{v}=\frac{Hf}{4\pi}\nabla\int\frac{d^3r^1\delta(\mathbf{r}^1)}{|\mathbf{r}-\mathbf{r}^1|} \tag{1}$$

where $f=(a/\delta)(d\delta/da)$ with overdensity $\delta(r^1)=\{\varrho(\mathbf{r}^1)-\varrho_b\}/\varrho_b$ and scale factor $a(t)$. ϱ_b is the mean density of the universe, and H is the Hubble parameter (not to be confused with the present day Hubble constant H_0). Whilst linear perturbation theory applies and we are at a late enough epoch so that only the growing mode solution is present and the relativistic background can be ignored, then f is independent of r and is a function of the density parameter only. We will adopt Peebles' approximation $f(\Omega)=\Omega^{0.6}$; this is only used to set up the initial conditions and will be sufficiently accurate at a starting redshift at recombination of 1500 where Ω is very close to one.

Denoting initial quantities by the subscript (i) where necessary, if we specify the initial overdensity of the ellipsoid, $\delta_{(i)}=(\varrho_e-\varrho_b)/\varrho_b$, we can calculate the density ϱ_s outside the ellipsoid, given the assumption that the average density inside a sphere of radius $a_{1(i)}$ is ϱ_b. It is given by

$$\varrho_s=\varrho_b[1-a_{2(i)}a_{3(i)}\{1+\delta_{(i)}\}]/\{1-a_{2(i)}a_{3(i)}\} \tag{2}$$

where the $a_{j(i)}$ are the principal axes of the ellipsoid $\{a_{1(i)} \geq a_{2(i)} \geq a_{3(i)}\}$ and we choose our length unit such that $a_{1(i)}=1$. The overdensity of the matter immediately outside the ellipsoid is

$$\delta_s = -\left(\frac{a_2 a_3}{1-a_2 a_3}\right)_{(i)} \delta_{(i)}. \tag{3}$$

Clearly the assumption will not be good for near-spherical objects, as formally $\delta_s \to -\infty$, whereas we expect underdensities of the same order as the overdensities in all but the most unusual density fields. However, only when $a_{3(i)} \geq 0.9$ does the underdensity outside the ellipsoid greatly exceed the overdensity inside, so the inapplicability to near-spherical objects is not serious in practice.

Splitting the integral into two parts over a homogeneous sphere, overdensity δ_s and a homogeneous ellipsoid, overdensity $\delta_{(i)}-\delta_s$ which can be solved exactly and performing the divergence operation we find that the initial growing mode velocity perturbation is given by components [dropping subscript (i) for equations (4) and (5) only].

$$v_j = -\frac{\Omega^{0.6} H \delta r_j}{2(1-a_2 a_3)}(\alpha_j - \tfrac{2}{3} a_2 a_3) \tag{4}$$

with the α_j coefficients defined by

$$\alpha_j = a_1 a_2 a_3 \int_0^\infty (a_j^2+\lambda)^{-1} \prod_{k=1}^{3} (a_k^2+\lambda)^{-1/2} d\lambda. \tag{5}$$

The chosen initial axial ratios $a_{j(i)}$ with $\alpha_{j(i)}$ values from (5) and proper velocities from (4) adding in a Hubble term constitute the initial conditions.

The potential for a homogeneous ellipsoid, of density ϱ_e embedded in a uniform sphere of density ϱ_s is

$$\Phi = \pi G \sum_{j=1}^{3} \{(\varrho_e - \varrho_s)\alpha_j + \tfrac{2}{3}\varrho_s\} r_j^2 \tag{6}$$

[*cf.* WS equation (5)] where, if we ignore all other tidal effects, Birkhoff's theorem means that we can ignore forces from the surrounding average density universe.

This enables us to determine the equations of motion for the principal axes of the ellipsoid a_j. If we change the independent variable to z using

$$dz/dt = -H_0(1+z)^2(\Omega_0 z+1)^{1/2} \tag{7}$$

(e.g. Longair 1984), express all densities in terms of Ω_0 (the present value of Ω), we can eliminate H_0 to yield

$$\frac{d^2 a_j}{dz^2} = -f_1(\Omega_0, z)\frac{da_j}{dz} - f_2 \frac{(\Omega_0, z)}{\varrho_b} a_j \{\alpha_j \varrho_e + (\tfrac{2}{3} - \alpha_j)\varrho_s\} \tag{8}$$

where

$$f_1 = \frac{5\Omega_0 z + \Omega_0 + 4}{2(1+z)(\Omega_0 z+1)}; \qquad f_2 = \frac{3\Omega_0}{4(1+z)(\Omega_0 z+1)}.$$

If we convert equation (8) into two first-order equations and use the auxiliary formulae (7) of WS we can set up a system of differential equations in a_j, $\dot{a}_j$, $\dot{\alpha}_j$ which are solved numerically subject to the conservation equations

$$\varrho_e a_1 a_2 a_3 = \text{constant}; \qquad \varrho_s(s^3 - a_1 a_2 a_3) = \text{constant} \tag{9}$$

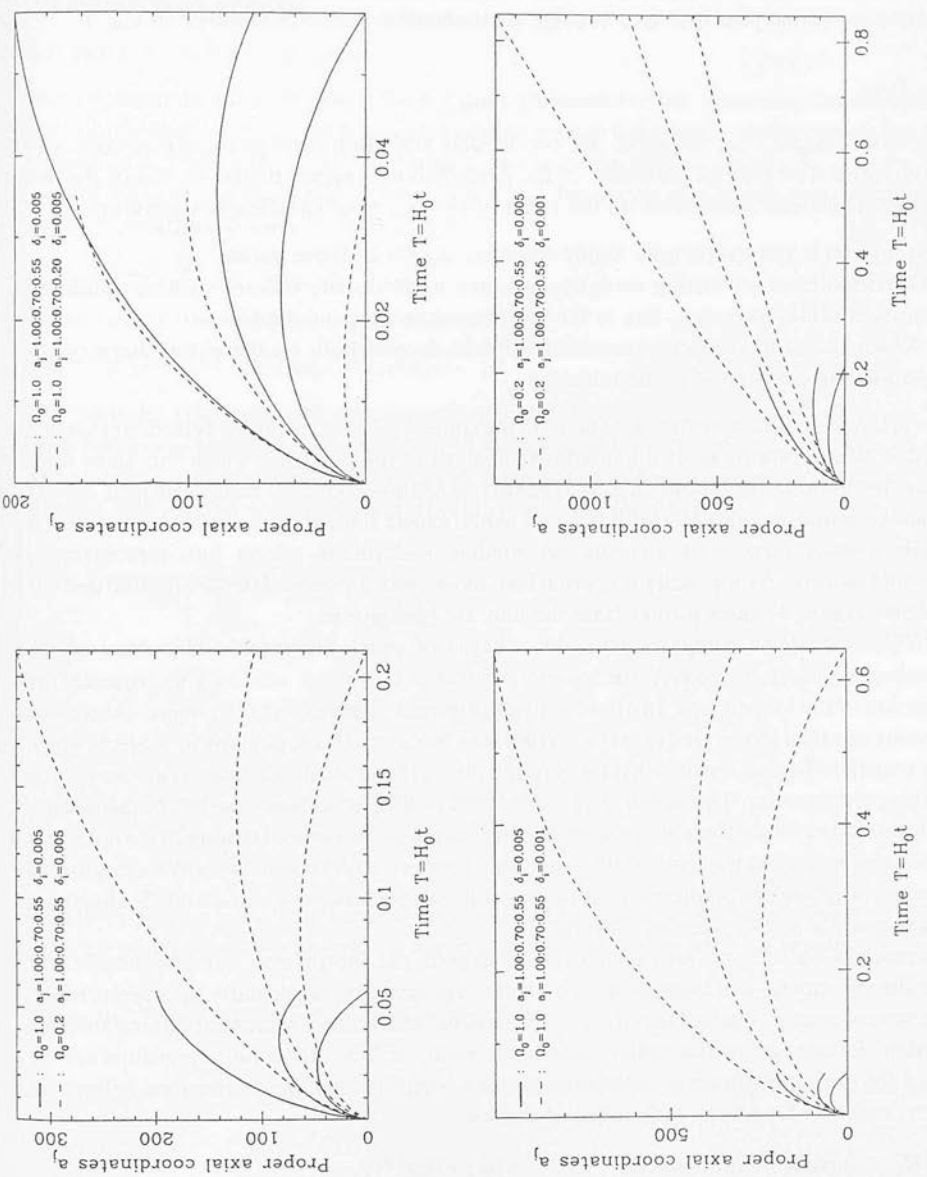

Figure 1. The pre-pancaking behaviour of the principal axes of a few representative ellipsoids is shown to illustrate the effect of a change in background density, ellipsoid density, and initial configuration. The axes, normalized to the initial major axis, are plotted against dimensionless time $T=H_0t$.

where s is the comoving radius of the sphere containing our perturbation. For the particular case of oblate or prolate spheroids the α_j values can be written in closed form [adapted from equations (21)–(24) of Lin *et al.* with a misprint corrected].

We began each calculation at a redshift 1500, in the recombination era. For our purposes, the initial epoch is not too important as the shape is more or less preserved while $\delta\varrho/\varrho \ll 1$. The behaviour of the principal axes of some representative ellipsoids is shown in Fig. 1.

2.2 RESULTS

We can now compare the results of the two models and offer some physical explanation of the differences. The general behaviour of the perturbation is rather similar to that of the WS model and their basic conclusions on the effect of varying input parameters are confirmed:

(i) At a given initial overdensity highly eccentric objects collapse fastest.

(ii) Deviation from self-similar evolution is larger in low-density universes where significant overdensity is achieved earlier, due to the more rapid background expansion.

(iii) Kinematic properties of a pancaked ellipsoid depend both on the initial shape of the perturbation and on the background density.

We will have more to say with regard to (ii) in the context of post-pancaking behaviour (Section 2) but it is informative to apply a quantitative analysis of the last point which will allow us to compare the two approximations directly. The two calculations agree for highly eccentric objects given similar initial conditions. This is what we would expect since at a given overdensity the flat ellipsoids contain little mass and the surrounding underdense region has approximately background density. As sphericity is approached, more mass is enclosed in the ellipsoid and the underdense region deviates further from the uniform background.

As WS found, when compared with the collapse of isolated ellipsoids, the effect of the surrounding region is to reduce the deceleration of the shortest axis and to increase the deceleration of the longest axis. In other words, the growth of asphericity is reduced. At a given overdensity our tidal forces are generally smaller than those of WS, particularly for objects which are not very flat. The net result is that fairly round objects form caustic surfaces at earlier epochs with our approximation. This result, and indeed that of WS, is not quite trivial, as the smaller deceleration of the longest axis in our approximation slows the increase of density of the ellipsoid, counteracting somewhat the reduced tidal support. However, with knowledge of WS's results and those of Lin *et al.*, we can predict that our objects will collapse faster than those of WS, since they believe they are in a lower-density universe.

As a result of the different treatment of the tidal field, the approximate expressions given by WS for the velocity field at collapse are no longer very accurate, particularly for objects which are not very eccentric. We find that the middle and long axes behave somewhat differently from each other, in contrast to the rather remarkable result of WS. Accurate expressions can be obtained for our approximation at the cost of some complication. The expressions below are, however, accurate for a very wide range of shapes.

$$1-H_1/H_{(p)}=0.66\,\Omega_{(p)}^{0.55}\{s_1(a_1/a_3-1)\}^{-1.13} \qquad s_1=1+10a_3^{3.5}(a_1-a_3)$$

$$1-H_2/H_{(p)}=1.11\,\Omega_{(p)}^{0.55}\{s_2(a_2/a_3-1)\}^{-1.24} \qquad s_2=1+20a_3^{3.5}(a_2-a_3) \tag{10}$$

where $H_j \equiv (1/a_j)\,da_j/dt$ and $H_{(p)}$ and $\Omega_{(p)}$ are the Hubble constant and density parameter at the formation of the caustic surface. These are accurate to $0.2\,H_{(p)}$ for all ellipsoids with $a_{3(i)}<0.9$ provided the axes are not collapsing too fast $\{|H_j|<H_{(p)}\}$. As we might expect, the approximations break down for the most spherical objects.

The essential results are that the ellipsoids collapse earlier and the pancakes expand faster than those of WS. As expected, for highly eccentric objects ($s \to 1$) our velocity expressions agree reasonably with WS's approximate results.

3 Post-pancaking evolution

3.1 THE EQUATIONS OF MOTION

We now continue the evolution of the collapsed ellipsoids further. Assuming the caustic surface to remain thin (see Section 1), we may investigate further behaviour a similar way to the method of Section 2. The elliptical pancake formed, with principal axes $a_{1(p)}$ and a $a_{2(p)}$, is the limiting case of a highly flattened ellipsoid and, given the dissipation of motions perpendicular to the plane, has surface density

$$\sigma_{(p)}(x,y)=\tilde{\sigma}_{(p)}\{1-x^2/a_{1(p)}^2-y^2/a_{2(p)}^2\}^{1/2} \tag{11}$$

where conservation of mass implies that

$$\tilde{\sigma}_{(i)}=2a_{2(i)}a_{3(i)}\{1+\delta_{(i)}\}\,\varrho_{b(i)}/\{a_{1(p)}a_{2(p)}\}. \tag{12}$$

The pancake axial ratio and velocities along with (11) constitute the initial conditions for the post-pancaking evolution. The equation of motion is determined by the gravitational field of the elliptical pancake and the background matter. The gravitational potential of an elliptical surface with surface density of the form (11) is given in the plane by

$$\Phi(x,y)=\frac{\pi^2 G\tilde{\sigma}}{4a_1}\{A(\mathrm{e})x^2+B(\mathrm{e})y^2\} \tag{13}$$

with

$$A(\mathrm{e})=\frac{2(1-\mathrm{e}^2)^{1/2}}{\mathrm{e}^2}\{F(\tfrac{1}{2},\tfrac{1}{2};1;\mathrm{e}^2)-F(-\tfrac{1}{2},\tfrac{1}{2};1;\mathrm{e}^2)\}$$

$$B(\mathrm{e})=\frac{2}{(1-\mathrm{e}^2)^{1/2}\mathrm{e}^2}\{F(-\tfrac{1}{2},\tfrac{1}{2};1;\mathrm{e}^2)-F(\tfrac{1}{2},\tfrac{1}{2};1;\mathrm{e}^2)(1-\mathrm{e}^2)\}$$

$$\mathrm{e}^2=1-a_2^2/a_1^2 \tag{14}$$

and $F(a,\ b;\ c;\ z)$ the hypergeometric function (Abramowitz & Stegun 1968). To this we add the potential of the uniform background matter, as in Section 2, to obtain

$$\Phi(x,\ y)=\frac{\pi^2 G\tilde{\sigma}}{4a_1}\{A(\mathrm{e})x^2+B(\mathrm{e})y^2\}+\tfrac{2}{3}\pi G\varrho_s(x^2+y^2). \tag{15}$$

Since the potential is quadratic in x and y, the surface density of the ellipse maintains its form:

$$\sigma(x,y,t)=\tilde{\sigma}(t)(1-x^2/a_1^2-y^2/a_2^2)^{1/2} \tag{16}$$

where $a_1(t)=a_{1(p)}X(t)$, $a_2(t)=a_{2(p)}Y(t)$ and $\tilde{\sigma}=\tilde{\sigma}_{(p)}/XY$ with X and Y evolving according to

$$\frac{d^2X}{dt^2}=\frac{-\pi^2 G\tilde{\sigma}_{(p)}A(\mathrm{e})}{2a_{1(p)}XY}-\frac{4\pi}{3}G\varrho_s(t)X$$

$$\frac{d^2Y}{dt^2}=\frac{-\pi^2 G\tilde{\sigma}_{(p)}B(\mathrm{e})}{2a_{1(p)}X^2}-\frac{4\pi}{3}G\varrho_s(t)Y \tag{17}$$

given the initial conditions $X=Y=1$, $dX/dt=H_{1(p)}\geqslant H_{2(p)}=dY/dt$. If we let $T=H_0t$ and define the elongation parameter

$$\Delta\equiv 1-a_2/a_1=1-(Y/X)\,a_{2(p)}/a_{1(p)} \tag{18}$$

then we have

$$\frac{d^2X}{dT^2}=-\frac{\Omega_0}{2}\left[\mathcal{F}X(1+z)^3+\frac{SA(\mathrm{e})}{X^2(1-\Delta)}\{1+z_{(p)}\}^3\right]$$

$$\frac{d^2\Delta}{dT^2}=\frac{\Omega_0}{2}\left[\frac{S\{1+z_{(p)}\}^3}{X^3}\{B(\mathrm{e})-A(\mathrm{e})\}\right]-\frac{2}{X}\frac{dX}{dT}\frac{d\Delta}{dT} \tag{19}$$

where

$$\mathcal{F}\equiv 1-a_{2(\mathrm{i})}a_{3(\mathrm{i})}\{1+\delta_{(\mathrm{i})}\}$$

and

$$S\equiv\frac{3\pi a_{2(\mathrm{i})}a_{3(\mathrm{i})}}{4a_{1(p)}^3}\left(\frac{1+z_{(\mathrm{i})}}{1+z_{(p)}}\right)^3\{1+\delta_{(\mathrm{i})}\} \tag{20}$$

measures the relative importance of the disc gravitational field to that of the background matter at pancaking. Converting to independent variable z as before (equation 7) we can integrate this pair of equations using series expansions for A and B. In the later stages of collapse,

$$\varepsilon=1-e^2\ll 1,$$

we can use the asymptotic expansions

$$A(\mathrm{e})\rightarrow\frac{2}{\pi\mathrm{e}^2}\varepsilon^{1/2}\left\{\ln 16-2-\frac{(1+\mathrm{e}^2)}{\mathrm{e}}\ln\varepsilon\right\};\quad B(\mathrm{e})\rightarrow\frac{2}{\pi\varepsilon\mathrm{e}^2}\left(1+\mathrm{e}^2-\frac{\varepsilon\ln\varepsilon}{2}-\frac{\varepsilon\ln 16}{2}\right) \tag{21}$$

(Abramowitz & Stegun). As will be apparent from (19), the ellipse increases its eccentricity with time. The minor axis may then reach zero in a finite time, and a filament will be formed. Whether this happens or not depends on the shape of the pancake, its density and expansion velocities at formation. In low-density universes ($\Omega_0<1$), it is possible for the ellipse to expand asymptotically at constant velocities in both of its principal directions.

3.2 RESULTS

For a given value of Ω_0 and pancake collapse redshift, the evolution is described entirely by the axial ratios $(a_2/a_1)_{(\mathrm{i})}$ and $(a_3/a_1)_{(\mathrm{i})}$. The evolution of the three axes is shown in some representative cases in Fig. 2. Essentially three types of behaviour are possible:

(i) The middle axis collapses before the present epoch, while the long axis is contracting.
(ii) The middle axis collapses before the present epoch, while the long axis is still expanding.
(iii) The pancake has not collapsed to a filament by the present epoch.

In the third case, corresponding to highly flattened initial ellipsoids, the pancake may exist for a long time. Indeed, in a low-density universe, the pancake may undergo asymptotic undecelerated expansion, never forming a filament. In the other cases, the eccentricity increases with time until the middle axis collapses, and a filament is formed. In the absence of further dissipation (e.g. if all the matter fragments into collisionless galaxies at pancaking), the filament will not remain thin, but possibly relax into a cigar shape. We make a crude distinction between these filaments which

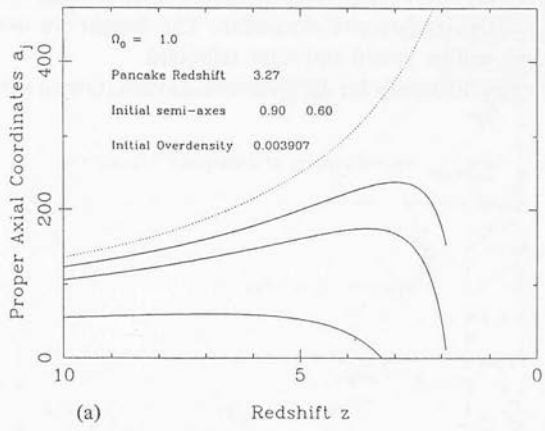

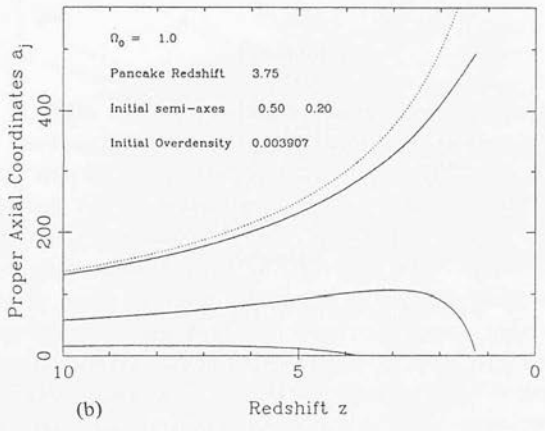

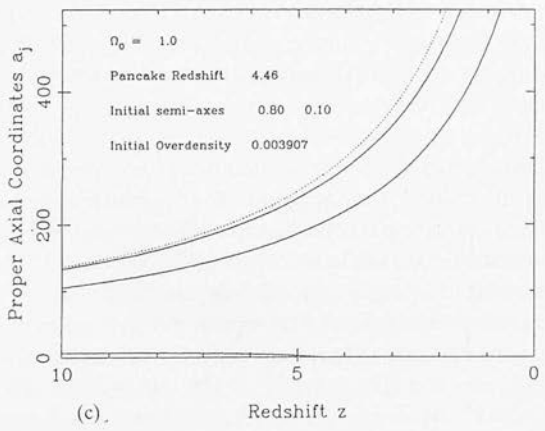

Figure 2. We illustrate the behaviour of the ellipsoid axes through pancaking identifying three cases: (a) Clusters – the long axis is contracting when the middle axis collapses. (b) Filaments – the long axis is expanding when the middle axis collapses. (c) Pancakes – the major axes have not collapsed by the present.

are still expanding along the long axis when the middle axis collapses, and those which are contracting. We assume that the latter relax into more isotropic configurations, which we shall describe as 'clusters' for the purposes of discussion. The former we assume will remain as filaments, although some will be bound and some unbound.

It is convenient to display the results for different initial axial ratios on a triangular diagram, as

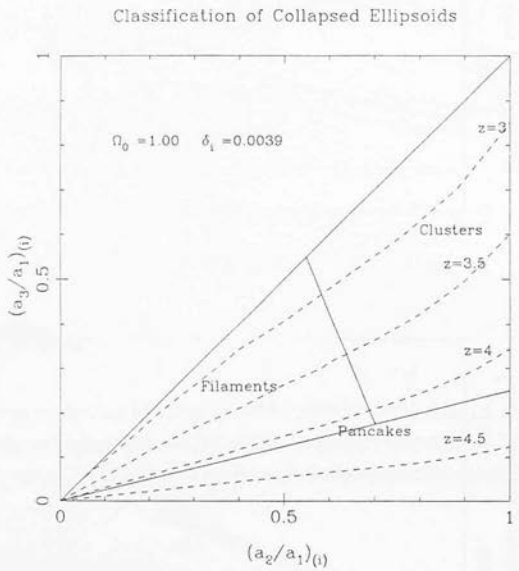

Figure 3.

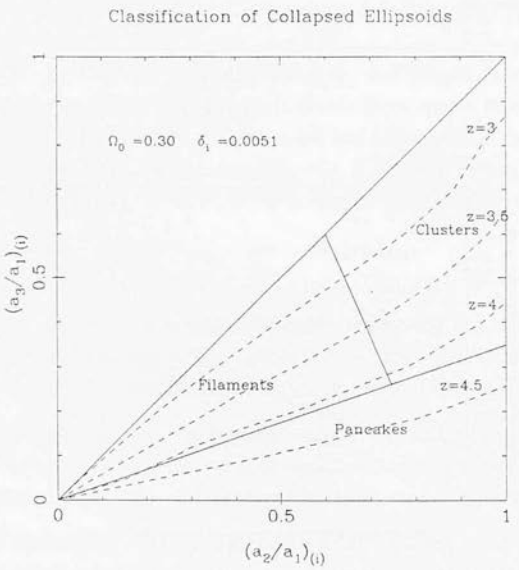

Figure 4.

Figures 3–5. Identified here are the regions in the initial shape plane which evolve into clusters, filaments and pancakes for different background densities. The overdensity $\delta\varrho/\varrho$ is chosen so that a typical object (see text) collapses at redshift 3. Also shown are the lines of constant collapse redshift.

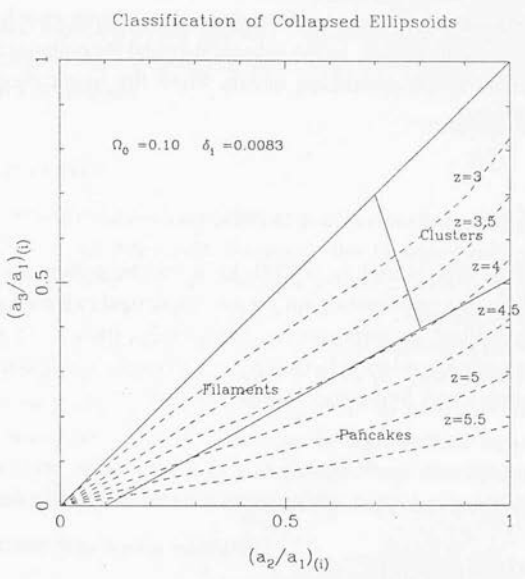

Figure 5.

shown in Figs 3–5. A point on this diagram represents one particular shape of ellipsoid characterized by the two coordinates $(a_2/a_1)_{(i)}$ and $(a_3/a_1)_{(i)}$. The apex represents spheres, the right-hand side oblate spheroids, and the diagonal prolate spheroids. The figures show the divisions between clusters, filaments and pancakes (characterizing the three cases above) for different initial shapes and background densities. This begs the question 'What is a typical initial shape?' This has been tackled by Peacock & Heavens (1985), hereafter PH, who analysed Gaussian random density perturbations to obtain shapes of primordial maxima. If we compare Figs 3 and 5 with their Fig. 3, we see that, for a given overdensity, more structures survive as pancakes in a low-density universe than in a high-density universe. This fits in with result (ii) of the pre-pancaking evolution since earlier deviation from self-similar evolution is more likely to lead to collapse of the minor axis, leaving two expanding axes. The most interesting result of such a comparison is the extreme rarity of objects which are expected to persist indefinitely as pancakes. There are very few local density maxima with $a_3/a_2 \leqslant 0.4$ in the work of PH (a result which is insensitive to the precise details of the perturbation spectrum). We see from Figs 3–5 that virtually no long-lived pancakes should exist unless $\Omega_0 \leqslant 0.1$. Even for $\Omega_0 = 0.1$ maxima with $(a_3/a_2)_{(i)} \leqslant 0.4$ have changing major-axis expansion parameters after pancaking, of order $0.2\,H_0$ over a redshift interval of $2 \rightarrow 0$ (i.e. any particular configuration is transitory). Notice, however, that these conclusions depend on the initial overdensity chosen, since that determines the collapse redshift of objects and hence, by the nature of our definition, the position of the pancake region on the diagram. We have taken our normalization from the work of PH. A 'typical' object has axial ratios 1:0.7:0.55 (more or less independent of the fluctuation spectrum), so we choose the initial overdensity so that this object pancakes at a redshift of 3. Flatter initial shapes tend to collapse earlier, but the variation in collapse redshift due to shape variation is rather smaller than that due to variations in overdensity (PH), at least for the common range of shapes. It is worth noting that if the WS background matter approximation is employed for the pre- and post-pancaking collapse, fewer filaments and more clusters result. Their approximation assumes a substantial infall of matter, and the average density within the sphere containing the ellipsoid can be much higher than the universe as a whole. It is not surprising, therefore, that the major axis of the ellipse turns round quickly.

It is possible to derive a simple yet powerful result on the collapse epoch of objects of a given overdensity with different initial shapes. In the spherical model for collapse in a flat universe (see e.g. Zel'dovich & Novikov 1983) pancaking occurs when the linear theory predicts that the overdensity $\delta_{\rm lin}=1.69$ where

$$\delta_{\rm lin}=\delta_{\rm (i)}\frac{\{1+z_{\rm (i)}\}}{\{1+z_{(p)}\}}.$$

If we put $\delta_{\rm (i)}=0.0039$ (see Fig. 3) and $z_{\rm (i)}=1500$ this gives the collapse redshift of a spherical object to be 2.47 which gives a consistent limit on our numerical calculations. The fact that the constant collapse redshift lines, or equivalently constant $\delta_{\rm lin}$ lines are approximately straight allows us to find an approximate relation between $\delta_{\rm lin}$ and $(a_2/a_3)_{\rm (i)}$. It is a good approximation to say that collapse occurs when linear theory predicts that

$$\delta_{\rm lin}=1+0.6(a_3/a_2)_{\rm (i)}$$

i.e. at

$$1+z=\delta_{\rm (i)}\{1+z_{\rm (i)}\}/\{1+0.6\,a_{3(\rm i)}/a_{2(\rm i)}\}.$$

This result is valid for a wide range of initial shape and overdensities. The lower limit $a_{3(\rm i)}\rightarrow 0$, giving $\delta_{\rm lin}=1$, which implies that instantaneous pancaking does not occur, is entirely consistent with an analytic solution of the acceleration equation (8) for an oblate spheroid with infinitesimally small minor axis, and represents the fact that as we flatten the object at a given overdensity less matter is driving the collapse.

4 Discussion

4.1 COLLAPSE TO FILAMENTS

In this paper, we have extended the work of Lin *et al.* (1965) and White & Silk (1979) on the gravitational collapse of homogeneous triaxial ellipsoids. Including the effect of background matter in an idealized manner, we find that (assuming the caustic surface, formed during the collapse, remains thin), the anisotropic collapse continues after pancake formation, increasing the eccentricity of the pancake with time. This is partly effected by the anisotropic gravitational field in the plane of a non-circular pancake, but is principally due to the fact that the anisotropic collapse prior to the formation of a pancake imparts an anisotropic velocity field to the pancake. The short axis expands less quickly (if indeed it expands at all) than the long, and collapses prior to the long axis.

In many cases, then, the anisotropic collapse of the pancake in its plane leads to the formation of a filament, which may be expanding or contracting along its axis. For highly flattened ellipsoids, however, the resulting pancake may persist for a long time. In a low-density universe the pancake may asymptotically expand undecelerated and never undergo secondary collapse in its plane to a filament. On fragmentation we might expect a sheet-like distribution of galaxies with approximately Hubble velocity expansion in the plane.

The secondary collapse of a pancake to a filament may result in further fragmentation of some of the gas which did not fragment before. Galaxies formed at pancaking may be regarded as collisionless, and will not be confined to a thin line. The galaxy distribution around a filament may therefore be expected to be closer to a cigar shape than to a one-dimensional structure.

In summary, the types of objects expected given the possibility of secondary collapse are

filaments, pancakes and more isotropic 'clusters', depending on the initial ellipsoid axial ratios. Filaments do not correspond to a degenerate case, as in the existing pancake theories, but arise naturally after pancake formation.

4.2 THE LOCAL SUPERCLUSTER

The general features of the pre-pancaking collapse (i.e. production of highly flattened structures with velocities in the plane retarded with respect to the Hubble flow), provide an interesting comparison with the observations of superclusters in general (see Oort 1983) and particular those of the Local Supercluster (LS; see e.g. Tully 1982). There are two possible explanations for the LS observations as mentioned by WS: first, that we are simply observing the LS near pancaking in a small-scale damping picture with galaxies forming prior to superclusters, or secondly, that it represents an object which collapsed whilst still gaseous at some earlier epoch. In principle, observation of the velocities normal to the plane can distinguish these two cases as the dissipative formation will result in low values. We can now discuss these descriptions in more detail. The observed flattening and velocity behaviour reported by Tully can be reproduced in two ways:

(1) The initial structure was highly eccentric:

$(a_3/a_1)_{(i)} \simeq 1/8 \qquad \Omega_0 = 1.0$

$(a_3/a_1)_{(i)} \simeq 1/4 \qquad \Omega_0 = 0.2$

which collapse quite early ($z > 4$ for our normalization). As discussed earlier these are unusual objects, particularly in the $\Omega_0 = 1$ case. If any of these objects exist, our post-pancaking calculations show that their major-axis velocity variation will be slow and so Tully's observed 27 per cent deviation from pure Hubble flow in the LS plane does not put tight constraints on the LS collapse epoch.

(2) If we restrict ourselves to shapes of objects which are common in the work of PH we find that, given our normalization, even in a low-density universe ($\Omega_0 = 0.1$) very few objects will not have undergone secondary collapse by the present. These statements are, however, valid for one normalization (i.e. one initial overdensity). Varying the overdensity will affect which shapes remain as pancakes at present and their major-axis velocities. We can set a limit on the collapse redshift for the LS in different background universes by considering the present major-axis velocity for ellipsoids with $a_2 : a_3$ of order 1:0.4, representing the limit of common objects (PH Fig. 3). Objects flatter than this occur with probability of 0.07 (PH Fig. 4). Requiring the expansion in the plane to be 0.73 H_0 at $z = 0$ gives the following limits:

$\Omega_0 = 0.1 \qquad z_{(p)} < 3.31$

$\Omega_0 = 0.3 \qquad z_{(p)} < 0.61.$

Earlier collapse will result in velocities in the pancake plane smaller than those observed in the LS. For shapes of order 1:0.5 which may occur reasonably often (12 per cent) we obtain

$\Omega_0 = 0.1 \qquad z_{(p)} < 1.46$

$\Omega_0 = 0.3 \qquad z_{(p)} < 0.10.$

We use inequalities here since, for later collapse epochs there will be some (common) initial shapes with $a_3 \geqslant 0.5$ which have $H_1 = 0.73 H_0$. For $\Omega_0 = 1.0$ we cannot model the LS field with the above structures, requiring a more eccentric and hence unusual initial perturbation. If we choose the overdensity so that our model of the LS collapses at $z = 0$, which corresponds to the least eccentric possible initial structure, we require minor to major axis ratio of 0.36 which has about 5

per cent chance of occurring. This agrees with the WS result that for $\Omega_0=1$ a viable model requires $(a_3/a_1)_{(i)}<\frac{1}{3}$ and demonstrates that the effect of using different background assumptions is not drastic for flat structures.

We see then that, for the higher density universes, LS collapse must have occurred recently and so a hierarchical clustering picture is favoured, whereas in low-density universes it is possible to reconcile the LS velocity behaviour with a pancake picture in which galaxies form later. There are of course ways to avoid this and allow $\Omega_0=1$. The most obvious solutions are to appeal to non-Gaussian initial conditions or to a non-zero cosmological constant. If this seems distastefully *ad hoc*, there remains the possibility of a more complex tidal field than the one we have considered. Allowance for the effects of discrete nearby clusters may relax the above limits somewhat. In the context of this work, however, the LS must have grown from an exceptionally flat perturbation, if $\Omega_0=1$ and the initial perturbations were Gaussian.

Acknowledgments

J. G. More acknowledges the support of a SERC research studentship.

References

Abramowitz, M. & Stegun, I. A., 1968. *Handbook of Mathematical Functions*, Dover, New York.
Barrow, J. D. & Silk, J., 1981. *Astrophys. J.*, **250**, 432.
Dekel, A., 1983. *Astrophys. J.*, **264**, 373.
Doroshkevich, A. G., 1970. *Astrophysics*, **6**, 320.
Efstathiou, G. & Silk, J. I., 1983. *Fundam. Cosmic Phys.*, **9**, 1.
Lin, C. C., Mestel, L. & Shu, F. H., 1965. *Astrophys. J.*, **142**, 1431.
Longair, M. S., 1984. *Concepts of Theoretical Physics*, Cambridge University Press.
Oort, J. H., 1983. *A. Rev. Astr. Astrophys.*, **21**, 373.
Peacock, J. A. & Heavens, A. F., 1985. *Mon. Not. R. astr. Soc.*, **217**, 805.
Peebles, P. J. E., 1980. *The Large Scale Structure of the Universe*, Princeton University Press.
Shapiro, P. R. & Struck-Marcell, C., 1984. *Astrophys. J. Suppl. Ser.*, **57**, 205.
Sunyaev, R. A. & Zel'dovich, Ya. B., 1972. *Astr. Astrophys.*, **20**, 189.
Tully, R. B., 1982. *Astrophys. J.*, **257**, 389.
White, S. D. M. & Silk, J. I., 1979. *Astrophys. J.*, **231**, 1.
Zel'dovoch, Ya. B. & Novikov, I. D., 1983. *Relativistic Astrophysics, Vol. 2: The Structure and Evolution of the Universe*, Chicago University Press.

Explosions in pancake models of galaxy formation

J.G. More and A.F. Heavens
Department of Astronomy, University of Edinburgh, EH9 3HJ, U.K.
M.J. Wilson
Department of Applied Mathematical Studies, University of Leeds, U.K.
& A.S. Trew
Department of Physics, University of Edinburgh, Edinburgh, U.K.

We have investigated the consequences of galaxies in pancakes releasing large quantities of energy, in the spirit of explosion models.

The explosion sends a blast wave through the baryonic material which is still falling in towards the pancake plane. Some of the shocked gas can cool, leading to a population of galaxies outside the pancake planes, reducing the strength of galaxy clustering. The large-scale structures (tens of Mpc) comes from the original pancake distribution.

We use a fluid-in-cell scheme, running on a 64x64 axisymmetric, comoving grid, with logarithmic grid spacings the highest resolution is where the density gradients are most severe. For speed, we use the University of Edinburgh Physics Department Distributed Array Processors.

In neutrino models, gas can cool, while not violating the X-ray background and Sunyaev-Zeldovich constraints, if the energy escaping into the infalling pancake is less than about 10^{52} J. However, the cooled gas does not extend very far away from the pancake plane (<1 Mpc), so the large-scale distribution should not be affected. For baryon-dominated universes, we expect the effect to be much more important.